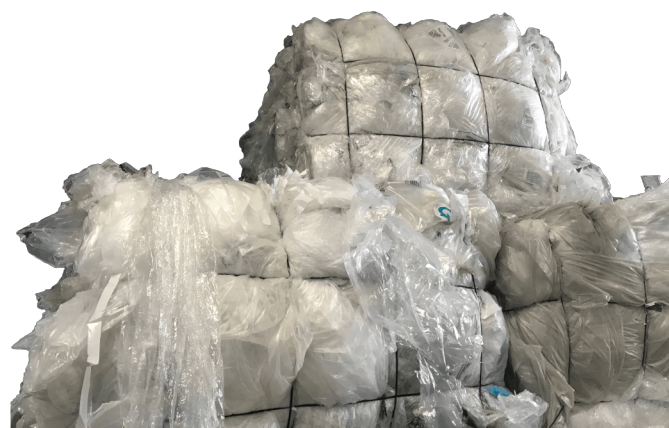




Compatibilization of polyethylene (waste) mixtures through reactive extrusion

Anne Raúl Nico Bussemakers



Cover photos:

- Pellets of recycled LDPE. Credit: Recyclon^[1]
- Bales containing End-of-Life LDPE film. Credit: Global Sources^[2]

Compatibilization of polyethylene (waste) mixtures through reactive extrusion

by

A.R.N. Bussemakers

to obtain the degree

Master of Science

in Materials Science & Engineering
at the faculty of Mechanical, Maritime and Materials Engineering (3mE)
of Delft University of Technology (TU Delft)

to be defended publicly on January 30th, 2023

Thesis committee:	Dr. Ir. S.T. Abrahami	TU Delft – Chair
	Dr. G.A. Filonenko	TU Delft
	Dr. Y. Yang	TU Delft
	Prof. Dr. S.J. Picken	TU Delft
	Dr. V. Decottignies	SUEZ France
	Dr. A. Dupas	SUEZ France

Thesis work duration:	April 11 th , 2022	January 30 th , 2023
Student number:	5409209	

This version of the thesis is intended for public view. An electronic copy of this thesis is available at <http://repository.tudelft.nl/>.

This work was performed in collaboration with SUEZ - CIRSEE,
Le Pecq / Croissy-sur-Seine, France

Acknowledgements

This thesis is the embodiment of the journey that I have made over the past ten months. A journey to earn the official title of Master of Science, but at the same time, a journey towards becoming a confident and independent academic. I am very proud to have dedicated my thesis to such a relevant and interesting cause. It would not have been possible without the opportunity provided by Virginie Decottignies, allowing me to combine this intellectual journey with gaining valuable experience in corporate life. For this, I am sincerely grateful to you. I would also like to thank both you and Adeline Dupas for your seemingly endless supply of knowledge of the world of plastic valorisation. You have both taught me an incredibly great deal during our fruitful discussions. Furthermore, I want to thank Shoshan Abrahami, for the long-distance support during my time in France, providing adequate advice or feedback whenever I needed it. You proved your dedication as a supervisor by visiting me in Paris to see for yourself where my research was taking shape. Lastly, thank you Georgy, Yongxiang and Stephen, for being part of my committee and facilitating this important moment for me.

I do not know where I would be right now without the undying support of my parents, Henk and Claudine, and brother, Matthijs, which started long before I set foot in Paris or at the TU Delft. You have always stimulated me to make the most out of my education, while never forgetting personal growth in the process. Thank you so much, Lise, for being as involved and loyal as you are, in both ups and downs. Life is one big adventure with you and I cannot wait where it will bring us. Then, a massive thanks to my faraway friends AJ, Job, Bart and Martijn, for whom travelling to Paris to see me was not a choice but a necessity. Finally, I want to thank my study buddies, Adi, Quentin and Linde, for making this Master's period so much fun.

I proudly present to you: my Master thesis. Enjoy!

Raúl Bussemakers
Paris, January 2023

Abstract

The production of plastic materials has experienced incredible growth over the past decades. Polyethylene constitutes the largest part (25%) of plastic production, finding its application mostly as film in industrial and food packaging and agricultural use. However, since packaging materials are getting increasingly complex, polyethylene waste is nearly always mixed with other polymers, making direct recycling impossible. Compatibilization of polymer blends can be used to convert an immiscible polymer blend into a homogeneous material with synergistic properties. When this compatibilization is carried out inside an extruder, one less reaction step is needed and the material can directly be processed according to its application.

This study addresses the reactive compatibilization of recycled LDPE (rLDPE) originating from industrial film waste with its polymer impurities, as well as virgin low-density polyethylene (LDPE)/polyamide 6 (PA6) blends of various compositions through reactive extrusion with PE grafted with MA (PE-g-MA). A literature review was carried out, summarising the current state-of-the-art of reactive compatibilization and reactive extrusion. The composition of the recycled stream was identified through various characterisation methods. Through a wide variety of characterisation techniques, the mechanical properties of the extruded sample pellets were investigated, as well as the mechanical and optical properties of the blown film.

The compatibilizing effect on the virgin LDPE/PA6 blends was found to grow in importance with increasing PA6 content. For 1 wt%, the samples did not exhibit any improvement upon compatibilization. The samples containing 5 wt% showed their improvements predominantly in the optical properties. The 10 wt% samples showed large enhancements overall, after being treated with the compatibilizer. Both the optical and mechanical properties of rLDPE saw a significant amelioration as a result of compatibilization. This study thus achieved compatibilization through reactive extrusion for an extensive variety of polymer samples.

Contents

Acknowledgements	i
Abstract	ii
List of abbreviations	ix
1 Introduction	1
1.1 Research questions	5
2 Theoretical background	6
2.1 Treatment of End-of-Life plastics	6
2.1.1 Polyethylene and its film waste	8
2.2 Compatibilization	11
2.2.1 Polymer blends	13
2.2.2 Reactive block copolymers	13
2.2.3 Reactive grafted polymers	16
2.2.4 Chain functionalisation	19
2.2.5 Dual compatibilization	23
2.3 Reactive extrusion	25
2.3.1 General process	26
2.3.2 Chemical reactions in a twin-screw extruder	27
2.3.3 Peroxide reaction kinetics	31
3 Materials and methods	34
3.1 Materials	34
3.2 Extrusion	35
3.2.1 Extruder correlation curves	37
3.3 Grain characterisation	37
3.3.1 Fourier-transform infrared spectroscopy (FTIR)	37
3.3.2 Melt flow index (MFI)	38
3.3.3 Differential scanning calorimetry (DSC)	38
3.3.4 Scanning electron microscopy (SEM)	38
3.4 Extrusion blowing	39
3.5 Film characterisation	40
3.5.1 Gel and black spots	40
3.5.2 Colorimetry	40
3.5.3 Tensile tests	40

4	Results and discussion	41
4.1	Extruder correlation curves	41
4.2	Pellet and film samples	43
4.3	FTIR	45
4.3.1	Additive calibration curves	45
4.3.2	Sample results	50
4.4	MFI	58
4.5	DSC	61
4.6	SEM	69
4.7	Gel and black spots	73
4.8	Colorimetry	77
4.9	Tensile tests	81
4.10	Synthesis of results	85
5	Conclusion and recommendations	88
5.1	Conclusion	88
5.2	Recommendations for future work	90
	References	93
	Appendices	106
A	Specifications extruder set-up CIRSEE - PLAST'lab	106
B	Screw design of twin-screw extruder	107
C	Extrusion blowing experiment	108

List of figures

1.1	Global annual primary plastics production (in Mt) by sector from 1950 to 2017 ^[4]	1
1.2	Schematic representation of the different layers that can be present in a multilayer film, all with their own functionality, and the repercussions that this might have for the recycling process ^[17]	3
1.3	Schematic representation of increased dispersion through polymer compatibilization.	4
2.1	Examples of PE material uses.	8
2.2	Different spatial structures of PE. Adapted from ^[38]	9
2.3	Structure of E-GMA.	14
2.4	SEM photographs of fracture surface of the blends: (a) HDPE/PET (90/10); (b) HDPE/PET/EBAGMA (90/10/3); (c) HDPE/PET/EBAGMA (90/10/5); and (d) HDPE/PET/EBAGMA (90/10/8) ^[63]	15
2.5	Structure of maleic anhydride.	16
2.6	The esterification reaction between PE-g-MA and PET (top) and the condensation reaction between PE-g-MA and PA6 (bottom) ^[69,81]	17
2.7	Scheme of a peroxide radical attacking a labile C–H bond.	19
2.8	General scheme of radical post-modification of a polyolefin ^[101]	20
2.9	Mechanism of GMA/St (or MA/St) multi-monomer grafting on a polyolefin ^[103]	21
2.10	The twin-screw extruder.	25
2.11	Schematic representation of processing zones of a twin-screw extruder ^[131]	26
2.12	Number of occurrences for different screw diameters in experimental studies in Section 2.2.	28
2.13	Number of occurrences for L/Ds in experimental studies in Section 2.2.	29
3.1	The extrusion line used for compounding and pelletizing the samples.	36
3.2	The mount used for SEM analysis, with a pellet fixed on it.	38
3.3	The extrusion blowing line used for transforming the samples into film.	39
3.4	A schematic of a roll of film with MD and TD illustrated.	40
4.1	Correlation curve for throughput as a function of screw speed.	41
4.2	Correlation curve for residence time as a function of screw speed.	42
4.3	The obtained pellets after extrusion of, from left to right, virgin LDPE, LDPE + 10 wt% PA6, LDPE + 10 wt% PA6 + PE-g-MA and rLDPE.	43
4.4	The obtained film after extrusion blowing the extruded pellets.	44
4.5	Correlation curve (bottom) for 1705 cm ⁻¹ peak intensity for various concentrations of MA, obtained from series of sample spectra (top).	46
4.6	Correlation curve (bottom) for 1736 cm ⁻¹ peak intensity for various concentrations of PE-g-MA, obtained from series of sample spectra (top).	47

4.7	Correlation curve (bottom) for 1705 cm^{-1} peak intensity for various concentrations of MA mixed with PE-g-MA, obtained from series of sample spectra (top).	48
4.8	Correlation curve (bottom) for 1736 cm^{-1} peak intensity for various concentrations of MA mixed with PE-g-MA, obtained from series of sample spectra (top).	49
4.9	FTIR spectrum of virgin, untreated LDPE.	50
4.10	FTIR spectrum of LDPE after extrusion.	51
4.11	FTIR spectrum of virgin LDPE with, 1 wt% (red), 5 wt% (black) and 10 wt% (green) of PA6, respectively.	52
4.12	FTIR spectrum of virgin LDPE with, 1 wt% (black), 5 wt% (red) and 10 wt% (green) of PA6, respectively, with 5 wt% of PE-g-MA added to each blend.	53
4.13	FTIR spectrum of PA6 grade C40L.	54
4.14	FTIR spectrum of PA6 grade B36LN.	55
4.15	FTIR spectrum of recycled LDPE before (red) and after (black) extrusion.	56
4.16	FTIR spectrum of recycled LDPE after being extruded with 2.5 wt% (black) and 5 wt% (red) PE-g-MA.	57
4.17	MFI values of references and formulations using virgin polymers.	58
4.18	Trends of Figure 4.17, differently presented.	59
4.19	MFI values of references and formulations using recycled LDPE.	60
4.20	DSC curve of virgin LDPE.	61
4.21	DSC curve of virgin LDPE after extrusion.	62
4.22	DSC curve of the first heating cycle of virgin LDPE with, from top to bottom, 1 wt%, 5 wt% and 10 wt% of PA6, respectively.	63
4.23	DSC curve of the first heating cycle of virgin LDPE with, from top to bottom, 1 wt%, 5 wt% and 10 wt% of PA6, respectively, with 5 wt% of PE-g-MA added to each blend.	64
4.24	DSC curves of the first heating cycle of the two different PA6 grades, followed by their respective second heating cycle.	65
4.25	DSC curve of the first and second heating cycle of recycled industrial film as received from the recycling plant.	65
4.26	Second cycle from Figure 4.25, with partial areas indicating LDPE/LLDPE ratio.	66
4.27	First and second heating cycle of rLDPE after going through an extrusion step.	67
4.28	First and second heating cycle of rLDPE after reactive extrusion with 2.5 wt% of PE-g-MA.	68
4.29	First and second heating cycle of rLDPE after reactive extrusion with 5 wt% of PE-g-MA.	69
4.30	SEM image of the fracture surface of a pellet containing virgin LDPE with 10 wt% of PA6.	70

4.31 SEM image of the fracture surface of a pellet containing virgin LDPE with 10 wt% of PA6 and PE-g-MA.	71
4.32 SEM image of the fracture surface of a pellet containing recycled LDPE after extrusion.	72
4.33 SEM image of the fracture surface of a pellet containing recycled LDPE and 5 wt% PE-g-MA.	73
4.34 Average number of black spots per m ² of film for the references and formulations using virgin polymers.	74
4.35 Average number of gel spots per m ² of film for the references and formulations using virgin polymers.	75
4.36 Average number of black spots per m ² of film for the references and formulations using rLDPE.	76
4.37 Average number of gel spots per m ² of film for the references and formulations using rLDPE.	76
4.38 Haze and thickness values for the references and formulations using virgin polymers.	77
4.39 L* and thickness values for the references and formulations using virgin polymers.	78
4.40 YI and thickness values for the references and formulations using virgin polymers.	79
4.41 Haze and thickness values for the references and formulations using rLDPE.	80
4.42 L* and thickness values for the references and formulations using rLDPE.	80
4.43 YI and thickness values for the references and formulations using virgin polymers.	81
4.44 Values of tensile strength and elongation at break in machine direction of films of all references and formulations using virgin polymers.	82
4.45 Values of tensile strength and elongation at break in transverse direction of films of all references and formulations using virgin polymers.	82
4.46 Values of tensile strength and elongation at break in machine direction of films of all references and formulations using rLDPE.	84
4.47 Values of tensile strength and elongation at break in transverse direction of films of all references and formulations using rLDPE.	85
C.1 The extrusion blowing setup during an experiment. The cylindrical plastic bubble can be identified, going from bottom to top.	108

List of tables

2.1	Properties of the three most common types of PE ^[39–42]	9
2.2	Composition of three bales of industrial LDPE film waste, as received by the SUEZ recycling plant.	10
2.3	Overview of experiments in literature using a reactive block copolymer for compatibilization.	14
2.4	Overview of experiments in literature using a reactive grafted copolymer for compatibilization.	18
2.5	Overview of experiments in literature using chain functionalisation for compatibilization.	24
2.6	Overview of experiments in literature grafting MA onto PE using reactive extrusion.	24
2.7	Arrhenius constants and half-life temperatures of some typical organic peroxides ^[144]	32
3.1	All used materials coming from external suppliers.	34
4.1	Summary of trends in mechanical and optical properties of the samples discussed in this chapter.	87
A.1	Extruder specifications ^[159]	106

List of abbreviations

ATR	attenuated total reflection
BMA	<i>n</i> -butyl methacrylate
BPO	benzoyl peroxide
BSE	back-scattered electrons
BTPB	<i>bis</i> [1-(<i>tert</i> -butylperoxy)-1-methylethyl]benzene
DCP	dicumyl peroxide
CIRSEE	International Centre for Research on Water and the Environment
CMR	carcinogenic, mutagenic and reprotoxic
DBP	di- <i>tert</i> -butyl peroxide
DBPB	di(<i>tert</i> -butylperoxyisopropyl)benzene
DMDH	2,5-dimethyl-2,5-di(<i>tert</i> -butylperoxy) hexane
DSC	differential scanning calorimetry
DVB	divinylbenzene
EaB	elongation at break
EBAGMA	ethylene-butyl acrylate-glycidyl methacrylate
EDS	energy-dispersive X-ray spectroscopy
E-EA-GMA	ethylene-ethyl macrylate-glycidyl methacrylate
EE-g-MA	ethylene elastomeric grafted with MA
E-GMA	poly(ethylene- <i>co</i> -glycidyl methacrylate)
EPR-g-MA	EPR grafted with MA
EoL	End-of-Life
EVA	ethylene vinyl acetate
FM	flexural modulus
FS	flexural strength
FTIR	Fourier-transform infrared spectroscopy
GHG	greenhouse gas
GMA	glycidyl methacrylate
HDPE	high-density polyethylene
HDPE-g-iPP	HDPE grafted with iPP
HDPE-g-MA	HDPE grafted with MA
HDPE-g-GMA	HDPE grafted with GMA
iPP	isotactic polypropylene
IS	impact strength
L*	whiteness
L/D	length-to-diameter ratio
LDPE	low-density polyethylene
LDPE-g-AA	LDPE grafted with acrylic acid

LDPE-g-BMI	LDPE grafted with bismaleimide
LDPE-g-MA	LDPE grafted with MA
LLDPE	linear low-density polyethylene
LLDPE-g-MA	LLDPE grafted with MA
MA	maleic anhydride
MD	machine direction
MFI	melt flow index
NIR	near infrared spectroscopy
PA6	polyamide 6
PA66	polyamide 6,6
PE	polyethylene
PE-g-MA	PE grafted with MA
PE-g-AA	PE grafted with acrylic acid
PET	polyethylene terephthalate
PP	polypropylene
PP-g-MA	PP grafted with MA
PS	polystyrene
rHDPE	recycled HDPE
rLDPE	recycled LDPE
rLLDPE	recycled LLDPE
rPE	recycled polyethylene
rPET	recycled PET
rpm	revolutions per minute
rPP	recycled PP
SE	secondary electrons
SEBS	styrene–ethylene / butylene–styrene
SEBS-g-DEM	SEBS grafted with diethyl maleate
SEBS-g-MA	SEBS grafted with MA
SEM	scanning electron microscopy
TAIC	triallylisocyanurate
TD	transverse direction
TPENR	thermoplastic epoxidized natural rubber
TS	tensile strength
TU Delft	Delft University of Technology
VLDPE	very low density polyethylene
YI	yellowness index
YM	Young's modulus
YS	yield stress

Introduction

In the 1950s, one of the biggest developments in material science history was put into effect; thermoplastics such as polyester, polystyrene and polyethylene (PE) were successfully produced on a large scale and made commercially available^[3]. Since then, plastic production has skyrocketed to staggering heights due to their lightweight, durable and inert nature, giving them a huge variety of possible applications. These applications vary from construction and transportation to agriculture and from household items to medical equipment. The sector that is most of all dominated by plastic consumption is packaging.

In Figure 1.1, the global annual primary plastic production is displayed, categorised into the different sectors where plastics play a role. The lifetime of plastics varies greatly per sector. Construction materials can have lifetimes spanning over multiple decades and consumer products might last several years, whereas packaging can find its end of use after weeks or even days.

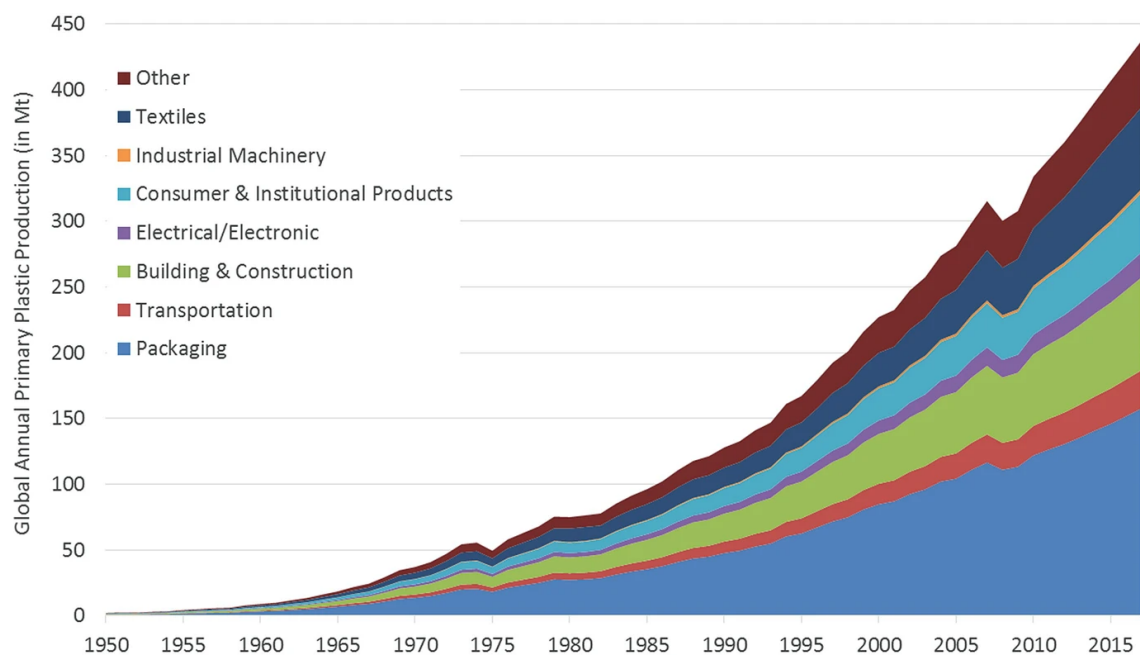


Figure 1.1: Global annual primary plastics production (in Mt) by sector from 1950 to 2017^[4].

Owing to their relatively inert nature and their astounding growth in production rate, however, plastic materials have been causing environmental problems worldwide. Greenhouse gas (GHG) emissions and energy use during production as well as discard in the environment are the two main reasons that make the plastic industry deeply problematic. Nearly all commercially used virgin plastics are petroleum-based, making them responsible for tremendous amounts of energy used (more than 6% of global coal electricity), as well as emissions during production (5% of global CO₂ emissions)^[5]. Furthermore, plastics are generally extremely inert materials, enabling them to stay intact and exist without significant degradation in nature for hundreds of years. Combined with the fact that an estimated 4 to 12 million tons of plastic end up in the oceans every year^[6], the effects are devastating.

The main reason why this problem has not yet been solved over the last decades, is the fact that no efficient and universally employable recycling and recovery strategies have come up. Furthermore, legislation around the recycling of materials is severely lacking in a large part of the world^[7]. Especially packaging material, due to their low lifespan, would benefit massively from better recycling and recovery. Therefore, especially for this plastic type, it is imperative that research is done in order to improve its End-of-Life (EoL) possibilities.

Notwithstanding, significant progress has been made over the past two decades, regarding the handling of EoL plastics. This has mainly been achieved through more and stricter legislation. An example of this is the European Commission's goal of increasing the recycling of packaging waste to 80% by 2030^[8]. In Europe, the recycling rate of plastic grew by nearly 120% between 2006 and 2020, the amount of waste that was used for energy recovery increased with nearly 80% and the amount of waste going to landfill shrunk by nearly 50%^[9]. Where polyethylene terephthalate (PET) used to be the only polymer for which a reasonable recycling infrastructure existed (30% share in total capacity), LDPE and high-density polyethylene (HDPE)/polypropylene (PP) have now caught up significantly (29% and 20%, respectively)^[10]. PE, predominantly finding its application in packaging and other films, remains mostly designed for single-use applications^[11].

PE materials constitute the largest groups of plastics that are commercially used, with a staggering 116 million tons (Mt) being produced in 2020^[12], out of nearly 450 Mt of plastic being produced in total^[13]. This number is only expected to grow in the upcoming years, due to the ever-increasing demand for plastic materials around the world^[14]. Furthermore, due to the growing demand of primary and secondary functions and thereby complexity of packaging, PE is nearly always combined with other materials^[15]. This can be done in many different ways, of which multilayer films is the most common for the case of PE (see Figure 1.2). Even though this concept has aided the packaging industry a great deal, it severely impedes straightforward recycling. It results in expensive and inefficient separating steps needing to be employed in order to achieve recovery of the different components. As of today, the economic incentive often remains

insufficient for the recycling industry to separate individual plastic fractions^[16].

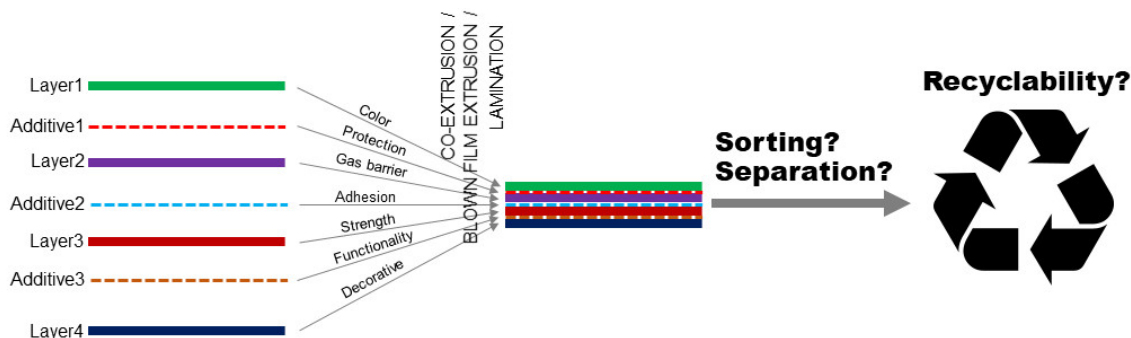


Figure 1.2: Schematic representation of the different layers that can be present in a multilayer film, all with their own functionality, and the repercussions that this might have for the recycling process^[17].

The recycling of industrial films at one of SUEZ' own recycling plants, has proven to be a viable process after which the material can be granted a new life as film. However, this film too, is dealing with impurities that cannot, or not cost-effectively, be removed. Since full separation has not yet proven to be an economically viable solution, the impurities need to somehow be incorporated in the material.

Polymer compatibilization or blending is an effective approach for the reuse of plastic waste^[18]. By reducing interfacial tension between the (immiscible) polymers of a blend, miscibility is promoted and the material will show much better mechanical and optical properties due to the increased dispersion of the minor phase in the major phase (see Figure 1.3). This method has great potential to be used for plastics that contain impurities of other polymers. If the right link is created between the polymer chains, making use of their respective molecular properties, a material might be conceived that is able to compete with virgin materials in terms of properties.

In order to achieve compatibilization at an appreciable cost and energy usage, reactive extrusion can serve as a very effective means. During the reactive extrusion process, an extruder is used as a reactor for polymerisation or polymer modification, after which the processing and shaping steps can take place immediately^[19]. The International Centre for Research on Water and the Environment (CIRSEE), SUEZ' main research centre, has a large history in plastics recycling and recovery. To serve this purpose, it is highly interested in exploring the world of plastic waste compatibilization through reactive extrusion.

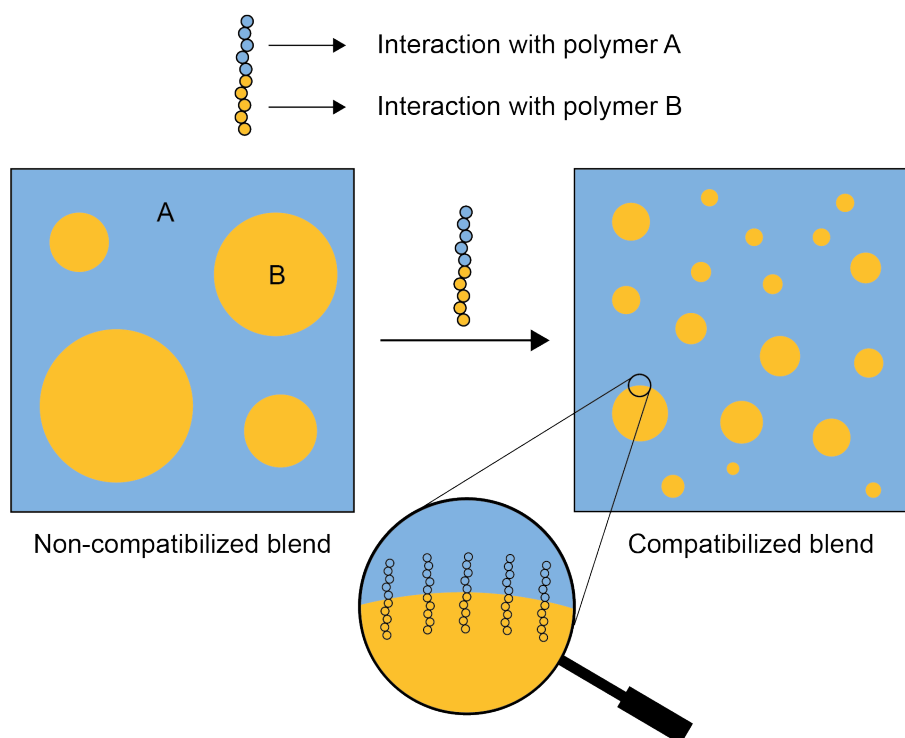


Figure 1.3: Schematic representation of increased dispersion through polymer compatibilization.

This study aims at researching the effects of compatibilizing virgin LDPE with impurities as well as recycled PE film, through reactive extrusion. To this end, an all-encompassing summary of the current state-of-the-art on the reactive compatibilization of (recycled) PE-containing polymer blends through reactive extrusion is first constituted. Subsequently, an experimental study will be carried out using blends of virgin LDPE and PA6 of different compositions, serving as a benchmark for recycled formulations. This will be followed by an experimental study where the composition of SUEZ' rLDPE will be estimated. Finally, this recycled batch will be subject to compatibilization research.

The research questions that form the guideline for this study, are given on the next page.

1.1 Research questions

The following research questions are aimed to be answered in the literature review:

1. Which main types of PE exist and what are their characteristics?
2. With which immiscible polymers is PE usually mixed in plastic industrial film waste and what causes the immiscibility?
3. Which types of polymer compatibilization exist and what is their current state-of-the-art?
4. What does the reactive extrusion process look like?
5. How is the reactive extrusion process carried out for polymer compatibilization in the current state-of-the-art?

The following questions are aimed to be answered through experimental work:

6. What is the effect on the mechanical and optical properties of compatibilizing virgin LDPE and PA6 of different compositions through reactive extrusion?
7. What is the composition of the researched batch of SUEZ' recycled LDPE stemming from industrial film?
8. What is the effect on the mechanical and optical properties of compatibilizing recycled LDPE from industrial film with its impurities through reactive extrusion?

This report is outlined as follows:

In Chapter 2, a theoretical background on the subject is combined with a review and summary of the current state-of-the-art.

In Chapter 3, the used materials and experimental methods for this study are elaborated on.

In Chapter 4, the experimental results are displayed and discussed.

In Chapter 5, conclusions are drawn based on the discussed results and recommendations for future work are given.

Theoretical background

This chapter will commence by covering the current state-of-the-art of plastic (film) waste management, after which the focus will be shifted towards PE. Subsequently, the theoretical background of compatibilization is treated, before reporting on the state-of-the-art thereof in light of PE. Finally, the state-of-the-art of reactive extrusion elaborated on, again followed by a specification towards PE compatibilization studies.

2.1 Treatment of End-of-Life plastics

Plastic waste can take many different forms. The first thing that might come to mind, is packaging of a product bought by a consumer. However, plastic waste can emerge without it being an EoL product. A distinction is first made between two types of plastic waste:

- Post-industrial waste: This type is created during the manufacturing process of the product. It is considered high-quality, since there are no impurities present and the composition is known^[20]. This scrap is usually being recycled or reused at the same facility.
- Post-consumer waste: When a plastic product reaches its EoL, it is called post-consumer waste. This waste is considered much more complex and of unknown composition, rendering the recycling process a great deal more difficult.

From here on, when the term plastic waste is used, it will be referring to post-consumer waste. This is the type of waste that is studied and treated by recycling & recovery teams at companies such as SUEZ. Nowadays, a vast spectrum of waste treatment methods exist, are developed and are applied to plastic waste. These techniques do not exclusively comprise recycling methods, since not all plastic waste is being recycled yet, as of today. The treatments can be categorised into four types, which will be elaborated on below.

Mechanical recycling is a technique characterised by the fact that it merely adopts mechanical processes, keeping the structure of the polymer chains unaltered. The process conventionally involves the sorting, washing and grinding of the material, all of which may occur multiple times^[21]. The plastic is often re-extruded, after which the pellets are ready to be used as feedstock for new products. Here, two scenarios can be

differentiated: the closed-loop and open-loop process^[22]. Closed-loop denotes the possibility of implementing the recycled material in a high-end product, which is only possible if its quality and properties are nearly identical to those of the original product. Open-loop indicates that the recycled material is to be used in mechanically and/or optically less demanding applications, e.g. industrial packaging film of which the recycled PE is re-implemented in garbage bags or garden hoses. The former is seen with single-plastic waste with few contaminants, whereas the latter arises from waste with remaining contaminants or a mix of compatible polymers.

Chemical recycling lends its name from the fact that the polymer is broken down into its monomers or other valuable chemicals. Popular approaches that have been applied for many years are pyrolysis and gasification, which produce gases, fuels and even monomers that can then be reused in a useful way^[23]. Much is still being experimented with this on both LDPE^[24–26] and HDPE^[27–29]. Besides, depolymerisation methods such as solvolysis has sparked the attention of researchers, where heteropolymers (polyesters, polyamides) are transformed into monomers that could be used as feedstock for new polymers^[30]. This method can, however, not be used to cleave C–C bonds and is therefore not applicable to polyolefins.

Energy recovery is applied when the plastic waste is incinerated, and the energy is used for heating or electricity production. Because polymers possess a very high calorific value, similar to those of other petroleum-based fuels ($\sim 45 \text{ MJ kg}^{-1}$), this is a feasible process. Additionally, incineration yields a volume diminution of 90-99%, reducing the reliability on landfilling^[31]. Where energy recovery used to be a much more harmful process due to toxic gases being emitted, legislation and closer monitoring have changed this for the better. This technique is quite universally called "recovery" instead of "recycling", also in EU's Waste Framework Directive^[32]. Whether or not energy recovery ought to be awarded the term recycling, is up for debate. Since the material is entirely destroyed and nothing tangible can be recovered for reuse, the term "recycling" would be misplaced. *Something* is obtained in return, though, namely energy, contributing significantly to fill our needs of power. The share of energy recovery has steadily increased over the past decade, mostly at the cost of landfilling^[21].

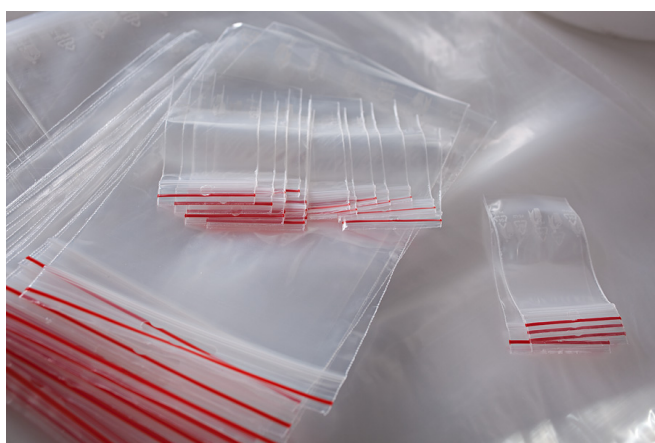
Landfill is the process of burying plastic waste in designated sites. Nothing is gained from this option in terms of materials or energy and the valuable resource that plastics could be, are not made use of. During landfill, the release of hazardous compounds is closely monitored, following some highly important steps taken by the EU Landfill Directive^[33]. In a number of countries throughout the EU, landfill is banned entirely. As a result, the share of landfill in the waste treatment sector has decreased tremendously, also due to energy recovery being a vastly more preferable means to treat non-recyclable plastic waste.

The three types of recycling/recovery (not taking landfill into account) are listed in order of priority; mechanical recycling will, if applicable, always be preferable over chemical recycling or energy recovery. This is due to several reasons. Firstly, chemical recycling

remains at least two to three times more expensive than mechanical recycling, because of the complexity of the process and expensive equipment that is needed. Secondly, breaking up the polymer chains means the plastic material will be irreversibly lost, resulting in the need of newly produced materials to replace it. Also in the case of depolymerisation methods the obtained monomers cannot always be directly reused, due to complex material structures^[30]. So even though investments by SUEZ are made in this field, the focus remains to be pushed towards retaining the thermoplastic material through the shortest possible recycling route, especially when merely a few percentages of impurities are present. If a feasible solution were to be found for either separating or compatibilizing the plastic waste with its contaminants, the quest towards full reuse and a circular economy would be dramatically simplified.

2.1.1 Polyethylene and its film waste

Plastic films constitute a vast part of the plastics market worldwide. As was touched upon in the introduction, packaging is the biggest end-use market for plastics (around 40%). Together with the agricultural sector, it comprises the majority of plastic film applications. PE, especially LDPE, is primarily used for film material, e.g. for food packaging, garbage bags or in agriculture. Other applications, although to a much lesser degree are squeeze bottles, tubes, pipes or bins^[34]. Its immense popularity in the food industry stems from various appreciable qualities, such as being low cost, heat sealable, chemically inert and odour free. Moreover, it can be used as multilayer wrapping in combination with other materials^[35]. LDPE can be polymerised with vinyl acetate, creating ethylene vinyl acetate (EVA). Strength and flexibility at low temperatures are hereby increased. EVA is commonly applied in agricultural films and multilayer food packaging.



(a) As packaging film^[36].



(b) As tubing material^[37].

Figure 2.1: Examples of PE material uses.

PE has the simplest of polymer structures, with the repeating unit



The polymer chains can, however, take on a different structure as a result of the synthesis conditions. A further distinction arises, based on density (and thereby crystallinity): LDPE, linear low-density polyethylene (LLDPE) and HDPE. Their respective structures are displayed in Figure 2.2.

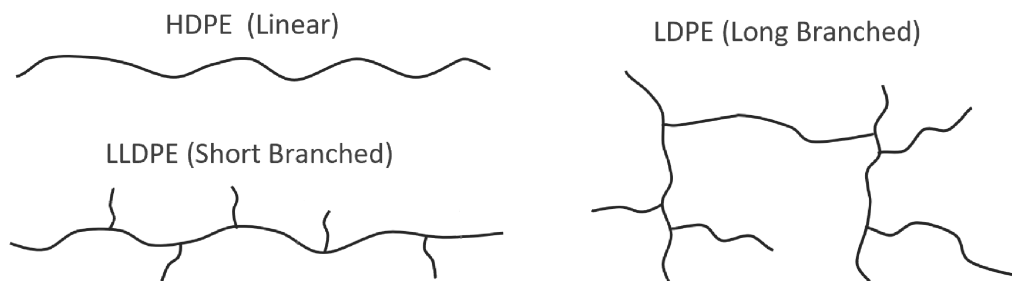


Figure 2.2: Different spatial structures of PE. Adapted from^[38].

As the figure shows, the structures differ in degree of branching, where HDPE is hardly branched, LLDPE contains the most (but only short) branches and LDPE on average has slightly fewer, yet much longer branches. Naturally, such differences on a microscopic scale cause the three grades to behave differently. A higher degree of branching will result in a lower density and lower crystallinity of the material. This makes HDPE stronger, more brittle and less tough than LDPE. Since they are all products of radical polymerisation, LDPE is the product of lowest reaction pressure, while HDPE is obtained at highest pressure. Some noteworthy properties of the three grades, that follow from their varying structures, are summarised in Table 2.1.

Property	LDPE	LLDPE	HDPE
Density, g/cm ³	0.917–0.940	0.925–0.950	0.940–0.970
Melting point, °C	106–110	120–124	130–135
Crystallinity, %	40–55	50–60	70–80
Short branches, /1000	10–25	20–35	1–3
Molecular weight, g/mol	30,000–50,000	60,000–100,000	200,000–500,000
Tensile strength, MPa	10–20	25–45	30–40
Hardness, Shore D	40–50	55–56	60–70

Table 2.1: Properties of the three most common types of PE^[39–42].


This study entails LDPE originating from EoL industrial film. As the name suggests, this film comes from industry, differentiating itself from municipal film (e.g. from curb side collection) or agricultural film. SUEZ performs mechanical recycling on this stream, at its own recycling site in France. The industrial film is received at the site, coming from a sorting centre^[43]. The bales are subsequently shredded to handleable pieces, after which a manual sorting step takes place to remove non-industrial or coloured film, different plastics and other contaminants. The film is then shredded to much smaller pieces, washed and dried. At this point, it is ready for re-extrusion, with which the recycling site produces pellets to be resold. These mechanically recycled pellets of EoL industrial

film, are subject of this research.

During a characterisation study performed at SUEZ' recycling site, the composition of several bales was determined. In Table 2.2, this composition is summarised.

Constituent	Average fraction level (wt%)
Transparent LDPE films	81.2
Coloured/printed LDPE films	5.9
PP films	0.3
Other plastics (PA6/PP/PET/PS)	0.9
Metal/wood	0.1
Cardboard/paper	0.9
<i>Total transparent LDPE films</i>	81.2
<i>Total coloured/PP films</i>	6.1
<i>Total impurities</i>	2.0

Table 2.2: Composition of three bales of industrial LDPE film waste, as received by the SUEZ recycling plant.


 Besides this, some other remarks should be made about the table above. The exact identification of (the quantity of) other plastics cannot be done on site, since no IR spectroscopy or differential scanning calorimetry (DSC) is present. Furthermore, PET and PA6 often come in the form of multilayers with PE, making analysis difficult since near infrared spectroscopy (NIR) is used for characterisation. In addition, the LDPE is usually mixed with LLDPE and sometimes even with HDPE, but again, this cannot be verified without the use of a DSC.

As mentioned above, a second sorting is carried out manually. Understandably, pieces of wood, metal or coloured film are relatively easy to spot and take out of the waste stream. However, minuscule fragments of other plastics such as PA6, PET and PP can easily go unnoticed. Furthermore, the fact that multilayer films are present, makes separation very difficult. For this reason, a few wt% of polymer impurity is known to exist in SUEZ' recycled industrial film. Although the extruder is equipped with a filter before the die, which purifies substantially, not all impurities will be caught. These impurities are one of the main reasons why recycled PE films underperform when compared to virgin films, due to polymer incompatibility. The next section will treat polymer compatibility and its possible role in PE recycling, as investigated in this research.

2.2 Compatibilization

Whether or not two polymers form a physical blend, creating a homogeneous phase on microscale, primarily depends on their thermodynamic miscibility. If two polymers do not show affinity towards each other they are considered immiscible, showing little to no interfacial interaction and forming two distinct phases. The boundaries between these phases act as source of fracture, causing the material to have very poor mechanical properties^[44]. The miscibility of two polymers is determined by the Gibbs free energy of mixing:

$$\Delta G_m = \Delta H_m - T\Delta S_m \quad (2.2)$$

where ΔH_m and ΔS_m are the enthalpy and entropy of mixing respectively, and T is the temperature. This free energy needs to be negative for the mixture to be considered miscible. With mixtures of relatively small molecules, the entropy of mixing is the main driving force for ΔG_m , since it contributes hugely compared to ΔH_m . For macromolecules, however, the contribution of the entropy factor is impeded immensely, due to their practical inability to move freely. Therefore, ΔG_m almost exclusively depends on the the enthalpy of mixing, i.e. the extent of interactions among the molecules^[44]. The following relation is obtained for the requirement of negative free energy, with negligible entropy of mixing:

$$\begin{aligned} \Delta G_m &= \Delta H_m - T\Delta S_m < 0 \\ \Rightarrow \Delta H_m &< T\Delta S_m \\ \Rightarrow \Delta H_m &0 \end{aligned} \quad (2.3)$$

implying that exothermic mixtures occur spontaneously, while endothermic mixtures have a high temperature threshold in order for ΔG_m to become negative^[45]. However, only very seldom does a blend of polymers exhibit a negative enthalpy of mixing. Explaining how polymers do manage to blend into a homogeneous mixture, can be done through the well-known Flory-Huggins lattice model for polymer blends^[44]:

$$\frac{\Delta G_m}{RTn_r} = \frac{\phi_1}{N_1} \ln \phi_1 + \frac{\phi_2}{N_2} \ln \phi_2 + \phi_1\phi_2\chi_{12} \quad (2.4)$$

where R is the gas constant, n_r is the number of moles, ϕ_1 , ϕ_2 and N_1 , N_2 are the volume and number fractions of both polymers, respectively, and χ_{12} is the Flory-Huggins interaction parameter. This parameter is calculated as follows:

$$\chi_{12} = \frac{V}{RT} (\delta_1 - \delta_2)^2 \quad (2.5)$$

where δ_1 and δ_2 are solubility parameters of both components. The lattice model also states the enthalpy of mixing, as a function of the interaction parameter:

$$\Delta H_m = RT \chi_{12} \phi_1 \phi_2 V \quad (2.6)$$

As stated before, the entropy of mixing, although slightly positive, is negligible with respect to the enthalpy of mixing for case of polymers. Therefore, the following relation for the free energy of mixing is obtained:

$$\Delta G_m \cong \Delta H_m = RT \chi_{12} \phi_1 \phi_2 V \quad (2.7)$$

implying that in order to satisfy Equation 2.3, χ_{12} should be (close to) zero. For highly similar polymers, this can be achieved through minimising the difference in the respective solubility parameters of the two polymers^[46] (see Equation 2.5).

In order to evaluate the mutual miscibility of two polymers, the most conventional approach is a glass transition temperature (T_g) measurement. A (nearly) single T_g means the polymers are miscible and form a homogeneous phase. When two transition temperatures are distinguishable, two separate phases exist¹ and the blend is immiscible^[47]. The T_g of a system is usually determined through DSC.

Miscibility of two structurally different polymers, albeit even slightly, is hardly ever naturally encountered. PE and PP have very similar structures, yet still show poor interfacial adhesion and stress transfer between phases, resulting in unworthy mechanical properties^[48]. Furthermore, HDPE and LLDPE are generally immiscible, even though their structures are nearly identical^[49] (see Figure 2.2). Consequently, help is needed from exothermic intermolecular forces such as hydrogen bonding and dipole interactions. In order to establish these forces, compatibilization is used.

Compatibilization is the process of modifying interfacial activity for establishing a heterogeneous polymer blend^[50]. A successful polymer blend is formed when two (co)polymers are mixed, having the synergistic properties of each polymer combined. Compatibilization achieves this by increasing the adhesion and reducing interfacial tension between the two phases. As a result, the number of defects and voids in the material will be drastically diminished. The stress concentration throughout the blend interfaces will thereby be reduced, positively impacting macroscopic properties such as tensile strength^[51]. The optical characteristics of a compatibilized polymer blend can be impinged upon, as compared to those of the pure polymers^[52]. This is due to the fact that their respective refractive indices are heavily affected during the blending process. Since PE is primarily finds its application as (transparent) film, the re-implementation of its recycled form could be severely limited as a result. This being said, compatibilization has widely proven its potential to ameliorate PE films' optical properties, mostly by reducing gels. Gels, or gel spots, can be caused by a large variety of things, the most common of which are the following^[53]:

- Highly oxidised polymeric materials (also called "black spots" for their colour)
- Locally crosslinked polymeric materials
- Non-dispersed polymeric materials (not crosslinked)
- Non-polymeric contaminants

¹The two phases will crystallise separately into different segments, as indicated by the DSC curve.

Oxidation and local crosslinking both occur as a result of polymer degradation. This can happen during extrusion, but is far more predominantly caused by the lifespan of EoL films. Non-dispersed polymeric materials include polymer impurities, subject of this study.

A distinction arises between physical and chemical compatibilization. Physical (or non-reactive) compatibilization (or blending) is the mixing of two polymer melts, upon introducing a blending agent. Since no chemical reaction takes place, it is a convenient approach without that can be carried out in conventional machinery^[54]. Chemical (or reactive) compatibilization occurs by chemically modifying one or both of the polymers, rendering them compatible. In the following sections, the different variants of compatibilization will be covered in light of PE recycling.

2.2.1 Polymer blends

Physical blending is done by introducing a coupling agent to a polymer melt. These molecules form a bridge between immiscible polymers as a result from their ability to bind to both simultaneously. They are often times block copolymers, with two different ends, both being highly compatible with one of the blends. Coupling agents are widely used in the plastics industry, for blending plastics or for compatibilizing inorganic fibres to polymer matrices in composites^[55]. Styrene–ethylene / butylene–styrene (SEBS) block copolymers have been used to an enormous extent for the compatibilization for polyesters with polyolefins, mainly contributing to impact modification^[56]. Because of their elastomeric nature they provide toughness, while still being similarly processable to thermoplastics. They form separated phases on micro-level, due to the incompatibility of polystyrene with the elastomeric blocks. As a result, they allow for physical blending of non-polar with polar polymers. PE has undergone much research in compatibilization through SEBS^[57,58].

From research within SUEZ, it followed that coupling agents constituted the vast majority of additives used for PE compatibilization^[59]. Since prior studies from their part have mainly focused on polymer blending with coupling agents, this study will emphasise chemical compatibilization, and its attainment through reactive extrusion.

2.2.2 Reactive block copolymers

Block copolymers are able to undergo reactive compatibilization, if they possess reactive groups that can covalently bond to one or both of the to-be blended polymers. If the other block is miscible with the other polymer in the blend, successful compatibilization arises. An example of such a block copolymer is poly(ethylene-*co*-glycidyl methacrylate) (E-GMA) (see Figure 2.3). The epoxy group readily dissociates to form a hydroxide side group and bind to, preferably, a carboxyl end group of another molecule. This renders it highly suitable to be used as a compatibilizer of polyolefins with PET. At high enough E-GMA concentrations, however, it will bind to the hydroxide end groups as well. This will cause a crosslinking effect, negatively affecting the final properties of the blend^[15].

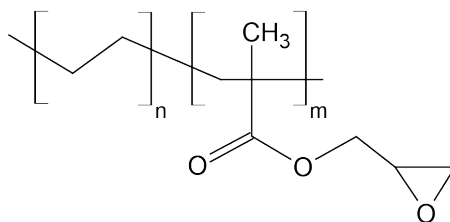


Figure 2.3: Structure of E-GMA.

E-GMA has played a role in a great amount of PE/PET compatibilization studies over the past decades. Other reactive block copolymers have been assessed as well, though almost exclusively with a GMA block. An overview of studies done in literature, including their qualitative results, is given in Table 2.3.

Ref.	Polymer blend	Copolymer	Results
[60]	rHDPE/rPET	E-GMA	Increased TS, FS, dispersion, toughness.
[61]	rLDPE/rPET (PP, PA6)	E-GMA	Increased TS, EaB, YM.
[62]	HDPE/rPET	E-GMA	Increased IS, EaB. Decreased FS, FM, TS, YM.
[63]	HDPE/PET	EBAGMA	Increased interfacial adhesion.
[64]	rPE/rPET	E-GMA	Increased interfacial adhesion.
[65]	HDPE/PET	E-GMA	Increased EaB, IS, phase dispersion.
[66]	HDPE/rPET	E-GMA	Increased dispersion, TS.
[67]	HDPE/PET	E-GMA	Increased TS, YM, IS, phase dispersion.
[68]	HDPE/PET	E-GMA E-EA-GMA	Increased EaB, IS. Decreased YM, TS.
[69]	LLDPE/PET rLLDPE/rPET	E-GMA	Increased EaB, IS. Decreased YM. Increased IS. Decreased YM.
[70]	HDPE/rPET	E-GMA	Increased TS, EaB. Decreased YS.
[71]	LDPE/PET	EBAGMA	Increased dispersion
[72]	LDPE/PET	EMA	Increased EaB, fracture toughness
[73]	HDPE/rPET	E-GMA	Increased adhesion, TS, EaB
[74]	HDPE/PET	Surlyn (EMA)	Increased EaB, IS
[75]	HDPE/rPET	EBAGMA	Increased dispersion, EaB, IS
[76]	LDPE/PA6	E-GMA	Increased dispersion
[77]	LDPE/PA6	TPENR	Increased dispersion, IS

Table 2.3: Overview of experiments in literature using a reactive block copolymer for compatibilization.

It becomes clear from Table 2.3 that block copolymers are mainly used to compatibilise PE with PET. Virgin PE is researched about as much as their recycled congeners (rHDPE, rLDPE and rLLDPE). Furthermore, it clearly follows from Table 2.3 that copolymers containing a glycidyl methacrylate (GMA) block are the main focus of research for PE/PET compatibilization. Certain studies used ethylene-butyl acrylate-glycidyl methacrylate (EBAGMA), a terpolymer containing a GMA block.

A number of aspects can be noticed from the results of the experiments. First of all, in the vast majority of cases, an increase in phase dispersion or interfacial adhesion was obtained upon compatibilizing with a copolymer and in no case a decrease in these parameters was seen. Both aforementioned effects indicate similar behaviour; when the interfacial adhesion goes up, the two phases will be more inclined towards mixing with one another, enhancing the overall dispersion. The degree of dispersion is generally assessed by means of a scanning electron microscopy (SEM) image of a fracture surface of a sample. A striking example of this can be found in Figure 2.4. In the non-compatible blend, a clear two-phase structure is seen, with droplets of PET being dispersed in the HDPE matrix. Upon adding a compatibilizer, the particle size diminishes and the blend is significantly homogenised because of the increased interfacial adhesion.

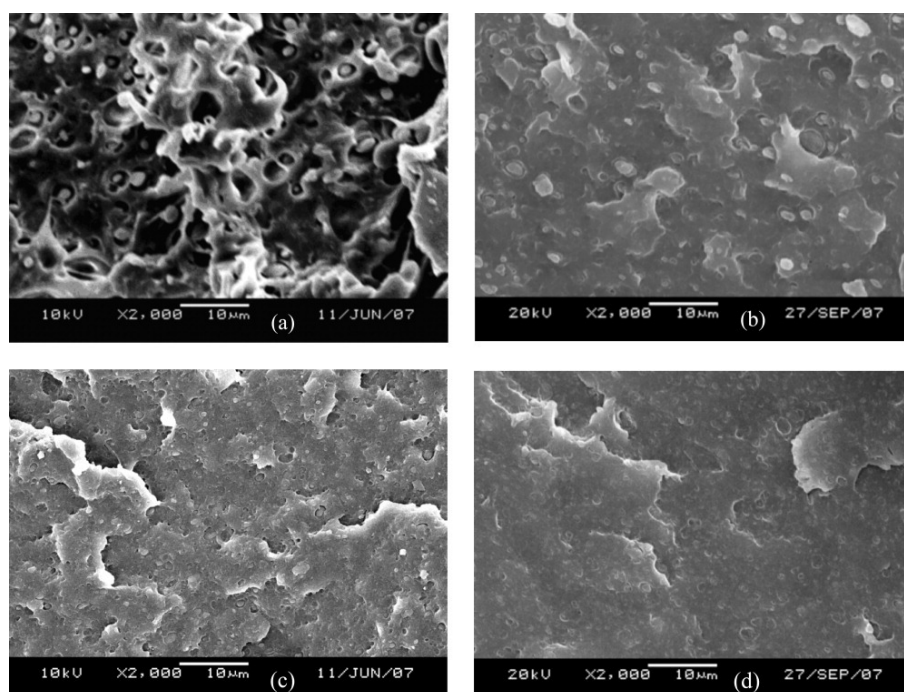


Figure 2.4: SEM photographs of fracture surface of the blends: (a) HDPE/PET (90/10); (b) HDPE/PET/EBAGMA (90/10/3); (c) HDPE/PET/EBAGMA (90/10/5); and (d) HDPE/PET/EBAGMA (90/10/8)^[63].

Besides microscopic interfacial properties, many different macroscopic mechanical properties were tested in the various experiments. Tensile properties (tensile strength (TS), Young's modulus (YM), elongation at break (EaB)) were evaluated in the majority of cases. Impact strength (IS) was often measured as well, and in a few cases, the flexural properties (flexural strength (FS), flexural modulus (FM)). What is noteworthy, however, is that not all mechanical properties show consistent trends upon compatibilization. Tensile strength and Young's modulus increased in some studies, whereas they decreased in others.

Lei *et al.*^[62] attribute the decrease to the decreased crystallinity level χ_c , which is calculated as follows:

$$\chi_c = \frac{\Delta H_{\text{exp}}}{\Delta H} \times \frac{1}{w_f} \times 100\% \quad (2.8)$$

where ΔH_{exp} denotes the experimentally obtained heat of crystallisation, ΔH is the theoretical heat of crystallisation of the fully crystalline polymer and w_f is the weight fraction of the polymer in the blend. Elongation at break and impact strength both clearly profit from compatibilization, as all studies that included them, showed an enhancement. According to Fasce *et al.*^[72], EaB is highly dependent on interfacial adhesion among the different phases, explaining the improvement after any kind of compatibilization. The same goes for impact strength, seeing significant growth with increased dispersion. This might not always be the case, though, since it has been found previously that the highest impact strength did not belong to the blend with the highest interfacial adhesion^[78].

2.2.3 Reactive grafted polymers

Block copolymers can also be chemically modified, or grafted, in order to render them eligible for reactive compatibilization. Similar to the aforementioned approach, a copolymer is made which is miscible with one component of the blend and undergoes a reaction with the other component. This forms a network of grafted copolymers, turning it into a synergistic blend. Since PE does not possess any functional groups, a copolymer should be chemically bonded to the other melt, while undergoing hydrogen bonding or Van der Waals bonding (and thereby being miscible) with PE. A great example of such a grafted copolymer, are maleic anhydride (MA) grafted copolymers^[79]. The MA (see Figure 2.5) provides the copolymer with an anhydride ring that will readily react with a hydroxide group of PET, for instance.

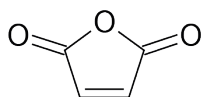


Figure 2.5: Structure of maleic anhydride.

The succinic ring will split up in a carboxyl group and ether group, connecting the former PET molecule to the formerly grafted MA. In Figure 2.6, a possible chemical compatibilization is displayed between PE-g-MA and the end of both a PET molecule and a PA6 molecule. In the case of PA6, the ring splits open as well, but close again afterwards, forming a double amide bond in the ring, with a bond to the PA6 chain instead of the otherwise present hydrogen. This is a condensation reaction.

It seems logical that the chemical attachment of the compatibilizer to one of the polymers, results in a vast increase in compatibilization efficiency. H. Zhang *et al.*^[80] carried out a comparative study in which both SEBS and SEBS grafted with MA (SEBS-g-MA) were used to compatibilise a blend of recycled PET (rPET) and LLDPE. Although both compounds did effectuate an increase in impact strength and elongation at break, this was done much more profoundly by the SEBS-g-MA.

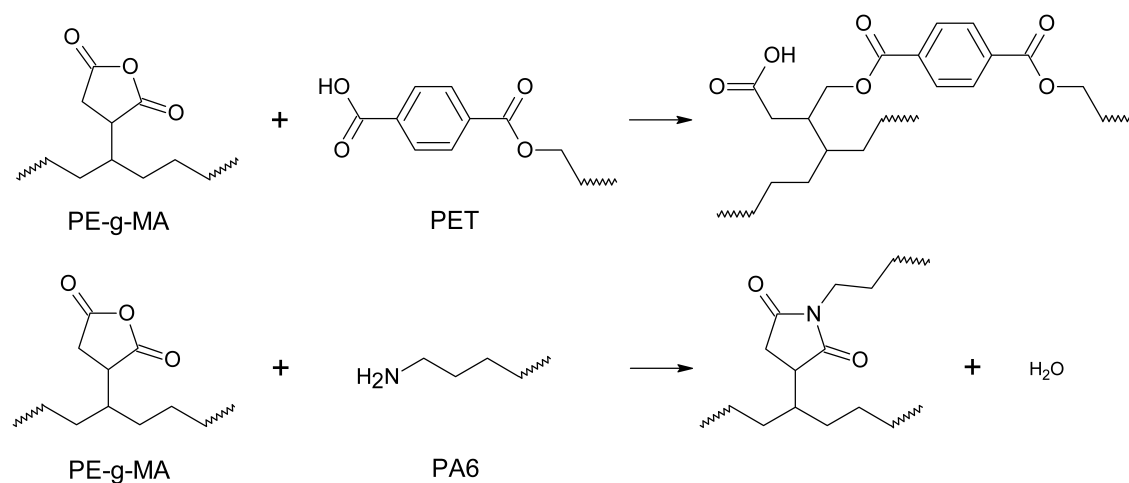


Figure 2.6: The esterification reaction between PE-g-MA and PET (top) and the condensation reaction between PE-g-MA and PA6 (bottom)^[69,81].

In Table 2.4, an overview is provided of studies done in literature using a grafted co-polymer for PE compatibilization.

It becomes clear that a larger variety exists regarding the copolymers that are used, compared to the block copolymers. However, the vast majority of polymers is grafted with MA. Furthermore, the polymer that is mostly blended with PE is again PET, although others are represented slightly more in this case.

The results shown by Table 2.4 are clearly in line with those in Table 2.3. Phase dispersion and interfacial adhesion were boosted in every experiment in which they were tested. The same goes for both impact strength and elongation at break; in no research did they show lower values after compatibilization. Similarly, tensile strength, Young's modulus, flexural strength and flexural modulus demonstrate inconsistencies throughout the experiments. Kasama *et al.*^[83] state that in general, when toughness is increased, YM declines. Indeed, the cases in Table 2.4 where both IS and YM were tested, the former went up at the cost of the latter. Mechanical properties can be negatively affected by the compatibilizer as well. H. Zhang *et al.*^[80] attribute the loss in TS, FS and FM to the rubbery nature of the SEBS copolymer. Lei *et al.*^[62] obtained an analogous result; the blend compatibilized with PE-g-MA exhibited improved TS, FS and FM, while the reaction with SEBS-g-MA yielded a decay in those same properties. Torres *et al.*^[88] suggest that because crystallinity is compromised to a certain degree upon compatibilization, rigidity (and thereby YM) of the material will decline.

A review done by Kumar *et al.*^[98] including various compatibilizers, among which E-GMA, EBAGMA and MA-grafted polymers, states that significant increases in impact toughness, elongation at break and chemical resistance are obtained after compatibilization, while tensile and flexural strength and moduli are generally slightly compromised. This confirms the findings in this section to a great extent.

The reader might be wondering how it is possible that a number of studies manage to

Ref.	Polymer blend	Copolymer	Results
[82]	HDPE/rPP	PE-g-MA	Increased TS, adhesion.
[58]	HDPE/rPET	PE-g-MA	Increased IS, compatibility. Decreased TS.
[83]	HDPE/rPET	PE-g-MA	Increased TS, EaB, IS, adhesion. Decreased YM.
[62]	HDPE/rPET	PE-g-MA	Increased TS, FS, FM, EaB.
		SEBS-g-MA	Increased EaB. Decreased TS, FS, FM.
[64]	rPE/rPET	SEBS-g-MA	Increased interfacial adhesion.
[84]	HDPE/PET	HDPE-g-GMA	Increased interfacial adhesion.
[65]	HDPE/PET	SEBS-g-MA	Increased EaB, IS, phase dispersion.
		HDPE-g-MA	Increased EaB, IS, phase dispersion.
[66]	HDPE/rPET	HDPE-g-MA	Increased dispersion.
		SEBS-g-MA	
		EPR-g-MA	
[85]	LDPE/rPET	SEBS-g-MA	Increased dispersion, EaB, IS. Decreased FS, FM, TS.
[86]	HDPE/PET	LLDPE-g-MA	Increased TS, EaB, dispersion.
[80]	LLDPE/rPET	SEBS-g-MA	Increased IS, EaB. Decreased TS, FS, FM.
[87]	LLDPE/HDPE/PET	PE-g-MA	Increased TS, YM, YS, EaB, IS, hardness.
[69]	LLDPE/PET	PE-g-MA	Increased EaB, IS. Decreased YM.
	rLLDPE/rPET		Increased IS. Decreased YM.
[70]	HDPE/rPET	PE-g-MA	Increased dispersion.
[88]	HDPE/PET	HDPE-g-GMA	Increased EaB, IS. Decreased YM, TS.
[89]	VLDPE/PET	SEBS-g-DEM	Increased dispersion.
[90]	HDPE/iPP	HDPE-g-iPP	Increased TS.
[91]	HDPE/PS	EE-g-MA	Increased EaB.
[92]	HDPE/rPP	PP-g-MA	Increased dispersion, TS, EaB, YM.
[75]	rPE/rPP	PP-g-MA	Increased IS, dispersion.
[93]	HDPE/PP	PP-g-MA	Increased dispersion, TS.
		HDPE-g-MA	
[94]	LDPE/PA6	PE-g-MA	Increased IS, TS, YS
[95]	LDPE/PA6	PE-g-AA	Increased interfacial adhesion
		SEBS-g-MA	
[96]	LDPE/PA6	LDPE-g-MA	Increased interfacial adhesion
		LDPE-g-AA	
		LDPE-g-BMI	
[97]	HDPE/PP	PE-g-MA	Increased TS, YM, toughness.

Table 2.4: Overview of experiments in literature using a reactive grafted copolymer for compatibilization.

ameliorate the properties of PE/PP blends through compatibilization with an MA-grafted additive. Since PP does not possess any functional groups and nor does PE, the MA cannot covalently bond like it can to PA6 or PET. Graziano *et al.*^[97] give the following explanation: the anhydride groups of the MA undergo π - π stacking with the chains of the PP, i.e. their respective π -orbitals that overlap and cause an attraction force.

2.2.4 Chain functionalisation

Another method for compatibilizing polyolefins is to functionalise their backbone. This is done through free radical reactions in the polymer melt^[79]. Usually by means of a peroxide initiator, a radical is formed, which attacks a labile carbon-hydrogen bond, extracting a hydrogen atom, thereby creating a radical site on the polymer chain (see Figure 2.7). Generally, only tertiary radicals are formed, since they are vastly more stable than secondary or primary radicals^[99]. This is confirmed by the difference in rate constant for the abstraction of a tertiary hydrogen, being about 4 and 20 times higher than those for secondary and primary hydrogens, respectively^[100].

The radical macromolecule can subsequently act as a compatibilizing agent, in several ways:

- It can cause (moderate) crosslinking with the backbone of a polymer with which it would otherwise be immiscible. These crosslinked complexes are formed at the interface and act as interfacial agents.
- Indirect crosslinking can take place, where a coupling agent forms the crosslink between the polymer chains at the radical sites.
- The radical sites can be used to attach a functional group, creating a grafted material *in situ*, after which a similar compatibilization occurs as described in Section 2.2.3.

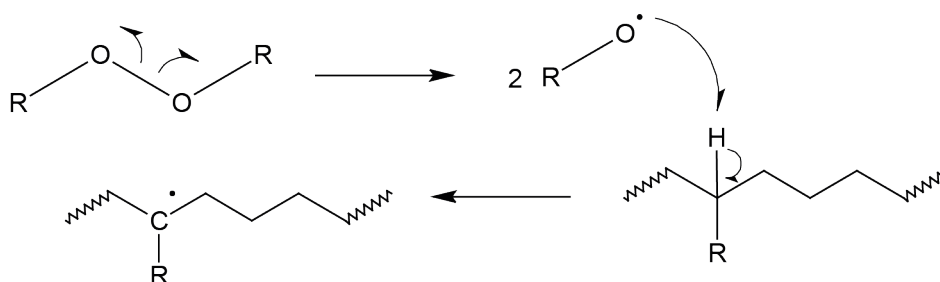


Figure 2.7: Scheme of a peroxide radical attacking a labile C–H bond.

For the latter of the aforementioned mechanisms, a distinction can be made between the one-step and two-step process^[79]. In the one-step process, functional group attachment and reactive blending with the other polymer happen in a single extrusion step. The two-step process is characterised by having two separate extrusion steps for the chain functionalisation and the blending afterwards. The method using two steps is used to a far greater extent.

In Figure 2.8, the chain functionalisation (or post-modification) of a tertiary polymer segment is schematically depicted. The three aforementioned functionalisation techniques can be distinguished here. After a radical site is created on the carbon backbone, it can be terminated by another backbone radical (denoted by the arrow with K_C). A crosslink has then arisen between the polymer chains. If a functional monomer is first attached, however, the created radical ($-M\cdot$) can terminate by reacting with another backbone radical site, functioning as indirect crosslink. The monomer extracting a

hydrogen from another carbon backbone, creating a functionalised polymer segment and a new radical site (denoted by the arrow with K_{Ht}).

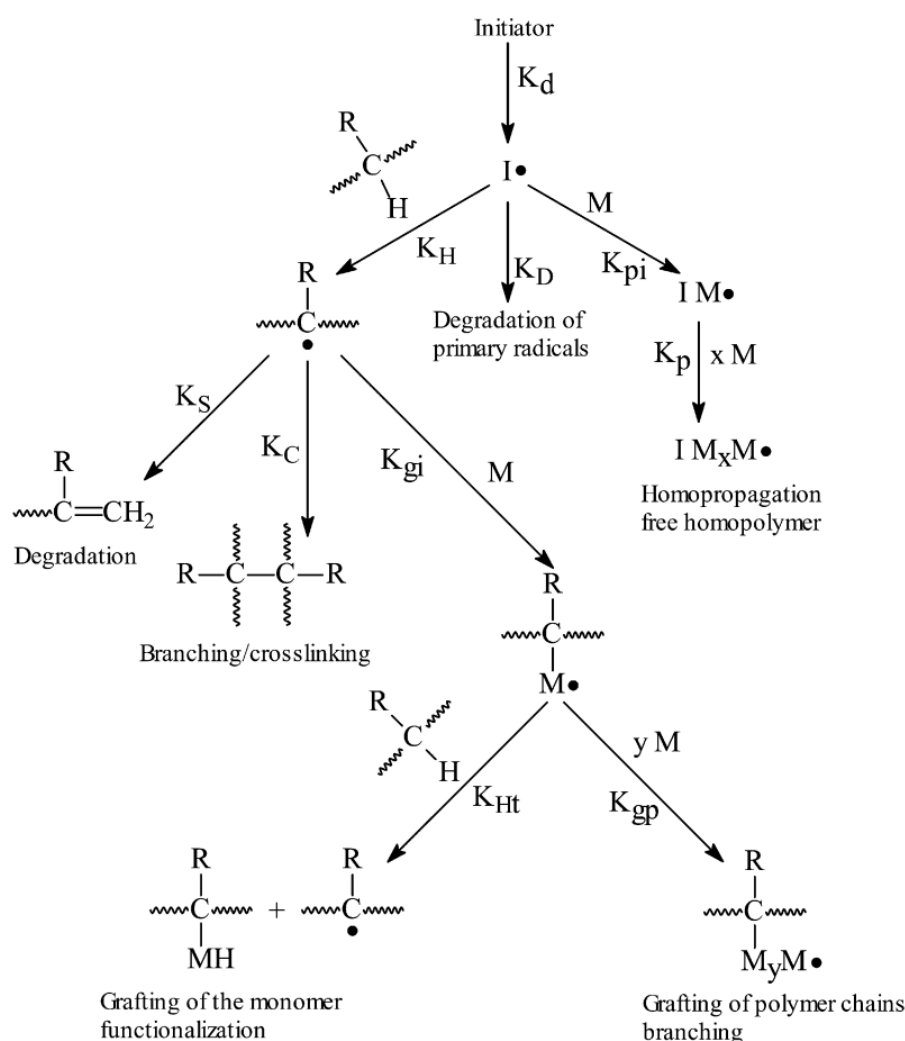


Figure 2.8: General scheme of radical post-modification of a polyolefin^[101].

An important setback that comes with this compatibilization approach is the fact that radicals are highly reactive and non-selective molecules, especially at elevated temperature. The PE chains that contain radical sites, readily undergo side reactions which affect blend properties such as molecular weight, polydispersity and chain linearity^[102]. Three side reactions are described in Figure 2.8: the monomer M can undergo homopolymerisation (K_p), the polymer backbone can show degradation (K_S) and a branch polymer can grow from the radical site (K_{gp}). Branching and degradation are the most notable.

The extent to which these side reactions occur, is heavily dependent on reaction parameters like residence time, temperature profile, reagent and additive nature and screw design and speed. Co-agents (or inhibitors) can be deployed to control the stability of the macroradicals, rendering them less reactive and pointing their reactivity towards the desired reaction.

Two kinds of co-agents are effectively used for this purpose^[102]:

- Unsaturated co-agents: compounds that quickly reacts with the macroradical, forming a new macroradical that is stabilised by resonance.
- Radical-mediating co-agents: compounds that impede the macroradical concentration by engaging in reversible radical reactions.

A widely used example of an unsaturated co-agent is styrene. It is particularly useful for functional group attachment. It attaches itself to the macroradical to generate a much more stable styryl radical^[103]. Monomers such as GMA and MA can then undergo a reaction with the styryl radical forming PE-g-(MA-co-Sty) grafted chains (see Figure 2.9). Undesired side reactions are hereby suppressed and the grafting ratio is greatly ameliorated. For the functionalisation of PE/PP blends, an unsaturated co-agent can be a huge aid in counteracting the degradation (chain scission) of PP^[104].

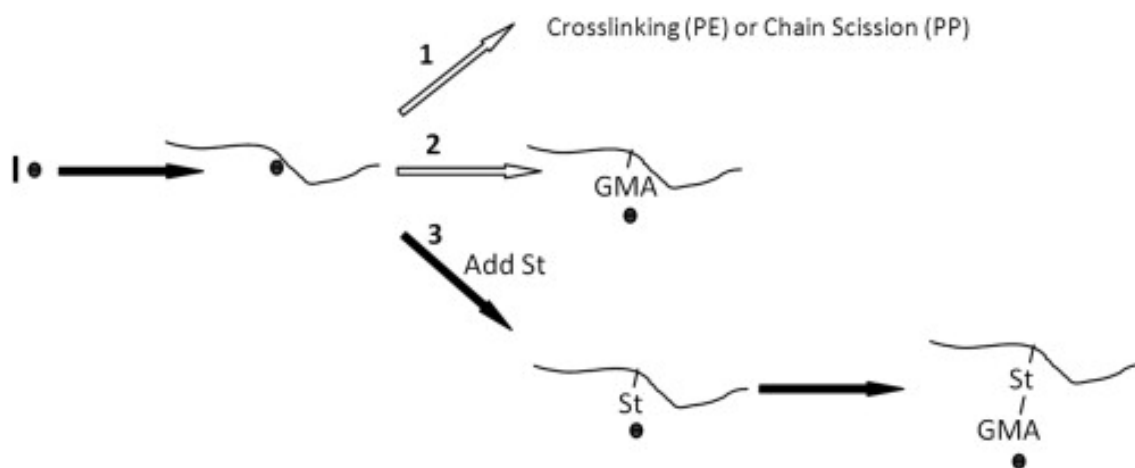


Figure 2.9: Mechanism of GMA/St (or MA/St) multi-monomer grafting on a polyolefin^[103].

A significant advantage, on the other hand, associated with *in-situ* chain functionalisation, is the fact that the additives are fairly basic chemicals, making them much less costly than pre-synthesised block or grafted copolymers. If side reactions can be held to a minimum during the functionalisation, this compatibilization approach becomes most interesting for economic reasons.

In Table 2.5 on page 24, a number of studies using chain functionalisation for the compatibilization of PE-containing blends are summarised. The different methods of chain functionalisation are shown in the fourth column. In case of indirect crosslinking, the coupling agent is stated and in case of functional group attachment, the grafted monomer is given. An inhibitor was used in some cases of chain crosslinking and in all cases of functional group attachment.

It becomes clear from Table 2.5 that different functionalisation methods are used for different kinds of blends. Chain crosslinking, whether it is direct or indirect, is used for compatibilization of PE with PP, while functional group attachment is used for blends of PE with PET and PA6. This is logical, since PP does not possess any groups that could

be targeted through functional group attachment of PE. PET and PA6 do, rendering them eligible for a reaction with a functionalised PE, which was discussed in Sections 2.2.2 and 2.2.3.

Various initiators were used in the studies. The common dicumyl peroxide (DCP) and benzoyl peroxide (BPO) were employed in the majority of cases, but a few studies chose the large peroxide molecules 2,5-dimethyl-2,5-di(*tert*-butylperoxy) hexane (DMDH) or *bis*[1-(*tert*-butylperoxy)-1-methylethyl]benzene (BTPB). Besides styrene, hydroquinone is a widely used inhibitor, due to the radical stability following from resonance. Divinylbenzene (DVB) is used for the same reason.

A number of conclusions can be drawn from the results. Firstly, functional group attachment increases the dispersion, which is in agreement with prior results of polymers having similar functional groups. Secondly, indirect crosslinking seems a viable compatibilization method, since it yields an improvement in a number of mechanical properties without compromising others. Lastly, chain crosslinking can result in a deteriorated material if no inhibitor is adopted. Jeong *et al.*^[105] crosslinked a PE/PP blend both with and without inhibitor, obtaining positive results from the former, yet negative results from the latter experiment. This is in agreement with the aforementioned theory.

Interestingly, even though grafted MA is used to a great extent for compatibilization, as was seen in Table 2.4, the cases of functional group attachment displayed in Table 2.5 only include this monomer once. This does not imply, though, that the grafting of MA onto PE is not studied². It is a rather well-known phenomenon, of which the knowledge remains mostly within the performing chemicals companies. Furthermore, the ceiling temperature for homopolymerisation, i.e. the temperature at which depropagation becomes favourable, is below 150°C. For methacrylate esters, such as GMA, this is around 200°C^[106]. Homopolymerisation as an undesired side reaction is therefore much less of an issue when the anhydride is employed. It was still found, however, that the addition of styrene as inhibitor led to a elimination of crosslinks for highly branched PE^[107].

In Table 2.6, an overview is provided with studies carrying out the grafting of MA onto PE through reactive extrusion. Similar organic peroxides as before are seen in this table, with the addition of another common initiator: di-*tert*-butyl peroxide (DBP). For both the initiator and the MA quantity, the optimal value is stated if a comparison was made in the concerning study. The initiator quantity lies roughly between 0 and 1 wt%, while the MA quantity lies between 3 and 5 wt%. A too high concentration of initiator creates an excessive amount of chain radicals that cannot be covered by the MA present, stimulating unwanted side reactions such as degradation and crosslinking (see Figure 2.8). A redundant amount of MA will favour crosslinking and might even cause

²Naturally, since pre-grafted PE-g-MA is commercially sold on the market, the grafting mechanisms must have been studied extensively.

phase separation^[108]. The temperature at which grafting is carried out varies substantially, in some cases being just around the melting temperature of PE, and in other cases being much higher. Furthermore, a very gradual temperature profile is opted for in some cases, while other studies maintain one temperature throughout.

2.2.5 Dual compatibilization

Two methods of compatibilization can be used simultaneously in order to achieve a larger effect. For instance, a physical blending agent can be combined with a reactive copolymer. Lei *et al.*^[58] combined SEBS with PE-g-MA and obtained results superior to those after using the compatibilizers separately. It seems, however, that dual compatibilization is not yet being explored on a large scale in literature.

When looking at all state-of-the art on reactive compatibilization that has been treated in this section, no studies are among them that produced film of the compatibilized blend. All mechanical properties stated in Table 2.3 through 2.5 are bulk properties, and no optical film properties were reported. This is logical if the target product for the recycled material is not film, but it is rarely mentioned what the target product will be. It would, for this study, have been more relevant to compare literature on film experiments, but they hardly seem to exist.

Ref.	Polymer blend	Initiator	Method	Coupling agent	Grafted monomer	Inhibitor	Results
[109]	LLDPE/PP	DCP	Indirect crosslinking	TAIC			Increased TS, IS.
[110]	LLDPE/PP	BPO	Chain crosslinking				Increased disp., EaB, TS, FS, IS.
[104]	LDPE/PP	DMDH	Chain crosslinking				Decreased EaB, IS.
			Indirect crosslinking	BMA			Increased dispersion, EaB, IS.
[105]	LLDPE/PP	DCP	Chain crosslinking			Hydroquinone	Decreased dispersion, EaB. Increased melt strength.
[111]	LDPE/iPP	DMDH	Chain crosslinking			Hydroquinone	Increased EaB, YM, TS.
[112]	rPE/rPP	BPO	Chain crosslinking				Increased IS.
						DVB	Increased IS, TS, EaB.
[113]	LDPE/PA6	BTPB	Functional group attachment		GMA	Styrene	Increased dispersion.
[84]	HDPE/rPET	BPO, DCP	Functional group attachment		GMA	Styrene	Increased dispersion.
[114]	HDPE/PP	DCP	Chain crosslinking				Increased interfacial adh., IS, EaB.
[115]	LDPE/PA6	BTPB	Functional group attachment		GMA	Styrene	Increased dispersion.
[116]	LDPE/PA6	BPO	Functional group attachment		MA		Increased dispersion, TS.
[117]	LDPE/PA6	BPO	Functional group attachment		MA		Increased dispersion, TS.

Table 2.5: Overview of experiments in literature using chain functionalisation for compatibilization.

Ref.	Polymer	Initiator used	(Optimal) initiator quantity	(Optimal) MA quantity	Temperature (profile)
[118]	HDPE	DBP	0.89 wt%	4 wt%	120-210 °C
[119]	HDPE	DMDH	0.94 wt%	4.7 wt%	200 °C
[120]	LDPE	DCP	0.1 wt%	3 wt%	150-160 °C
[121]	HDPE	DMDH			140-200 °C
[122]	HDPE	DCP	0.2 wt%	4 wt%	180-200 °C
	LDPE	DCP	0.2 wt%	3 wt%	140-200 °C
[123]	LDPE/PP	DCP	0.3 wt%		
[124]	LDPE	BPO	1 wt%	5 wt%	110-130 °C

Table 2.6: Overview of experiments in literature grafting MA onto PE using reactive extrusion.

2.3 Reactive extrusion

Reactive extrusion is a flexible alternative to conventional polymerisation or polymer processing. It relies on an extruder that is conventionally used for melting and homogenising of polymer feedstock, but is now used as a horizontal chemical reactor to facilitate the polymerisation reaction itself^[125]. Besides bulk polymerisation, many other types of reactions have shown great potential to take place by reactive extrusion, such as *in situ* polymerisation of a single phase or polymer, chemical modification or functionalisation of polymers and reactive blending or compatibilization of immiscible polymers^[126]. An important advantage thereby, is the fact that polymer melts of different viscosities can be processed together. Furthermore, extruders provide a large reactor surface, enabling sufficient heat removal³. The desired reactions are hugely simplified by not requiring reaction solvents or separate melting, mixing and degassing.

This study will treat a particular type of extruder, namely a twin-screw extruder (see Figure 2.10). After their first employment in the 1950s, they have gained immense popularity over single-screw extruders. They are eminently suitable for reactive extrusion, due to their ability to cover vast ranges of viscosity values and excellent mixing capabilities^[127]. Particularly co-rotating twin-screw extruders, which can be distinguished by their screws turning in the same fashion, show great mixing capability and generate larger shear forces than the counter-rotating equivalent. For PE and the other polymers concerned in this study, which show relatively high thermal stability, the co-rotating variant is very adequate^[128]. In Figure 2.10, a twin-screw extruder and its screws are displayed.

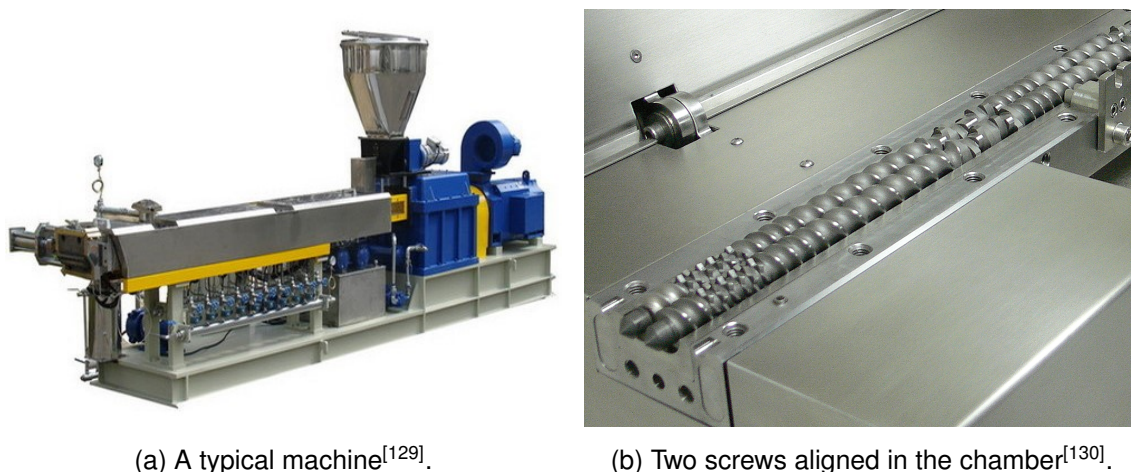


Figure 2.10: The twin-screw extruder.

³Polymer materials are known for their low thermal conductivity, rendering any polymerisation reactor prone to overheating.

2.3.1 General process

The twin-screw extrusion process is fairly constant for all applications. In Figure 2.11, the process is described schematically. The different zones within the extruder, which are arranged in series, all rely on a specific screw shape and dynamic. The different zones are also affected by one another, meaning that changes in one zone do have repercussions for the other zones. Additionally, most processes, such as dispersion, occur in multiple zones. The different zones can also be recognised in Figure 2.10b.

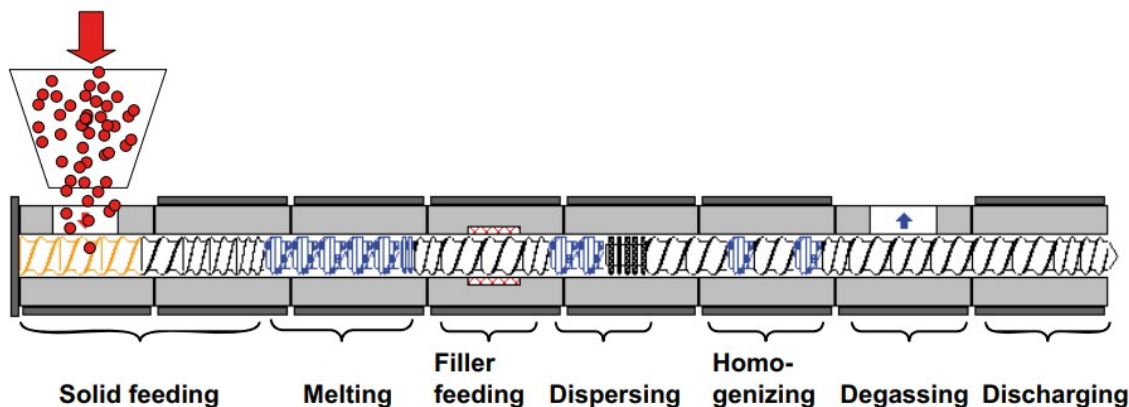


Figure 2.11: Schematic representation of processing zones of a twin-screw extruder^[131].

A distinction can be made between conveying and kneading screw segments^[132]. The conveying segments, coloured black in the scheme, are generally characterised by a larger channel depth, meaning no high pressures are present and the melt is merely heated up, mixed and transported. The kneading segments, displayed in blue, are used for exerting high pressures on the melt, for example to facilitate efficient melting. The shear force in these segments can be extremely high, resulting in changes in rheology and even material properties. Within conveying and kneading elements, many variations with respect to orientation and length-to-diameter ratio (L/D) exist. The screws are made up of different barrels, which can be combined in an endless number of ways, providing great flexibility as to which segments in the extruder serve which purpose^[133]. Different end products will need different screw designs. By means of barrel choice and location, each specific process is optimised in terms of melting, mixing, temperature and pressure regulation, etc. Furthermore, feeding locations can be created or omitted as a result of barrel order^[127].

At the beginning of the extruder, the feed inlet of the reaction is located. This is where polymer or monomer granules are added. The feed is subsequently heated up and put under high shear, converting it into a melt⁴. In the subsequent conveying section, a side feeder is usually located (downstream feeding). The L/D is usually fairly high at this point, and a vent is typically put above this section to allow air to escape which has entered upon side-feeding^[127]. (Low-viscosity) liquid additives should be added through downstream

⁴With the extruder size, the volume-to-surface ratio decreases rapidly, making surface heating elements less efficient. Therefore, energy transfer by mechanical force becomes dominant.

feeding or even in a kneading section (through a pressure valve), since they tend to affect pellets or powders that comprise the initial feed.

The second feeding location is followed by two mixing sections. Mixing knows two general disciplines: dispersive and distributive^[127]. Dispersive mixing, characterised by wide kneading sections, is used to break down particles into smaller units under high shear stress. Often times, the kneading blocks are followed by a restrictive screw, in order to increase filling extent as well as residence time (see Figure 2.11). Distributive mixing, characterised by several narrow kneading blocks, enables homogenisation and efficient particle distribution within the melt. It does not come as a surprise that the distributive mixing section follows the dispersive mixing section; particles have to be dispersed efficiently in order to be well-distributed.

After mixing, devolatilisation or degassing takes place, during which impurities are removed. These impurities involve moisture in initial feed, enclosed gases in side feeding or by-products from chemical reactions that have taken place^[127]. Even though impurities generally comprise less than 1%, it is a critical step in order to create an appreciable product. The screws in this section are designed in such a fashion, that sufficient residence time is achieved at relatively low degree of filling, to enable efficient volatile removal.

Following the degassing stage, the extrudate can be discharged. It is usually drawn through a die. As it exits the die, it is brought to a specific shape and quenched^[134]. The physical shape of the discharged product greatly varies with the final application. Films and sheets are quenched on rolls, blown film is quenched in a blown film tower by air, pipes and tubing are quenched in water tanks and various hollow shapes are blown quenched in moulds.

2.3.2 Chemical reactions in a twin-screw extruder

As mentioned before, twin-screw extruders are ideal to be employed as chemical reactors. Regardless of the viscosity of either reactants or products, chemical reactions can adequately take place in such a compounder, without the need for (often toxic) solvents^[135]. Various reaction types that a twin-screw extruder facilitates, are the following^[136]:

- Controlled depolymerisation or degradation
- Crosslinking
- Grafting
- Compatibilization
- Chain functionalisation
- Bulk polymerisation

For some of the reactions above, it has already been widely established that reactive extrusion is suitable. Others are still in the development phase and have yet to be applied on a large scale. A certain extent of overlap exists between the different list items, e.g.

grafting can be a form of chain functionalisation, which can be used for compatibilization.

The effectiveness of reactive compatibilization through reactive extrusion relies on the following process characteristics^[137]:

- High dispersion of one polymer in the other
- Sufficient amount of functional groups for interaction
- High reactivity of these functional groups with other phase
- Good stability of formed bonds during subsequent processing steps
- Lower reaction time than extruder residence time

A large part of the experiments that were highlighted Table 2.3 through 2.5, was conducted through reactive extrusion. The extruded samples could therefore immediately be used for characterisation and mechanical testing. The two-step method for chain functionalisation (Section 2.2.4) has been carried out in an extruder as well, although the internal mixer seems to be preferred for this process.

A large variation in reaction conditions existed among the studies that ran through reactive extrusion. Naturally, many of these conditions depend on the polymer blend that is compatibilized, as well as the method of compatibilization. Two parameters, however, do not vary but belong to the extruder set-up. These parameters are screw diameter and L/D. To see how they relate to the extruder that is used at SUEZ, an overview is given in Figure 2.12 and 2.13 of how many times different values occur in the consulted literature. In Appendix A, the specifications of the extruder present at CIRSEE are outlined.

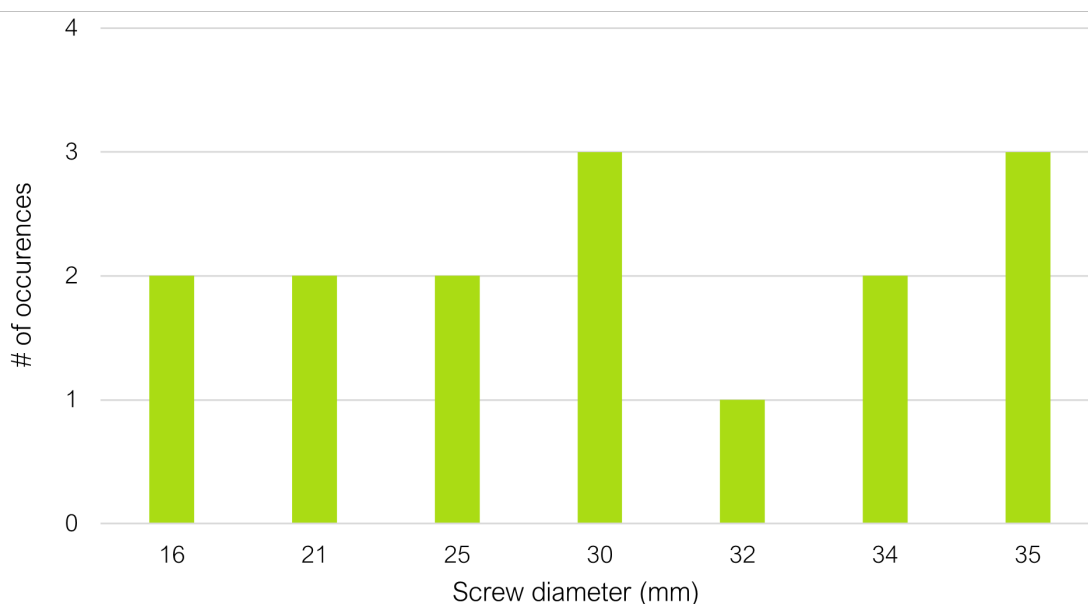


Figure 2.12: Number of occurrences for different screw diameters in experimental studies in Section 2.2.

A range of screw diameters is used to an equal extent in the studies. This range is quite broad; the thickest screw that was used has more than double the diameter of the thinnest screw. It is important to note that the extruders with a small screw diameter do not necessarily have high L/D values. The 26 mm screw diameter of the extruder at SUEZ falls nicely in-between the values found in literature.

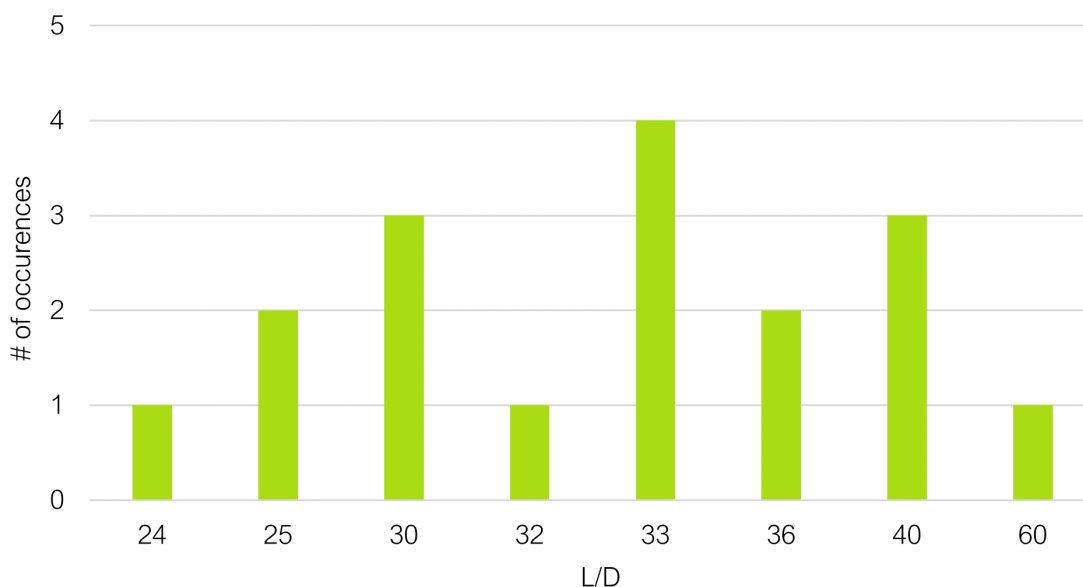


Figure 2.13: Number of occurrences for L/Ds in experimental studies in Section 2.2.

The extruders' L/D values too, vary a great deal throughout the studies. The largest value is again more than twice as big as the smallest one. It is often the sole extruder property that is stated in the experimental part of studies. This makes sense, since it provides more information than just the screw diameter and is relatable to other extruder set-ups. The L/D value of SUEZ' extruder, 44, is on the high side of the range. For polymers that are not excessively shear-sensitive, among which the polymers in this study, using a higher L/D value will ensure more efficient mixing and higher uniformity of the blend^[138].

As mentioned before, other reaction parameters depend on the type of polymer that is blended, the compatibilization method and sometimes simply the choice of the researcher. The temperature profile (which can be uniform or increasing from feed to die) that is appointed, is based on the polymer in the blend that has the highest melting temperature. However, subjecting the polymers to a too high temperature for too long will lead to uncontrolled degradation and deteriorate the polymer properties^[139].

PET has the highest melting point of the thermoplastics treated in this study, being 260°C. The studies that compatibilized PET through reactive extrusion therefore nearly exclusively attained 270°C as die temperature^[60–62,64,65,67,83]. Slightly lower temperatures of 265°C^[63] and 260°C^[69,85] are used as well. Interestingly, H. Zhang *et al.*^[80] adopt a die temperature of 240°C for rPET, which is under the melting point (they later determined this to be 253°C, through DSC). It is not stated why they opted for a lowered processing temperature, although it might be for anti-degrading purposes. No

issues were reported as a result of this lower processing temperature.

PA6, having a melting point around 223 °C, is mostly blended at 240 °C^[77,94,140] but also at 250 °C^[141]. Similarly, PP is treated with temperatures of 20–30 °C higher than its melting point (160 °C), at 180 °C^[75], 185 °C^[93] or 190 °C^[82,92].

The second reaction parameter that can be varied, which has a serious impact on the course of the reaction, is screw speed. Firstly, it is inversely proportional to the residence time of the reactants, meaning that a too high screw speed will not allow for the reaction to run until completion. Secondly, the screw creates very high local shear with the barrel wall that can cause, besides a local temperature increase, extra polymer degradation^[139]. This gives a second reason why the screw speed cannot be set too high. Contrarily, when the screw speed is not sufficient, the residence time becomes redundant, exposing the polymer melt to too high temperatures for an extended duration. This will cause degradation and branching of the polymers as well.

An immense variation is seen throughout the different studies when it comes to the screw speed. Chen *et al.*^[60] adopted a value as low as 30 revolutions per minute (rpm) to blend HDPE with PET using E-GMA. Morawiec *et al.*^[73] carried out the same blending reaction, opting for a screw speed of 88 rpm. Pietrasanta *et al.*^[68] performed it at 250 rpm, while Pawlak *et al.*^[65] even conducted the exact same experiment at 500 rpm. Naturally, different extruders were used in these studies, so merely the screw speed will not provide sufficient information for possible correlations. When an extruder's L/D is higher compared to that of another, the same screw speed will yield a higher residence time. Comparing residence time therefore seems to be a more logical option. However, this is hardly ever stated in literature, likely because it is not determined⁵. In the studies where residence time is given, any correlation seems impossible; a residence time of around 40 seconds is obtained for a screw speed of 500 rpm^[64,65], while 60 rpm yielded 63 seconds^[87] and 88 rpm resulted in a surprising 420 seconds^[73]. As many other factors can have an influence on the residence time, it would be interesting to compare the extruder specifications and reaction conditions in order to see which factors might cause such deviations in residence time, if they were universally available throughout the studies. All the same, it can be concluded that the process is highly empirical and that little theory and few correlations exist.

⁵The value for residence time is not constant for a certain screw speed, but depends highly on the viscosity and melt flow index (MFI) of the polymer. Therefore, for every experiment, it would in theory have to be calculated. At SUEZ too, such a correlation for different polymers does not exist.

2.3.3 Peroxide reaction kinetics

As concluded in the previous section, the residence time is a key factor in following the reaction that happens in the extruder. If a block copolymer or grafted polymer is used, though, the reaction is less complicated; the additive does not go through any transformation itself before reacting with the polymer blend. Furthermore, the reaction is not particularly time-sensitive; if the feed is blended well and kept at elevated temperature, the reaction will occur.

This is different in the case of chain functionalisation, i.e. where peroxides are involved. The peroxide needs to decompose (recall the first step in Figure 2.8) before the reaction can commence. This happens quickly, as radicals are known for their reactivity. This is followed by three more steps (creation of chain radical, grafting of monomer and reacting with polymer) before the compatibilization is achieved. This points to the fact that the reaction is substantially more time-sensitive; the conditions must prevent the peroxide from decomposing too quickly, while also allowing sufficient time for the subsequent reaction steps to take place. Herein the course of the decomposition reaction is the most important; without it, no eventual compatibilization will be possible.

Since the peroxide decomposition reaction solely depends on a single reactant, the reaction is said to be first-order and the reaction rate is therefore dependent on the peroxide concentration to the first order^[142]. This comes down to a simple multiplication:

$$rate = -\frac{\Delta[A]}{\Delta t} = k[A]^1 \quad (2.9)$$

Integrating this rate law on both sides and applying some Calculus yields the integrated rate law:

$$\ln \frac{[A]_t}{[A]_0} = -kt \quad (2.10)$$

Where $[A]_t$ is the concentration of A at time t, $[A]_0$ is the initial concentration, and k is the rate constant. This way, the half-life of a peroxide can be determined, i.e. the time at which the concentration has decreased to half of its initial value. In other words, $[A]_t = \frac{1}{2}[A]_0$, giving:

$$\ln \frac{1}{2} = -kt_{\frac{1}{2}} \Rightarrow t_{\frac{1}{2}} = \frac{\ln 2}{k} \quad (2.11)$$

The empirical value for k for organic peroxides is estimated by an Arrhenius-like equation^[143]:

$$k = A \exp\left(\frac{-E_a}{RT}\right) \quad (2.12)$$

where A is the so-called pre-exponential factor, E_a is the activation energy for dissociation, R is the gas constant and T is the temperature. A and E_a are constants, associated with a certain peroxide. Chemicals manufacturers have these values at hand, aiding them in offering fitting advice to customers. In Table 2.7 the values for the two aforementioned constants, as well as some commonly used half time temperatures are given for some typical organic peroxides used in reactive extrusion.

Peroxide	A (1/s)	E_a (J/mole)	Temperature for half time (°C)		
			0.1 hr	1 hr	10 hr
DBPB ⁶	7.65×10^{15}	1.53×10^5	156	134	114
DCP	9.24×10^{15}	1.53×10^5	154	132	112
BPO	6.94×10^{13}	1.22×10^5	113	91	71
DMDH	1.68×10^{16}	1.55×10^5	156	134	115

Table 2.7: Arrhenius constants and half-life temperatures of some typical organic peroxides^[144].

For the case of reactive extrusion, this provides insight into the percentage of peroxide that would be remaining at the extruder's die, when extruding at a specific temperature and using a specific residence time. When rewriting Equation 2.10, a relation is obtained to answer this problem:

$$\frac{[A]_t}{[A]_0} = e^{-k\tau} \quad (2.13)$$

where τ denotes the residence time in the extruder.

So for instance, if DBPB is taken for the reaction and the extruder runs at 200°C, k can be calculated by means of the table above and Equation 2.12:

$$k = 7.65 \times 10^{15} * \exp\left(\frac{-1.53 \times 10^5}{8.315 * 473}\right) = 0.1051 \text{ s}^{-1} \quad (2.14)$$

If the screw speed of the extruder is set so that the residence time equals one minute for the used polymer, the amount of peroxide that will be left at the die will be equal to:

$$\text{residual peroxide} = \exp(-0.1051 * 60) * 100\% = 0.183\% \quad (2.15)$$

This approach works the other way around, as well. If a certain peroxide residual is desired for an experiment, this will give a certain screw speed at which should be operated if the temperature of extrusion is not changed, or vice versa.

For this estimation to work, however, a precise estimation of the residence time during the experiment is required. As was touched upon at the end of Section 2.3.2, residence time is an indispensable piece of information when planning on carrying out a chemical reaction in an extruder. Of course, screw speed is the main factor influencing τ , but a universal trend would never be possible, since every extruder is different. Screw design will inherently affect τ as well, since different blocks are placed along the screw for different purposes, depending on the experiment. Furthermore, a factor that hugely impacts the residence time, is the actual material inside the extruder. Polymers can show a vast array of viscosities, which on themselves are dependent on temperature as well.

⁶It should be noted that di(*tert*-butylperoxyisopropyl)benzene (DBPB) is nearly identical to the previously seen BTPB, except that in this case the para variant of the molecule ring is mixed with the otherwise exclusively present meta variant.

For this reason, a correlation will need to be made for residence time as a function of screw speed, for the specific extrusion line setup at SUEZ. Additionally, a basic correlation will be established for throughput as a function of screw speed, since throughput is a universally utilised term on an industrial scale and provides useful info in this regard.

Materials and methods

This chapter covers the entirety of materials that were used for the study, as well as the experimental methods that were adopted to process and characterise them.

3.1 Materials

In Table 3.1, all materials are listed that were obtained from external suppliers. rLDPE was obtained from SUEZ' own recycling site.

Material	Commercial name	Supplier
<i>Virgin polymers</i>		
LDPE	Lupolen 2420D Lupolen 2420F	LyondellBasell
PA6	Ultramid® B36LN Ultramid® C40L	BASF
<i>Initiators</i>		
DCP		Sigma Aldrich
DBPB	Luperox® F	Arkema
DMDH	Luperox® 101 Luperox® 101XL45	
<i>Compatibilizing additives</i>		
MA		Sigma Aldrich
PE-g-MA (cont. 1.2 wt% MA ^[145])	Lucofin® 1492MHG	LUCOBIT AG

Table 3.1: All used materials coming from external suppliers.

With these materials, the different formulation are made. Firstly, a series of samples will be prepared based on virgin polymer blends. These samples will be the following:

- Lupolen 2420D (from hereon referred to as LDPE) without extrusion
- LDPE
- LDPE + 1, 5 and 10 wt% of PA6 (of which 50/50 w/w B36LN and C40L)
- LDPE + 1, 5 and 10 wt% of PA6 and 5 wt% of PE-g-MA
- LDPE + 1, 5 and 10 wt% of PA6 + 0.5 wt% of DBPB + 4 wt% of MA

Initially, DCP was supposed to be employed for the first trials of the reactive extrusion. However, shortly after ordering, it was brought to SUEZ' attention that this peroxide has recently been placed on the list of carcinogenic, mutagenic and reprotoxic (CMR) compounds. For this reason, the alternative (and non-CMR) two peroxides were ordered. DBPB will be used first, since this is a solid peroxide and well-known in the world of reactive extrusion, which became clear after consulting sessions with Arkema as well as Nouryon. The quantities of peroxide and MA are starting values based on literature (Table 2.6).

The two PA6 grades are used together in equal quantities to optimally simulate the PA6 material that is found in multilayer form in recycled streams. This was recommended by BASF. Since PA6 is mildly hydroscopic, it is dried before being used to remove present moisture. To this end, a FarragTech Card 10S dryer is used. The dryer is programmed to dry isothermically at 110 °C for four hours and subsequently go to a standby temperature of 80 °C.

The second series of samples will use recycled PE. The samples are constituted as follows:

- rLDPE without extrusion
- rLDPE
- rLDPE + 2.5 wt% of PE-g-MA
- rLDPE + 5 wt% of PE-g-MA
- rLDPE + 0.5 wt% of DBPB + 4 wt% of MA

3.2 Extrusion

The (reactive) extrusion was carried out in a LabTech Engineering LTE26-44 Standard co-rotating twin-screw extruder. It has a screw diameter of 26 mm and an L/D of 44. In Appendix B, the design of the screw is displayed, which was used in this study. The different modules can be distinguished along the screw length, each with their own purpose (conveying or kneading, see Section 2.3.1). In Figure 3.1, the extruder setup is displayed.

On the far right, the main feeder or hopper is seen. A mirror hanging above allows for visibility of the (amount of) feed inside. The feed is entered here. At the bottom of the hopper, a small screw is located, of which the speed can be adjusted for faster or slower feeding. From there, the polymer (mix) enters the barrel with the two screws, which is surrounded by the polished steel rectangular casing. Halfway down the length of the barrel, the side feeding system is located, standing in front of the extruder, which was not used in this study. Then, the degassing point can be observed at around 3/4th of the barrel length. Not visible in this picture, are the ten heating units located along the barrel. At the end, the replaceable filter can be seen with its small black handle, right before the (two-holed) die.

What follows is the water bath, through which the polymer strands are led. The strands go through a white brush, seen on the left side of the bath, as well as a suction system to remove most of the water. On the far left, the pelletizer is shown, starting with two black cylinders, providing the pulling force on the strands. A rotating knife cuts the strands into pellets against a stationary anvil.



Figure 3.1: The extrusion line used for compounding and pelletizing the samples.

Although the formulations for the different samples were varying, a general protocol was attained for all of them. The extruder is heated up, with the following temperature appointments: the three segments closest to the die are set to 240°C, and the other seven are set to 230°C. The water bath including suction and pelletizer are switched on. The screws are set to turn at a speed of 300 rpm, at which they will remain throughout the process. A scoop of LDPE, recycled or virgin depending on the formulation, is fed to the hopper with the hopper screw not turning. Then, the hopper screw speed is steadily increased, while monitoring the (rising) pressure in the barrel. When a speed of 15 rpm is reached, the screw is left as is. The polymer melt will start to come out of the extruder shortly after. The strands are not yet handled, but left to cool in the bath. Once the system seems to have stabilised, i.e. the pressure is constant and the polymer is fully melted and homogeneous upon exiting the die, the degassing is activated and the process of sample-making can begin.

Two kilograms of the to-be studied formulation is put together in a big bag, sealed and thoroughly tumble mixed. It is then fed to the hopper. Again, the system is left to stabilise, although this happens fairly quickly at this point. The polymer residue in the bath is cut off and thrown away. The newly ejected strands are pulled underneath the three rolls at the bottom of the bath, led through the brush and suction system and fed to the pelletizer. The process will keep itself running from here on, provided the entirety of the feed has

been supplied to the machine. The pressure in the barrel as well as the homogeneity of the strands are followed for the entire duration of the extrusion. When all polymer has been fed and the hopper runs empty, the strands will become increasingly thin and are cut off. The remaining polymer (mixture) in the barrel is left to exit the extruder and thrown away. The pellets are left to dry overnight, to remove any water present.

3.2.1 Extruder correlation curves

Since chemical reactions were going to be carried out in the extruder, it was deemed important to gain an understanding of the average time that the polymer spends in the extruder, or the residence time. Therefore, a series of extruder tests was carried out using virgin LDPE at varying screw speeds, to create a calibration curve for the residence time as well as the throughput. With these curves, the results of future experiments can then be linked to a residence time in the extruder. Naturally, the nature of this curve will slightly alter upon adding additives or polymer impurities, but it will still provide a good indication. The two different grades of LDPE that are processed at SUEZ, with a different MFI, will both be evaluated, since they will behave differently in the extruder.

The extruder is run with a certain screw speed and virgin LDPE is fed, until the process stabilises. Then, a colourant is added at the outlet of the feeder, so where the feed enters the extruder. This inlet can be recognised by its square, Plexiglas cover in Figure 3.1. The colourant consists of a few grains of heavily coloured PE. As soon as the colourant enters the extruder, the time measurement is started. The measurement is stopped as soon as the outgoing strands first start to fully adopt the colour (not yet when some first traces of colourant start to appear). Simultaneously, the throughput at the same screw speed is quantified. This is done by weighing the amount of plastic coming out of the extruder in one minute. This value in g/min can then easily be converted to a throughput in kg/h. The strands are cut at the moment of starting the time. When the time hits 60 seconds, the strands are cut again.

3.3 Grain characterisation

The following four characterisation techniques are (preferably) done with the sample in grain form.

3.3.1 Fourier-transform infrared spectroscopy (FTIR)

Fourier-transform infrared spectroscopy (FTIR) measurements were done using a Shimadzu IRTracer-100 with a GladiATR 10 as attenuated total reflection (ATR) accessory. Using an ATR accessory is ideal for the analysis of polymer pellets, since no additional sample preparation is needed. Furthermore, due to the soft nature of the pellets, they can be pushed well against the crystal, to ensure a maximum surface area while keeping the screw point from being damaged.

3.3.2 Melt flow index (MFI)

Although it did not play a large role in the compatibilization studies seen in Chapter 2, the MFI is of great importance to SUEZ. As their recycled LDPE is a commercial product for film production, they are held to certain product properties. It is therefore paramount to monitor the effect of the current study on the polymers' MFI. The MFI of the samples were analysed with an Instron CEAST MF20 melt flow tester. This was done in accordance with standard ISO 1133-1, procedure A (190 °C, 2.16 kg)^[146]. Four grams of material were taken for every measurement. The apparatus is set to cut every 120 seconds, so an MFI value for g/10 min can be taken after collecting five pieces that are cut. Three separate measurements are done on every sample.

3.3.3 Differential scanning calorimetry (DSC)

For the DSC analysis a Netzsch DSC F3 Maia, equipped with an autosampler, was employed. The granules are cut in half for the measurements, to obtain samples of around 10 mg. The used program depends on the type of sample that is analysed. For all PE samples, the program includes a heating from 25 °C to 190 °C with 10 °C/min, cooling with the same speed, and heating again from 20 °C to 190 °C with 10 °C/min. For PA6 (containing) samples, the procedure is the same, except for the fact that the two heating curves go up to 300 °C.

3.3.4 Scanning electron microscopy (SEM)

A JEOL JSM-IT100 is used for the SEM measurements of the samples. In order to gain the best understanding of the pellets' morphology, the fracture surface made by the pelletizer will be investigated. To this end, a small portion of the cylindrical shape is sliced off, providing the surface that can be inspected. Prior to the analysis, the pellets are carbon coated in upright position, so that the newly created fracture surface will be facing upwards and receive the coating. The thickness of the coating was chosen to be 10 µm. For the measurement, each pellets is fixed on the mount in this same position, using a carbon patch. Subsequently, a strip of copper tape is placed onto a small part of the fracture surface, leading to the mount (see Figure 3.2).

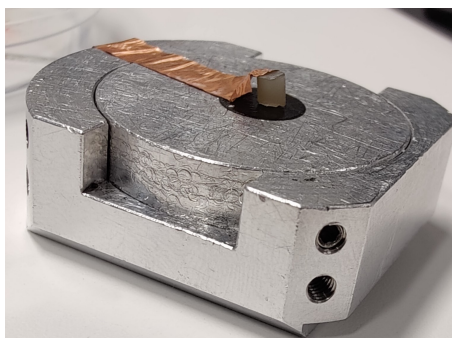


Figure 3.2: The mount used for SEM analysis, with a pellet fixed on it.

This way, the charge will not accumulate on the polymer's surface and the measurement should be conductible in full vacuum mode instead of low vacuum mode. An energy of

10 kV will be used. Low vacuum mode adopts back-scattered electrons (BSE), while full vacuum mode sends secondary electrons (SE) towards the sample.

3.4 Extrusion blowing

The extruded grains were processed into a film material by extrusion blowing. To this end, a Eur.Ex.Ma MiniBlown D20 blown film extrusion line was used. In Figure 3.3, its setup is displayed.

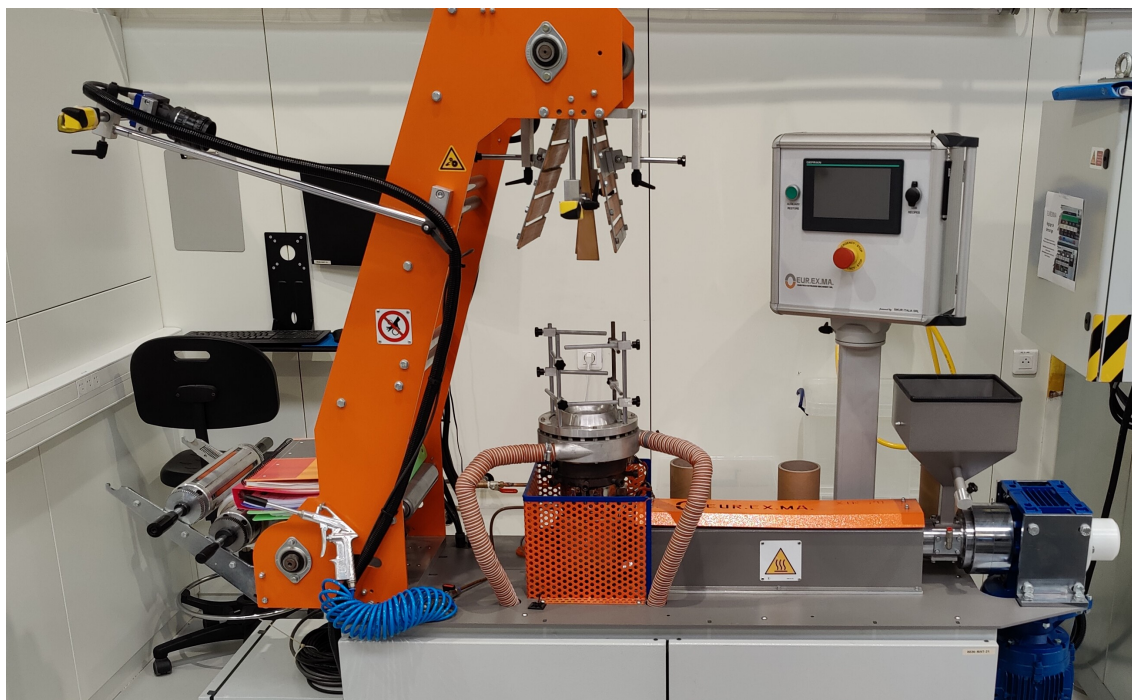


Figure 3.3: The extrusion blowing line used for transforming the samples into film.

Starting on the far right, a hopper can be identified, used to feed the polymer. The material then passes through a small, single-screw extruder. It is important to note that this screw merely serves as melting zone for the polymer and does not contain any kneading elements to exert shear force. The extruder is set at 200 °C. Although this is beneath the melting temperature of PA6, BASF advised that for a content of no higher than 10 wt%, extruding between 190 °C and 220 °C is acceptable. The melt is not pushed through a circular, but through a ring-shaped die, giving it a tube shape. At the same time, air is blown through the inside of this ring, pushing the sides of the tube further apart, and air is blown at the outside of the ring, to cool down the melt. This stretching out of the melt gives a thin-layered, cylindrical bubble. At the top of the picture, a reversed V-shape folds the cylindrical film into a flat state. It is subsequently guided downwards between the orange plates, where it is continuously inspected by a camera (seen on the top left). On the bottom left, the rolls are seen around which the film is wound.

The dimensions of the produced film are closely monitored. The width is measured with a ruler, after which the diameter of the bubble can be adjusted with the air inlet as well as the Teflon sticks that are laterally positioned around (see Figure 3.3). Two different directions are defined within the film; the machine direction (MD) and transverse direction (TD) (see Figure 3.4). The MD is parallel to the extruder and its die, while the TD is taken perpendicular to this direction. Since the mechanical properties of the film are not uniform in different directions, this will come into play for the tensile tests.

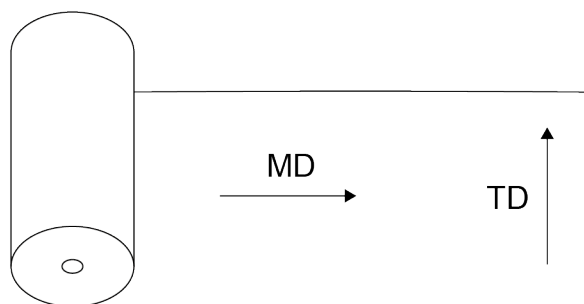


Figure 3.4: A schematic of a roll of film with MD and TD illustrated.

3.5 Film characterisation

The characterisation methods below were carried out on samples in film form.

3.5.1 Gel and black spots

The camera pointed at the film during extrusion blowing, which was highlighted in Section 3.4, serves as a means to quantify the number and size of gel spots and black spots that the film exhibits. The camera is directly transmitting a scan to the software connected to it, which does the counting and gives a number per m^2 . Three measurements are done on 8 m^2 , of which the average is taken.

3.5.2 Colorimetry

A Konica Minolta CM-5 spectrophotometer is used to quantify the whiteness (L^*) value, haze and yellowness index (YI) of the produced film. A strip of around 5 centimetres thick is cut from the film, after which it is cut open on one of the sides. On four different spots along the (now doubled) width of the film, a measurement is conducted. All aforementioned parameters are taken simultaneously and averaged afterwards.

3.5.3 Tensile tests

The tensile strength and elongation at break of the films is measured with an MTS Insight electromechanical testing system, using a 100 N load cell and mounted grips that are specialised for film tests. Out of a blown film 32 samples are cut, of which 16 in MD and sixteen in TD. The dimensions of the specimen, as well as the testing procedure, are in accordance with the ISO 527-3 standard^[147].

Results and discussion

First, the results of all experiments are treated individually. Subsequently, a synthesis of the results will be conducted, linking the outcome of the different analyses on a higher level.

4.1 Extruder correlation curves

The throughput out of the extruder as well as the residence time inside the extruder for Lupolen 2420D were determined at six different screw speeds. In Figure 4.1, the correlation curve for the throughput as a function of screw speed is shown.

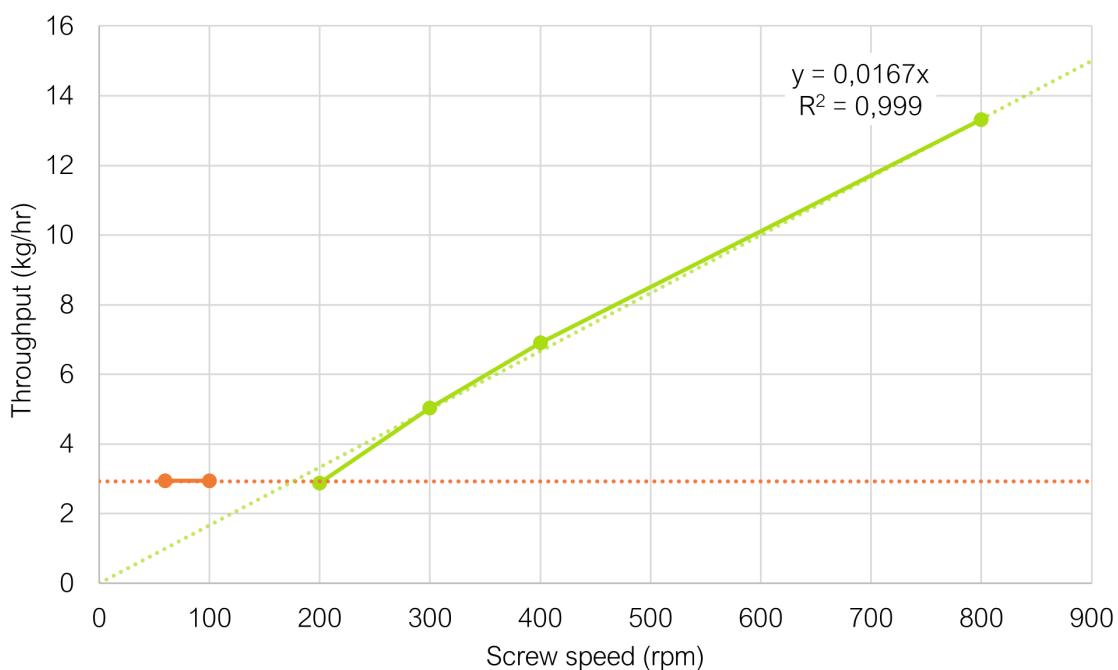


Figure 4.1: Correlation curve for throughput as a function of screw speed.

The curve takes on a peculiar shape, which has been emphasised by splitting up the two first points from the other four. The first three screw speeds yield the same throughput; only at the fourth speed (300 rpm) an increase in throughput is seen. From the third

point to the sixth point, a very neat linear relation arises, which can be described with great precision using a linear correlation curve going through the origin. At lower screw speeds (below ~175 rpm), the throughput seems to become independent of the screw speed and stay constant. Since the feed rate was constant for these three points (the extrusion was not manageable at lower feed rates), it becomes clear that the throughput is a function of feed rate at lower screw speeds. The obtained linear relation is confirmed by literature^[148].

The correlation of residence time measurements as a function of screw speed can be seen in Figure 4.2.

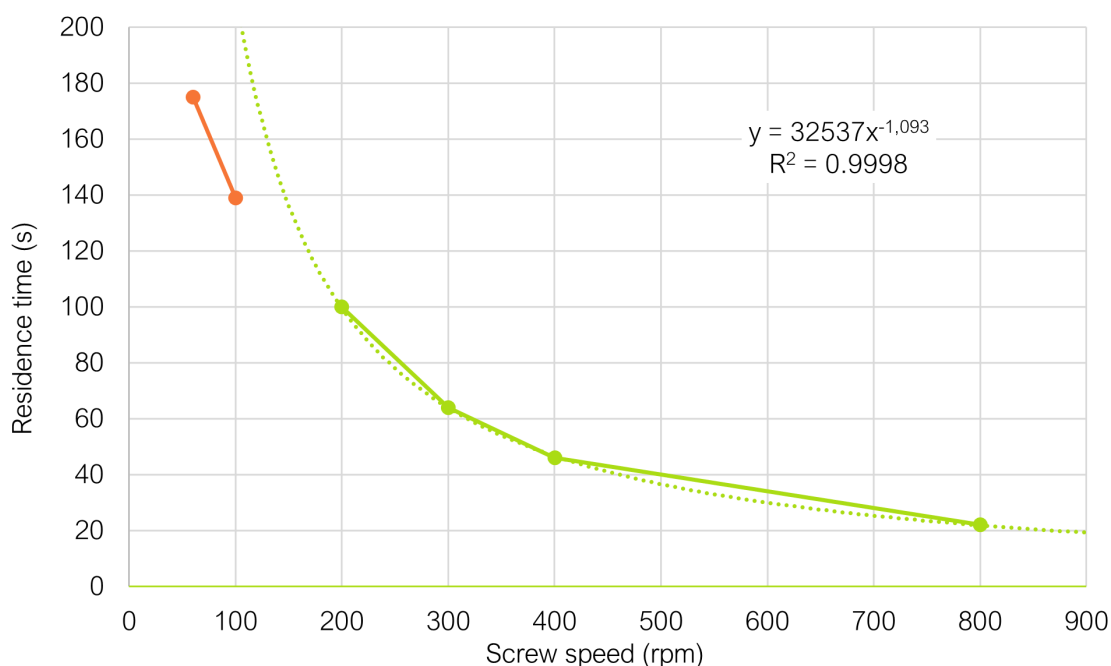


Figure 4.2: Correlation curve for residence time as a function of screw speed.

This time, an entirely different relation is seen, namely that of a power law. Based on the result of the throughput correlation, the first two points (marked in orange) were deemed not representative of the extruder's behaviour. Therefore, they were not included in the derivation of the correlation curve in this case, either. Again, the correlation curve represents the relation between the points with great precision, when looking at the R^2 value. The proposed trend for residence time is again confirmed by literature^[149]. Looking back at Section 2.3.3, the extruder conditions, i.e. temperature and screw speed can now directly be used in the calculations for the rate constant of a peroxide, and thereby an estimation can be made of its course of decomposition along the extruder.

Both variables were also measured for Lupolen 2420F, having a higher MFI value (0.75 instead of 0.25 g/10 min^[150,151]). This was done at 300 rpm. A residence time of 59 seconds was found, together with a throughput of 5.40 kg/hr. This outcome is in

agreement with what could be expected when subjecting a polymer of higher MFI to the same process: the residence time drops and the throughput rises (64 seconds and 5.04 kg/hr before, respectively). Both of these phenomena can be attributed to the higher flow of the melt.

4.2 Pellet and film samples

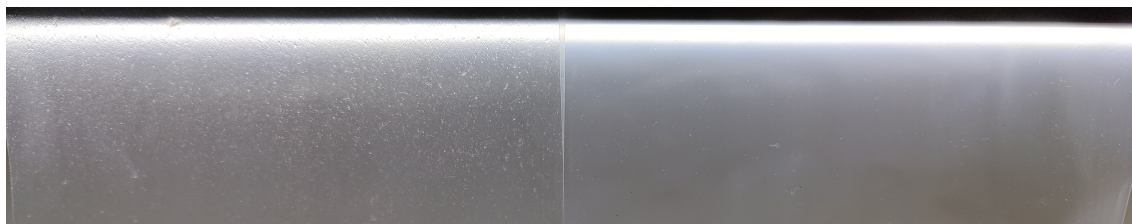
For illustrative purposes, the pellets as well as the films of some samples are given in this section. First, in Figure 4.3 the pellets can be observed of virgin LDPE, LDPE + 10 wt% PA6, LDPE + 10 wt% PA6 + PE-g-MA and recycled PE.



Figure 4.3: The obtained pellets after extrusion of, from left to right, virgin LDPE, LDPE + 10 wt% PA6, LDPE + 10 wt% PA6 + PE-g-MA and rLDPE.

The LDPE completely loses its "glassy" and grey look after the addition of PA6 and the pellets become more yellow. When extruded with the additive, the yellowness decreases and the pellet becomes whiter yet still rich in colour. Finally, the contrast between rLDPE and vLDPE becomes awfully clear when looking at the pellets on the far right. The pellets obtained from extruding rLDPE with PE-g-MA did not show a change in colour.

Then, in Figure 4.4, film samples are shown of LDPE + 10 wt% PA6 before and after compatibilizing with PE-g-MA, as well as samples of rLDPE before and after compatibilization.



(a) LDPE + 10 wt% PA6 before (left) and after (right) compatibilizing with PE-g-MA.



(b) rLDPE before (left) and after (right) compatibilizing with PE-g-MA.

Figure 4.4: The obtained film after extrusion blowing the extruded pellets.

For both cases, a definite transformation is observable upon introducing the additive. A more detailed analysis of the spots that are seen on the film, is given in Section 4.7. It should be noted that the films in Figure 4.4b have a much more brown colour than those in Figure 4.4a (as could be expected from the colour exhibited by the pellets), which does not immediately become clear from the pictures.

4.3 FTIR

4.3.1 Additive calibration curves

A series of samples of additive composition were prepared in the extruder, in order to create a correlation between the amount of additive present and the intensity of the peak in the FTIR spectrum. Virgin LDPE was extruded with MA, subsequently with PE-g-MA, and finally with a combination of the two.

The combined spectra of all three cases, together with their calibration curves and the associated equation, are given in Figure 4.5 through 4.8. For each correlation, the intensity of the concerning peak was compared to a known peak following from LDPE. Since FTIR spectra can go up or down in intensity as a whole, depending on the sample conditions, the value of a peak used to correlate a result will need to be standardised. This can be done by taking the ratio of two peaks. This ratio value will remain more or less constant for different spectra of the same sample, even if general intensity throughout some of them is lacking. Additionally, the peak that is used to generate the ratio value, is chosen at a wavelength not too far from the peak in question. The reason for this, is the fact that FTIR spectra can get asymmetrically more or less intense depending on the (plastic) material, meaning that a peak far away can yield a distorted result.

For each case, a peak was chosen that is prevalent in that specific spectrum, but not in the other. Otherwise, the different concentrations could never be differentiated in an eventual analysis with unknown quantities.

The first curve was made using MA. The superposed spectra and associated correlation can be found in Figure 4.5. One of the peaks caused by the MA present in the LDPE, is located at 1705 cm^{-1} . It does not immediately become clear which exact bond type is causing the peak. It is most likely a C=O stretching bond, caused by the succinic ring^[152]. However, the carboxylic acid group of maleic acid, which is a product of the hydrolysis of MA, shows a peak in a similar area^[153]. This means that water would have to be abundantly available, though, which is unlikely inside the extruder.

Although it is not the largest peak, it seems to be the only one that gradually increases its intensity as the quantity of added additive goes up. The added quantities of MA were 0.5, 1, 2.5, 4 and 5 wt%. In the table on the bottom right of the figure, the peak is shown with which the ratios were made. This is a constant peak at 1462 cm^{-1} , originating from LDPE and will be discussed later to more detail. The obtained correlation shows a very neat curve, with a great R^2 value of 0.933.

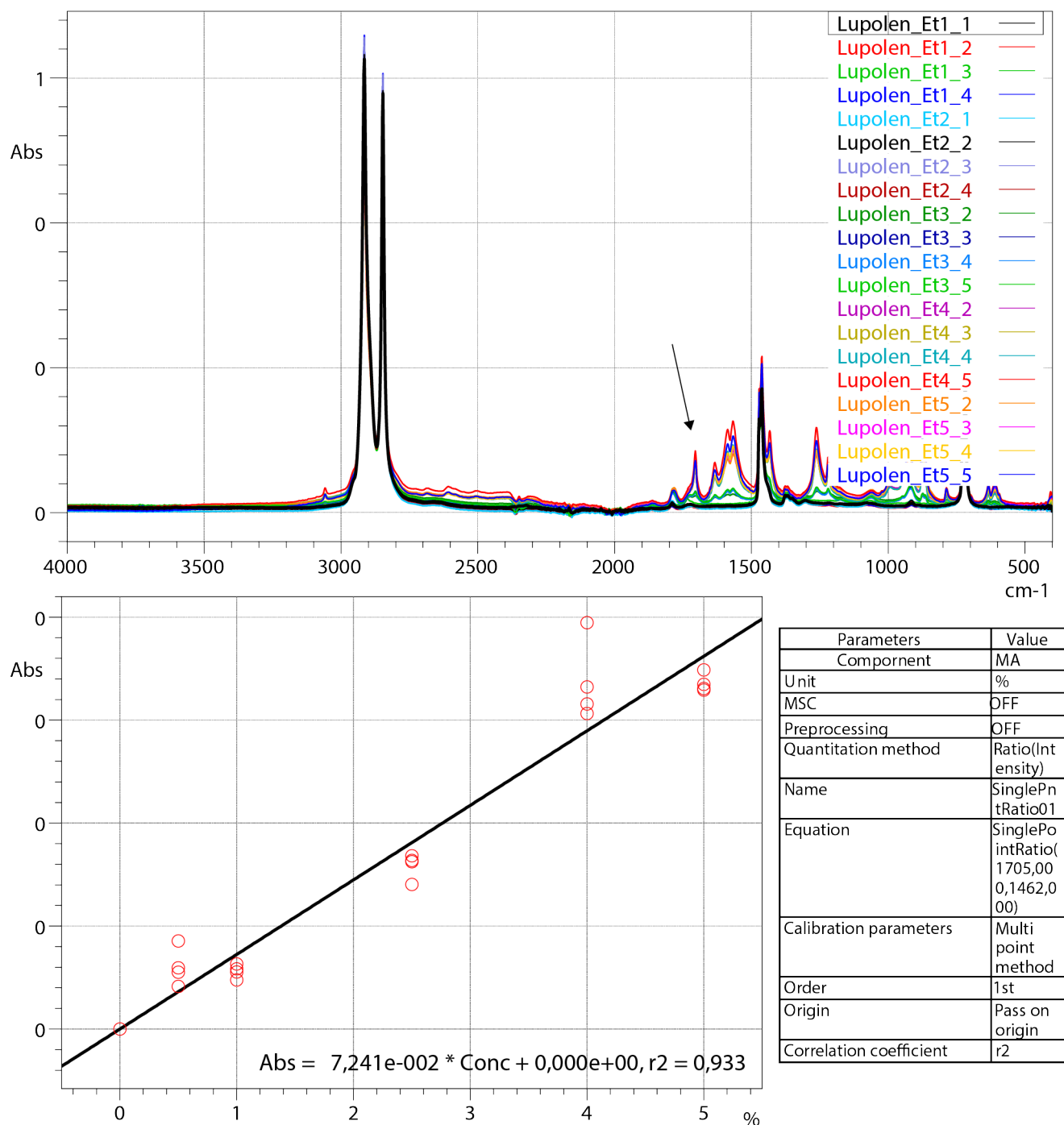


Figure 4.5: Correlation curve (bottom) for 1705 cm⁻¹ peak intensity for various concentrations of MA, obtained from series of sample spectra (top).

Subsequently, a curve was made using only PE-g-MA. Figure 4.6 reveals its spectrum and correlation curve. The added quantities of PE-g-MA were 16.67, 41.67, 83.33 and 100 wt% (recall that of these percentages, only 1.2 wt% is actual grafted MA). The peak at 1736 cm⁻¹ showed the best gradual augmentation, which was used for the ratio. The linear curve again shows a good correlation, with a very appreciable R² value of 0.901.

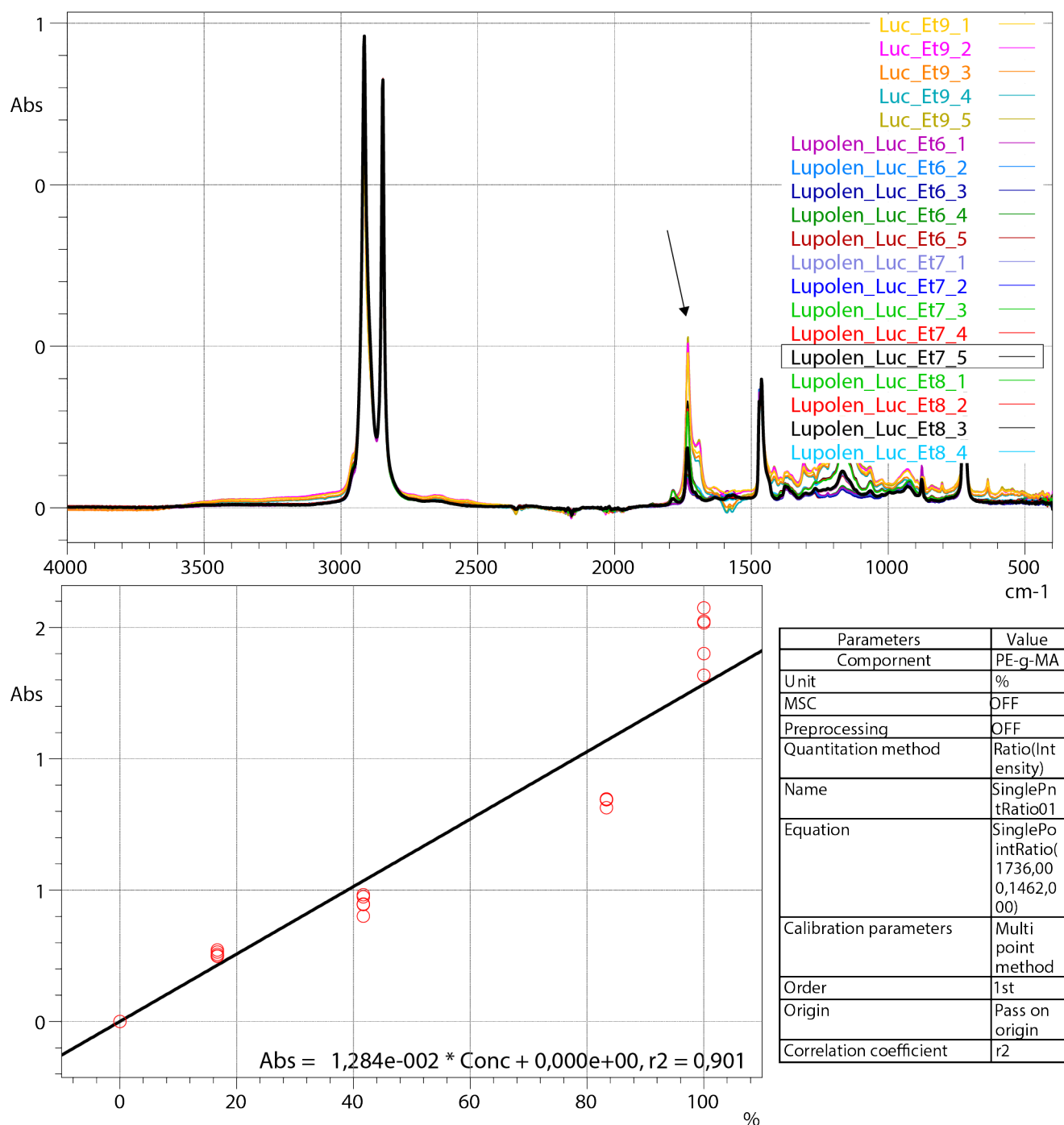


Figure 4.6: Correlation curve (bottom) for 1736 cm⁻¹ peak intensity for various concentrations of PE-g-MA, obtained from series of sample spectra (top).

Figure 4.7 shows the first of two curves where both additives were combined in the extruder, both with identical quantities to before. The same wavenumber as before, 1705 cm⁻¹, was used for the ratio of intensities. This time however, the curve does not show a great result. The peak at 1705 cm⁻¹ has disappeared in the spectra. It is unclear how the combination of the two additives can have caused this specific peak to vanish, but it is clear that these conditions cannot be used to establish a proper correlation.

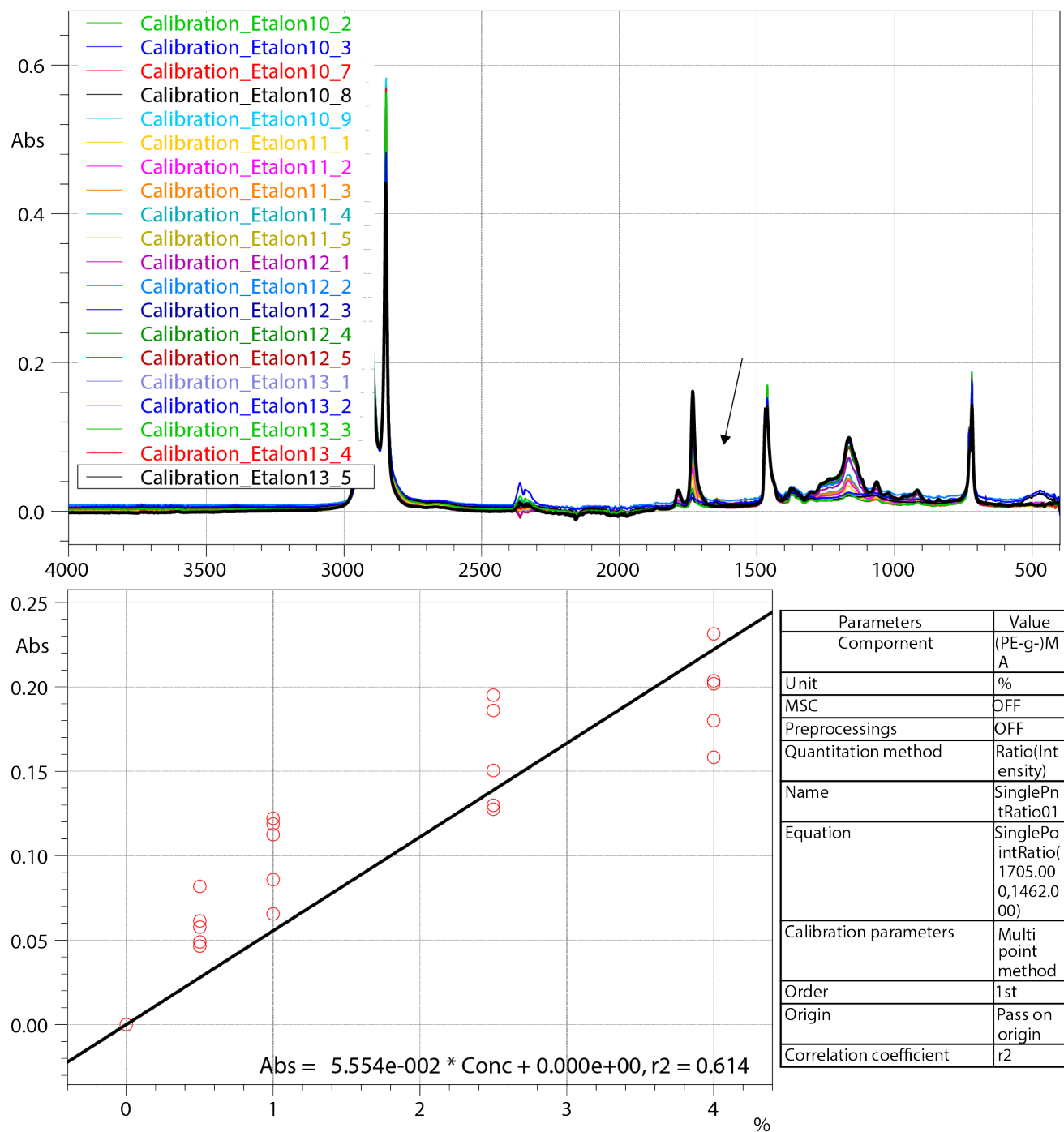


Figure 4.7: Correlation curve (bottom) for 1705 cm⁻¹ peak intensity for various concentrations of MA mixed with PE-g-MA, obtained from series of sample spectra (top).

Lastly, in Figure 4.8, the intensity at 1736 cm⁻¹ is taken for the correlation, for the same group of superposed spectra. Contrarily to the peak at 1705 cm⁻¹, this peak shows a nicely increasing intensity and shows to be legitimate basis for a correlation, with a very high R² value of 0.940.

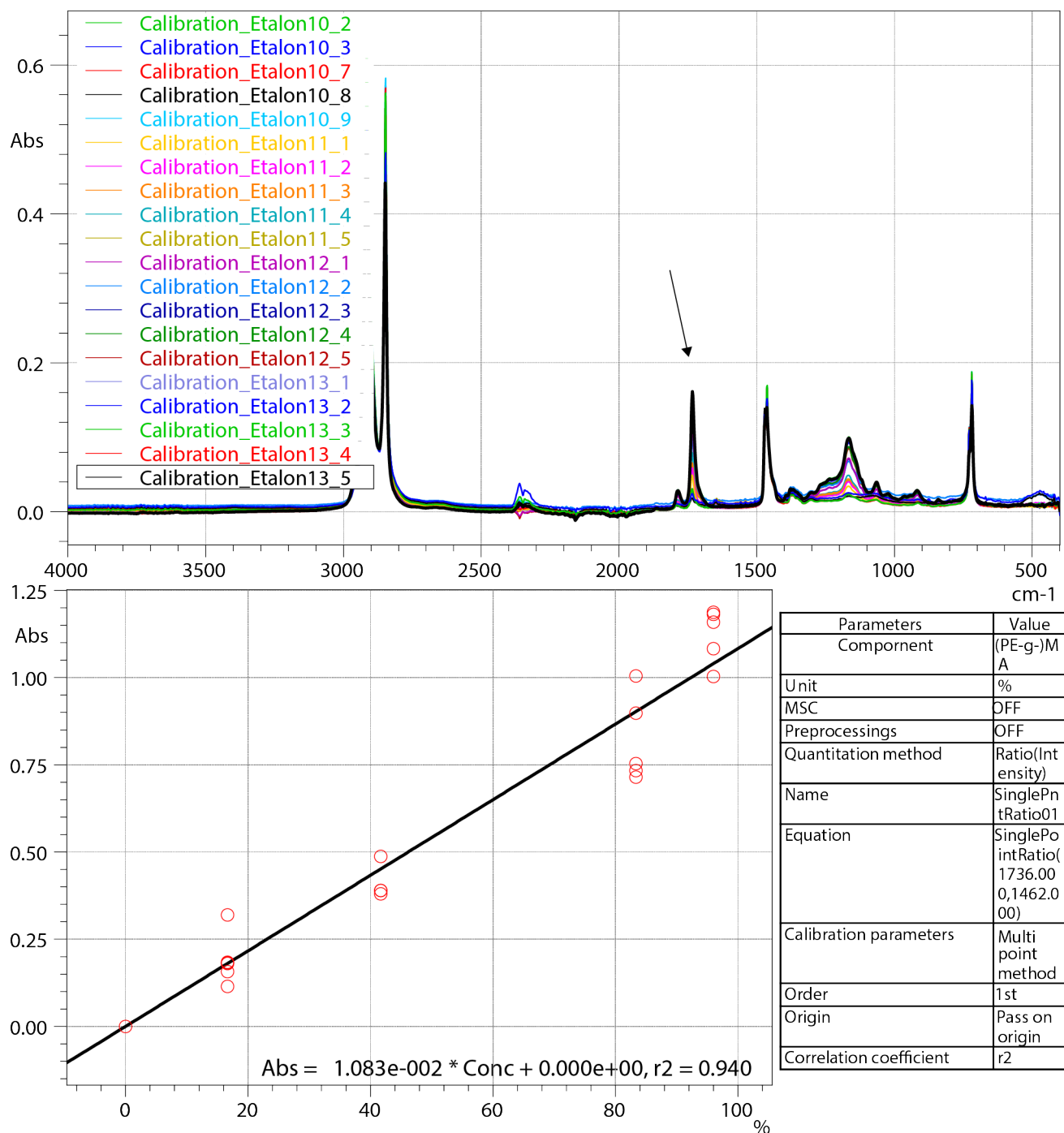


Figure 4.8: Correlation curve (bottom) for 1736 cm⁻¹ peak intensity for various concentrations of MA mixed with PE-g-MA, obtained from series of sample spectra (top).

The fact that an appreciable correlation curve can be established for MA in its grafted form but not in its free form, still provides a possibility to assess the degree of grafting for future experiments. If the amount of grafted MA can be estimated, this will automatically give an idea how much unreacted MA would be left. So even if the result of the experiment is not entirely satisfactory, it can might prove to be very useful.

4.3.2 Sample results

The different FTIR spectra of all samples will be covered in this section.

In Figure 4.9, the spectrum is shown of virgin LDPE, before extrusion. The fact that PE has the simplest of molecular formula of all polymers, is confirmed by looking at this spectrum, with only a few very distinctive peaks for LDPE. The peaks at 2914 and 2848 cm^{-1} stem from asymmetric and symmetric C–H stretching, respectively. The peaks at 1471, 1463 and 1377 cm^{-1} come from (umbrella) bending, and the peaks at 729 and 717 cm^{-1} are caused by split CH_2 rocking.

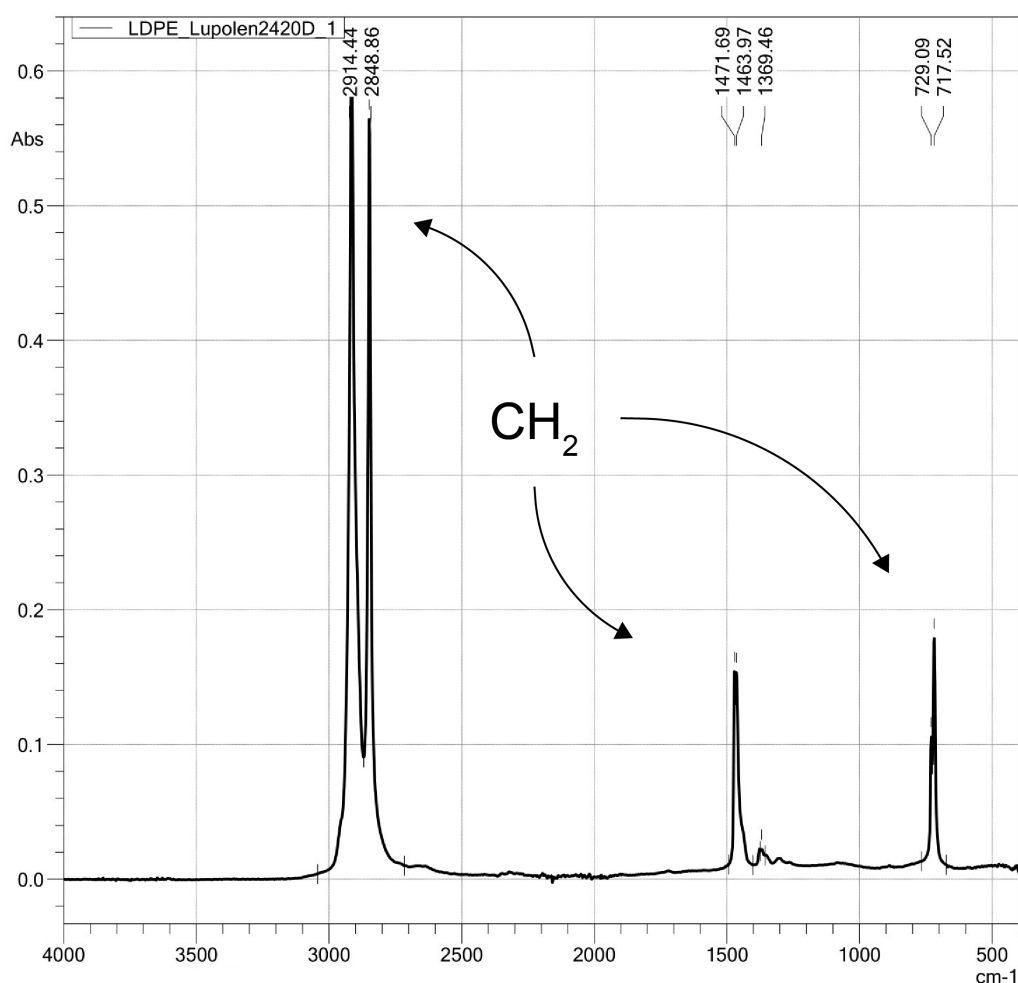


Figure 4.9: FTIR spectrum of virgin, untreated LDPE.

A spectrum of LDPE after one extrusion step is displayed in Figure 4.10. All peaks seem to correspond, except for a peak at 1647 cm^{-1} . This peak could in theory come from a C=C stretching bond, due to degradation. This is rather unlikely, however, since one extrusion step should not cause a peak with such intensity. Furthermore, minor peaks can be noticed at wavenumbers around 3200 and 3400 cm^{-1} , indicating an amide group. Since Lupolen 2420D was designed for film manufacturing, it is most likely lubricated, causing the appearance of these peaks. The fact that these peaks were not present in Figure 4.9, could be explained by the extrusion step, homogenising the polymer and causing the peaks to appear.

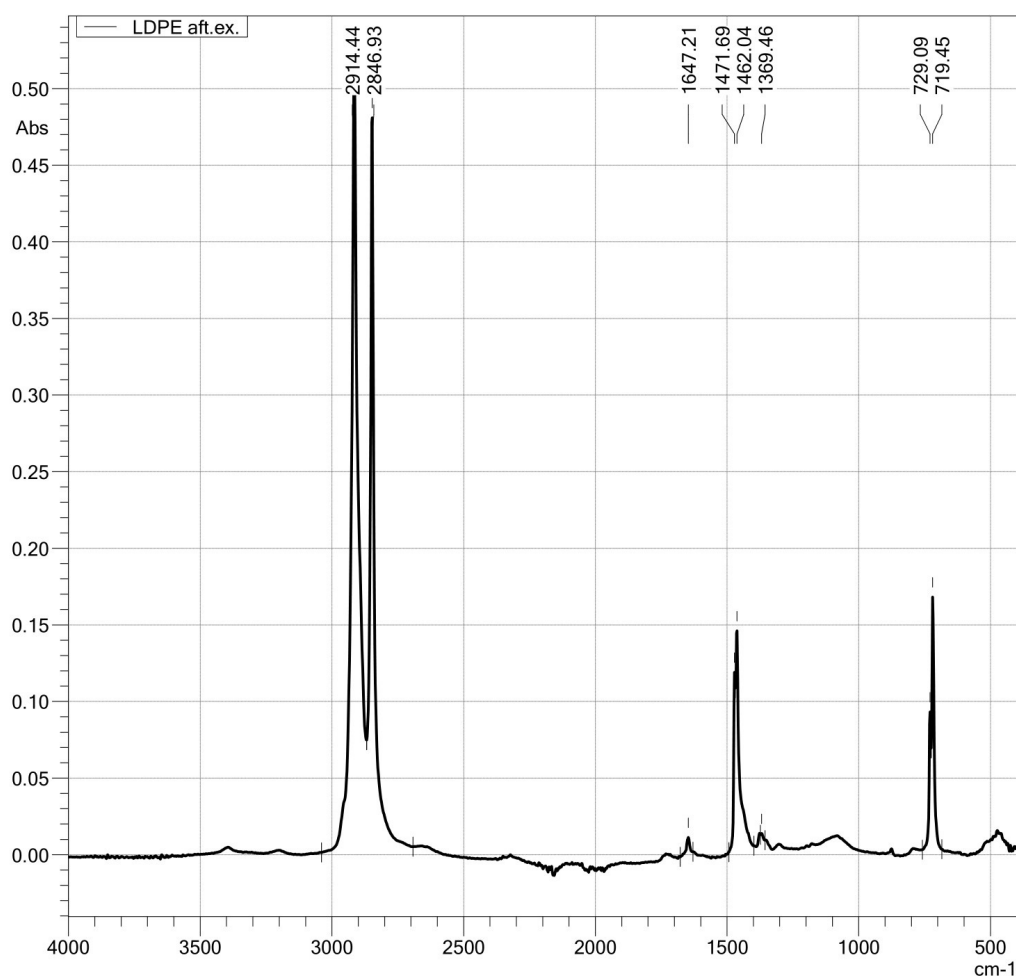


Figure 4.10: FTIR spectrum of LDPE after extrusion.

In Figure 4.11, the spectra of virgin LDPE with 1 wt%, 5 wt% and 10 wt% of PA6 are combined. Several peaks have appeared, caused by the amide group in the PA6. At 3298 cm^{-1} , a peak is caused by N–H stretching. The peak at 1645 cm^{-1} comes from C=O stretching and the peak at 1541 cm^{-1} arises due to N–H bending. For every one of these peaks, the intensity gradually increases with PA6 content, which is in line with expectations.

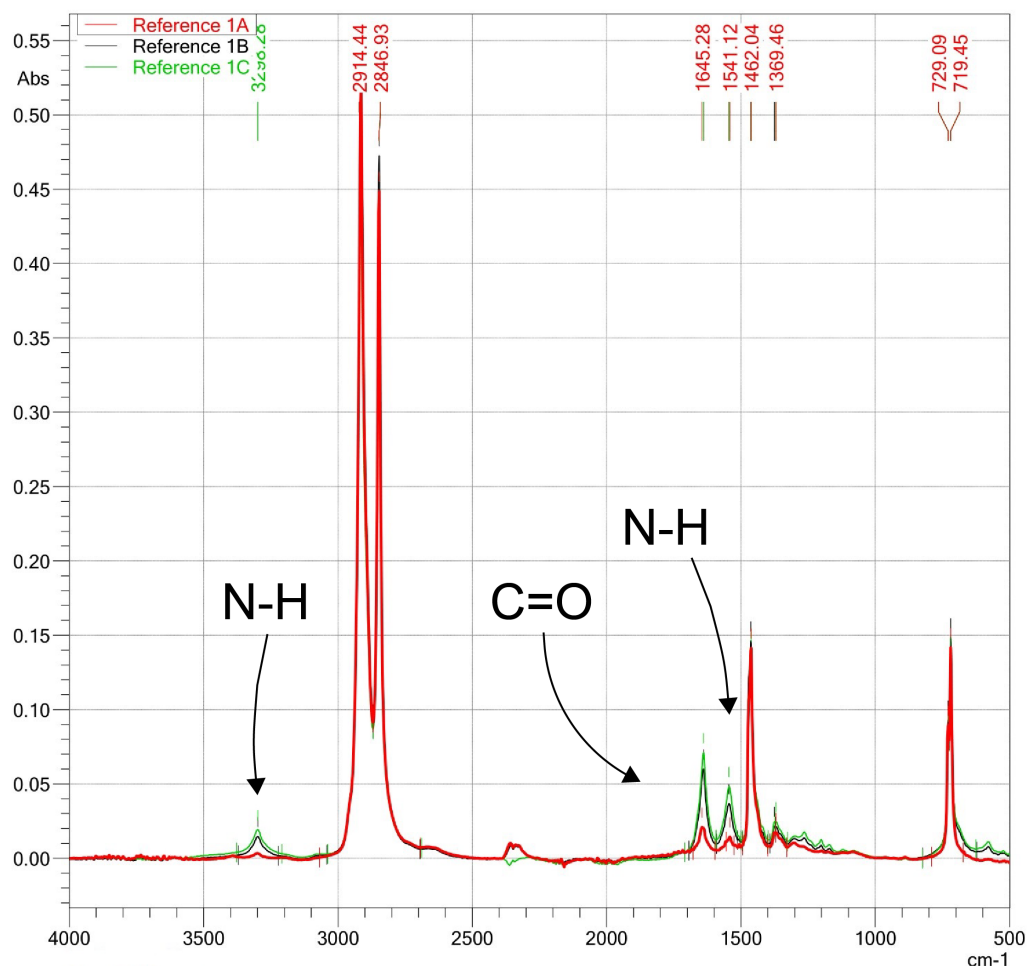


Figure 4.11: FTIR spectrum of virgin LDPE with, 1 wt% (red), 5 wt% (black) and 10 wt (green) of PA6, respectively.

Then, in Figure 4.12, samples of same composition had been extruded with 5 wt% PE-g-MA. Since only new amide groups are formed during the reaction of PE-g-MA and PA6, no newly distinguishable peaks are created, besides the peak arising at 1734 cm^{-1} . This peak was seen before in the calibration curves of PE-g-MA. This means that some additive remained unreacted during the extrusion, which was to be expected.

Now, even though the FTIR calibration curves were initially set up to follow the degree of grafting during *in-situ* compatibilization, the curve that was seen in Figure 4.6 could in theory be used to estimate the unreacted PE-g-MA for these cases. A look at the exact (corrected) intensities of the peaks at 1734 cm^{-1} yields respective intensities of 0.006, 0.007 and 0.005. Using the ratio with the peak intensities at 1462 cm^{-1} (0.132, 0.056 and 0.069, respectively), gives respective peak ratios of 0.045, 0.125 and 0.072. Using the equation stated in Figure 4.6, this gives concentrations of 3.54 wt%, 9.74 wt% and 5.64 wt% of unreacted additive. Naturally, since the starting concentration was 5 wt%, these results cannot be right. It can therefore be concluded that at these additive quantities, the minuscule peak intensities that are obtained cannot be used to accurately estimate unreacted PE-g-MA, since any minor noise in the spectra will overrule the results.

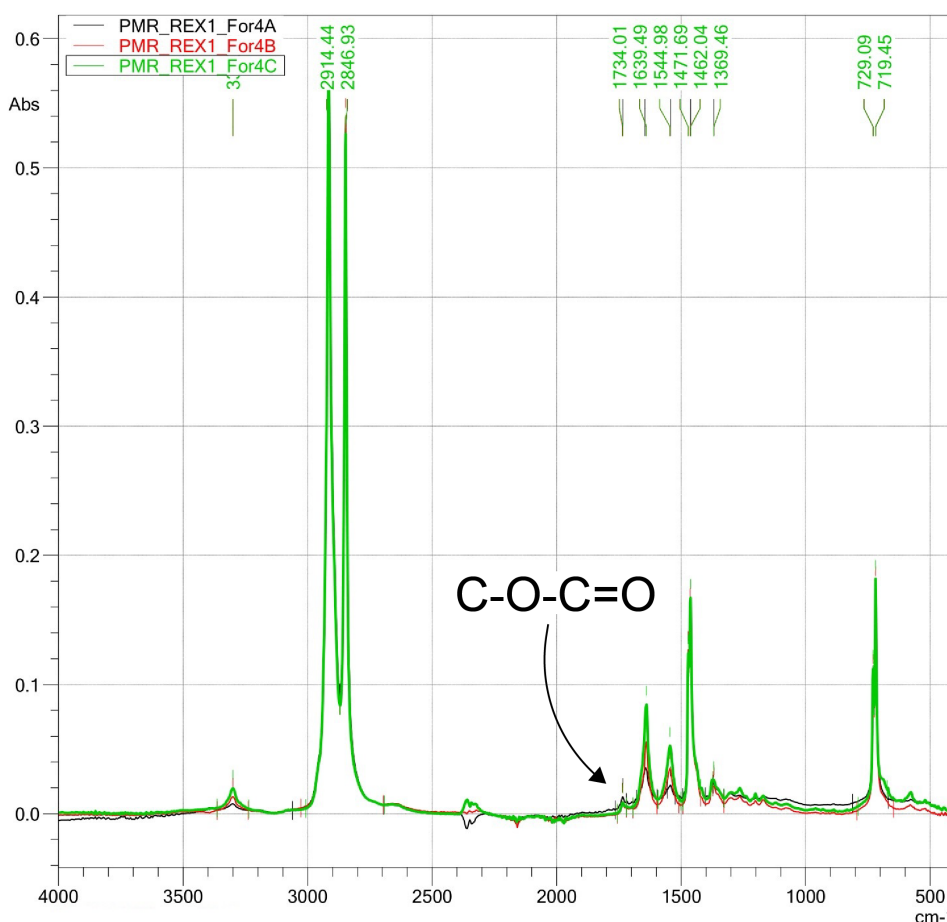


Figure 4.12: FTIR spectrum of virgin LDPE with, 1 wt% (black), 5 wt% (red) and 10 wt% (green) of PA6, respectively, with 5 wt% of PE-g-MA added to each blend.

The FTIR spectra of the two pure grades of PA6 are given in Figure 4.13 and Figure 4.14. They show a much more extensive array of peaks than LDPE which, naturally, follows from their more complex functional groups. The peaks at 3294, 1633 and 1537 cm^{-1} are the same, although marginally shifted, as those mentioned with regard to Figure 4.10. Furthermore, the peaks at 2918, 2850 and 1471 cm^{-1} stem from C–H interactions, similar to the case of LDPE. Some new peaks can be distinguished, such as the peak at 1261 cm^{-1} associated with C–N stretching, the peak at 1371 cm^{-1} coming from N–H bending and the peak at 3080 cm^{-1} created by C–N–H deformation.

Although they are very similar, the spectra of the two grades of PA6 are not identical. A small difference is the peak at 3676 cm^{-1} , being a little more intense for the B36LN grade. However, a substantial difference is seen when looking at the peak at 1014 cm^{-1} , it being the most intense peak in the whole B36LN spectrum, while being non-existent in that of the C40L grade. The presence of this peak is rather peculiar, since it not mentioned in literature. Furthermore, since the C40L is a specific lubricated copolymer of PA6, it would be easier to explain an unordinary peak in this spectrum, instead of in that of the B36LN.

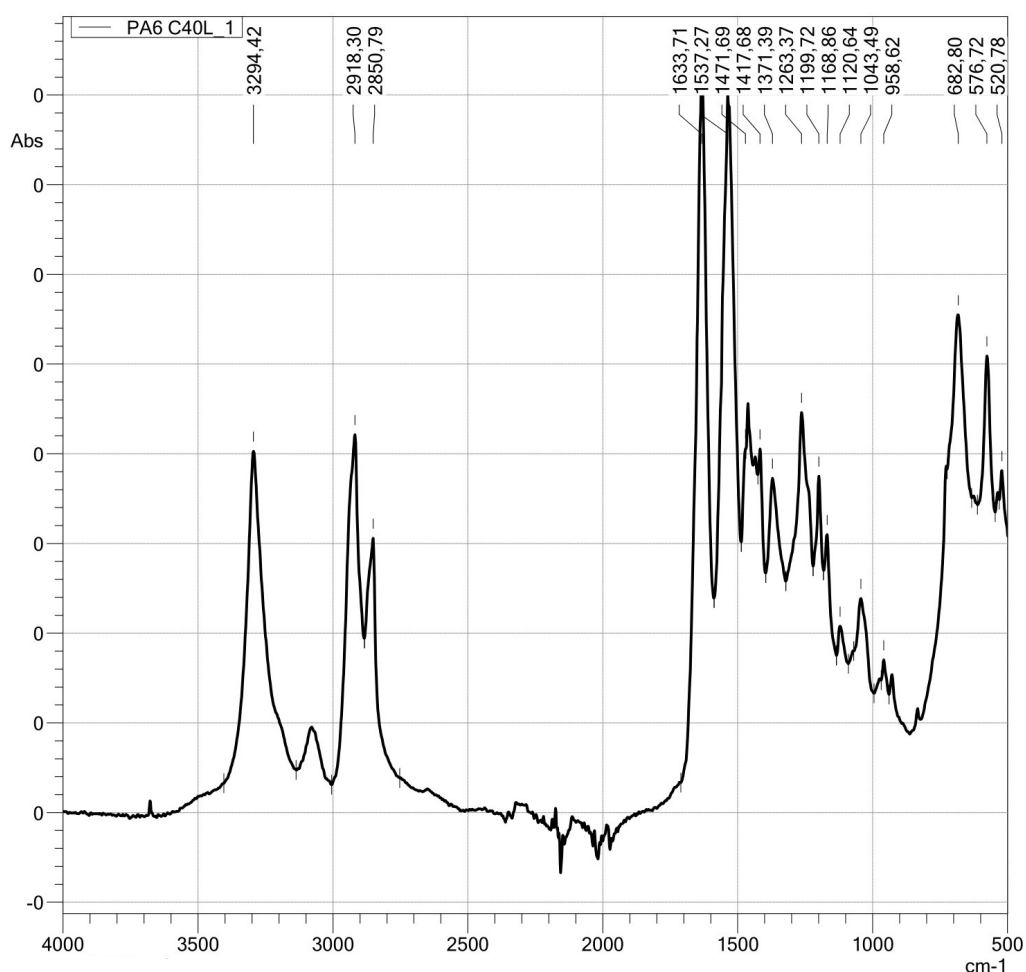


Figure 4.13: FTIR spectrum of PA6 grade C40L.

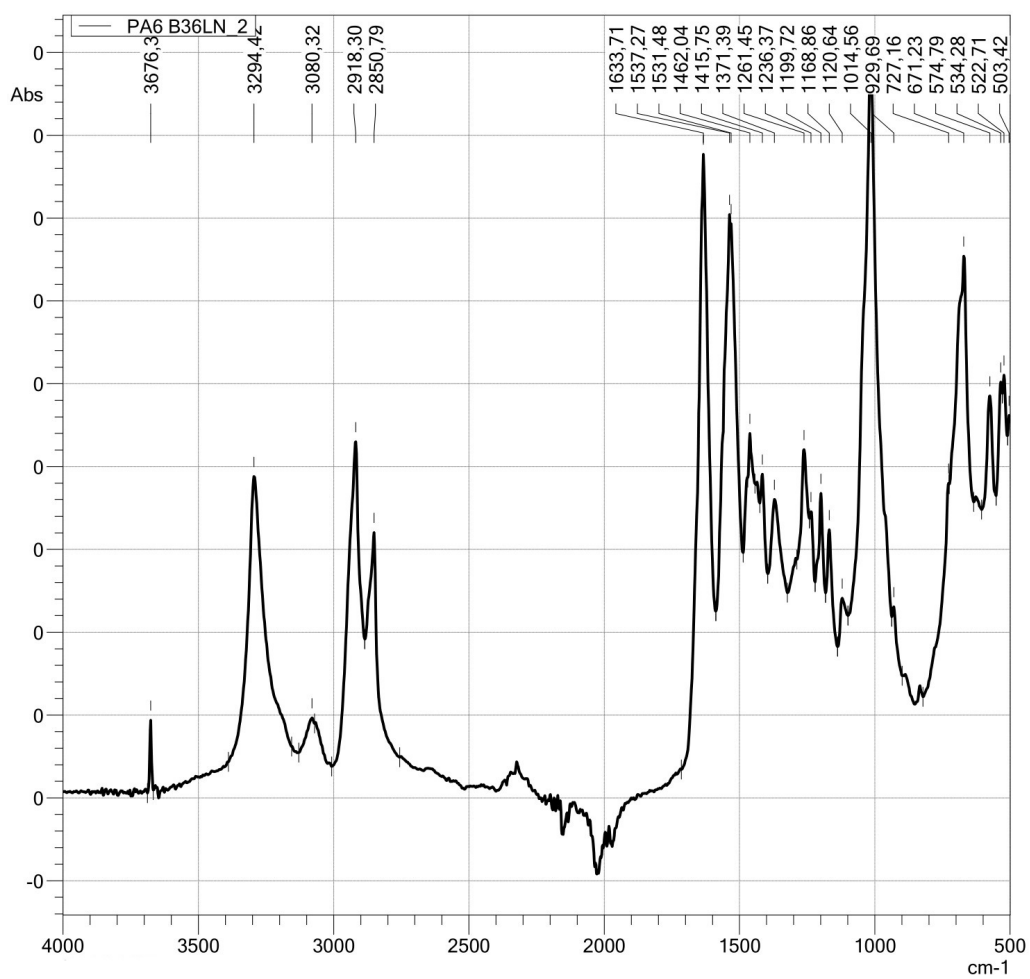


Figure 4.14: FTIR spectrum of PA6 grade B36LN.

In Figure 4.15, the FTIR spectrum of the recycled PE is given, both before and after extrusion. The spectra are extremely similar. Again, a peak is seen at 1645 cm^{-1} , combined with minor peaks around 3200 and 3400 cm^{-1} , most likely following from a lubricant or other additive in the PE. The peak at 1737 cm^{-1} indicates a C=O peak, possibly arising from the oxidation of PE. The peak was not detected in the rLDPE after extrusion, but this could be a result of noise.

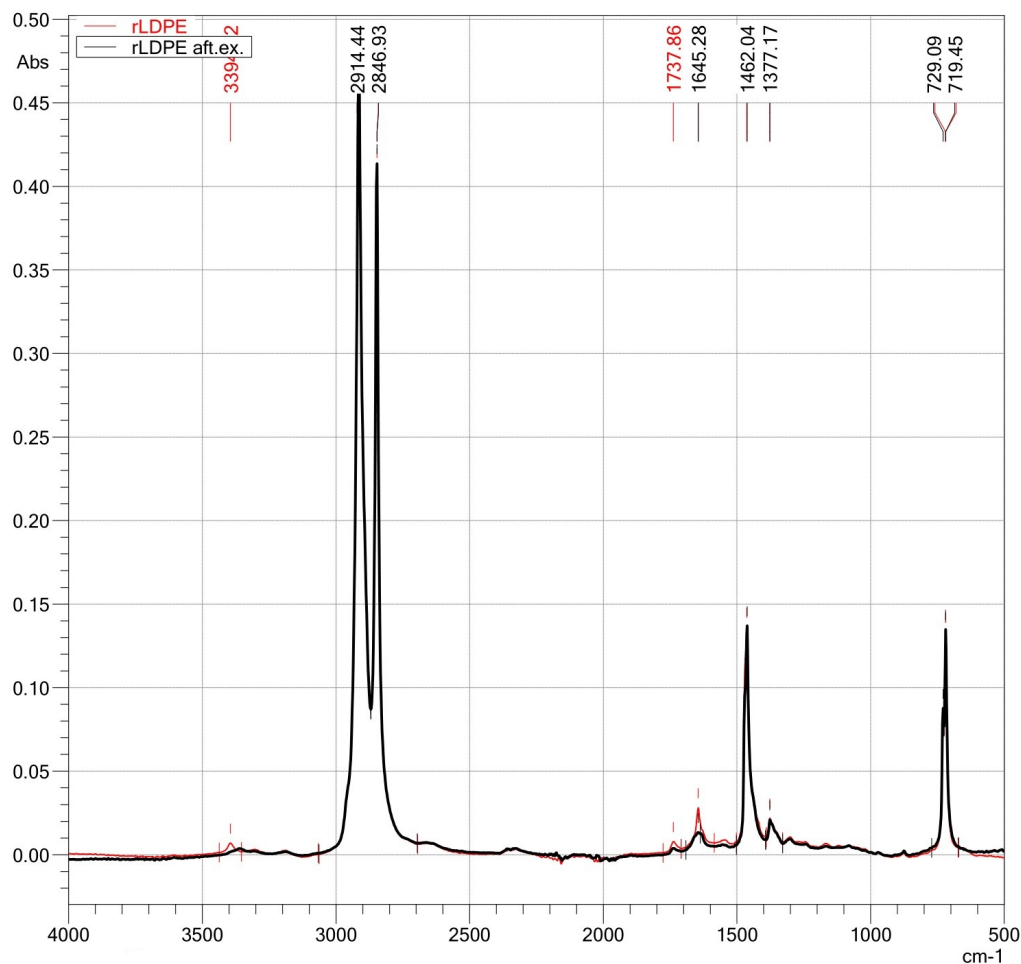


Figure 4.15: FTIR spectrum of recycled LDPE before (red) and after (black) extrusion.

Finally, in Figure 4.16, the spectra of recycled PE can be observed, after being extruded with two different quantities of PE-g-MA. As was the case before, a peak at 1735 cm^{-1} is created by the grafted MA groups. This is, interestingly, at almost the exact same wavenumber as the one shown in Figure 4.15. The respective corrected intensities for the two samples are 0.005 and 0.009, where it was 0.005 for the rLDPE before extrusion in Figure 4.15. Thus, it seems that the peak has not gotten more intense as a result of the additive. However, as was stated before, with peak intensities of this calibre, it is impossible to draw any conclusions with certainty. Lastly, the peak at 1645 cm^{-1} has shrunk as compared to the untreated recycled PE.

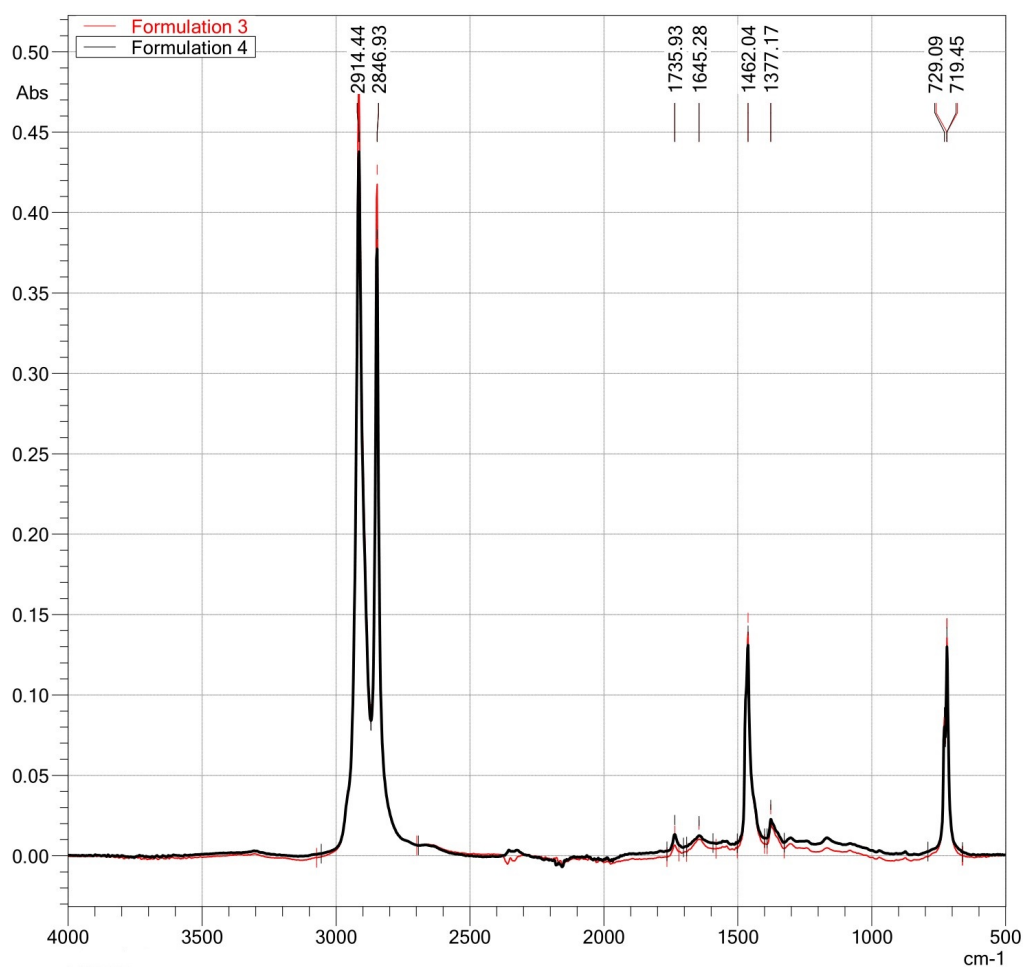


Figure 4.16: FTIR spectrum of recycled LDPE after being extruded with 2.5 wt% (black) and 5 wt% (red) PE-g-MA.

4.4 MFI

In Figure 4.17, the results of the MFI analysis of all references and formulations using virgin polymers are given.

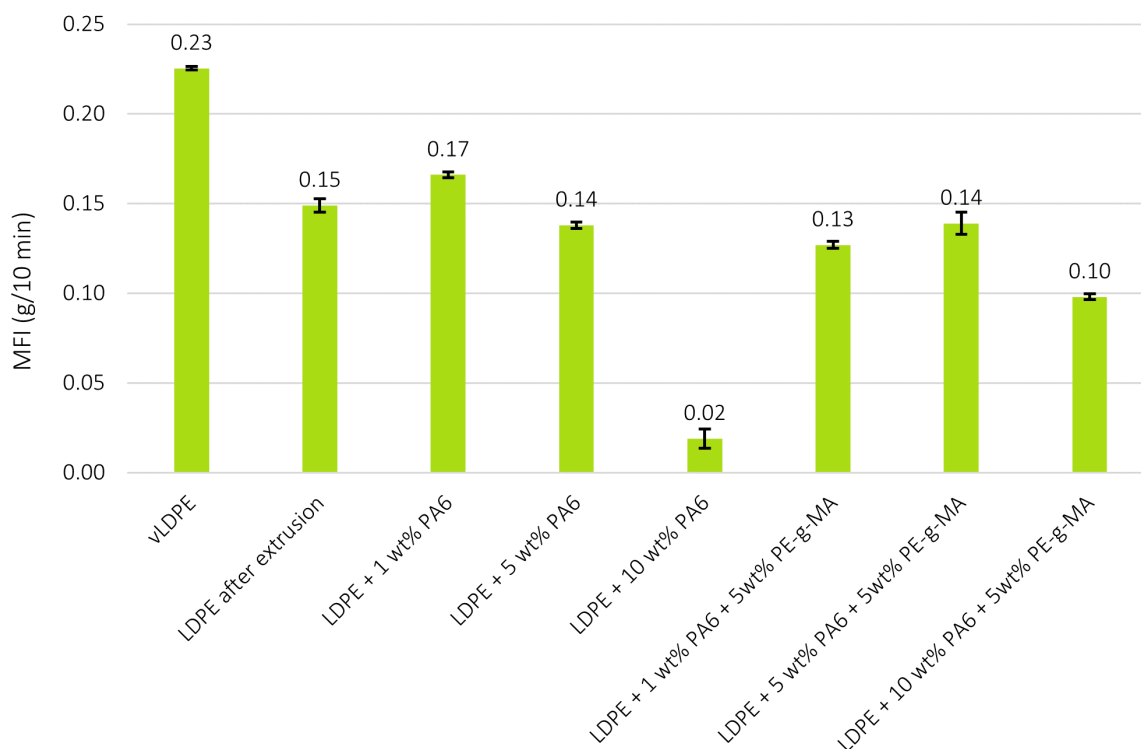


Figure 4.17: MFI values of references and formulations using virgin polymers.

The first result that stands out, is the LDPE after extrusion having a lower MFI than the virgin polymer. Due to thermomechanical degradation, the average molecular weight should slightly decrease after extrusion, resulting in a higher MFI (due to easier flow). However, the opposite is observed in this case (though it is not a big difference). The experiment was even repeated an extra time to confirm, resulting in the same value. One explanation could be a small amount of crosslinking, although this hardly occurs after merely one extrusion step.

To properly describe the correlations of the blends with and without compatibilizer, the scheme in Figure 4.18 was put in place.

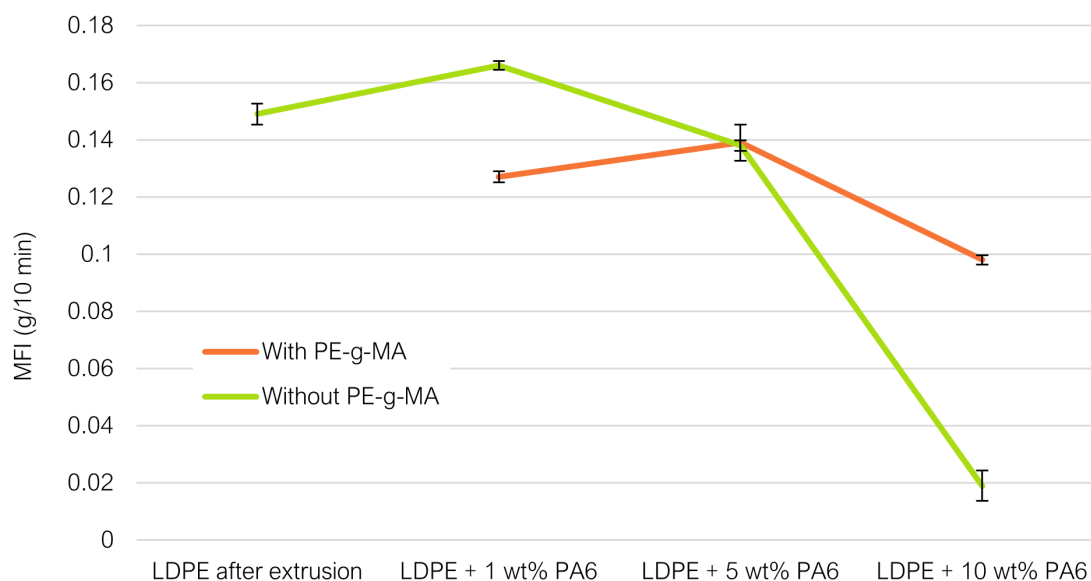


Figure 4.18: Trends of Figure 4.17, differently presented.

The results do not seem very straightforward at first glance. For lower amounts of PA6, the compatibilized blend shows a lower MFI, after which the values are nearly identical for 5 wt% PA6, followed by a much lower value for the non-compatibilized sample at 10 wt% PA6. To understand what might be causing this behaviour, it is important to highlight some molecular phenomena before and after compatibilization.

Before compatibilization, two separate phases exist, one being LDPE and one being PA6. Due to the hydrogen bridges present in the PA6 phase, this phase has a much higher melting temperature, and will therefore be expected to severely impede the flow of the blend at the temperature of measurement. However, it is possible that at low concentrations, the PA6 might act as a lubricant, weakening the van der Waals forces present throughout the LDPE. This could be an explanation to the increase in MFI for 1 wt% PA6. At higher percentages, the PA6 molecules will have a higher chance of finding each other, which will cause the MFI to drastically decrease for the aforementioned reason.

After compatibilization, a significant part of the PA6 molecules will have covalently bonded to the PE-g-MA. Due to steric hindrance of the LDPE branches, the PA6 phase will not be able to manifest itself as before, causing it to be dispersed throughout the PE phase. This will increase the ability of the blend to flow. However, the average molecular weight of the blend will be augmented because of these covalent bonds, diminishing the flow. It seems like at lower PA6 content, the increase in molecular weight seems to be dominant for flow, while at higher concentrations the greater PA6 dispersion seems to be dominant. Czarnecka-Komorowska *et al.*^[154], performing similar research on a 80/20 w/w PE/PA6 blend, observed a decrease in MFI after compatibilization with PE-g-MA which they attribute to the aforementioned complex forming. This indicates the opposite of what is observed for the 10 wt% PA6 sample in this study. They did not perform the test at

190 °C, though, but at 230 °C. This is of great influence on the result, since the PA6 will be in its fully molten state.

This being said, it should be noted that all values, except that of the LDPE + 10 wt% PA6, find themselves in a span of 0.12 g/10 min. This is a very small interval, so even when certain results do not seem to have an immediate explanation, the results are marginal and will not demand any large operational changes on an industrial scale. It seems as though the extrusion step is the main contributor to the drop in MFI, after which the effect of the compatibilizer is not very significant.

In Figure 4.19, the MFI results are given of all references and formulation using rLDPE.

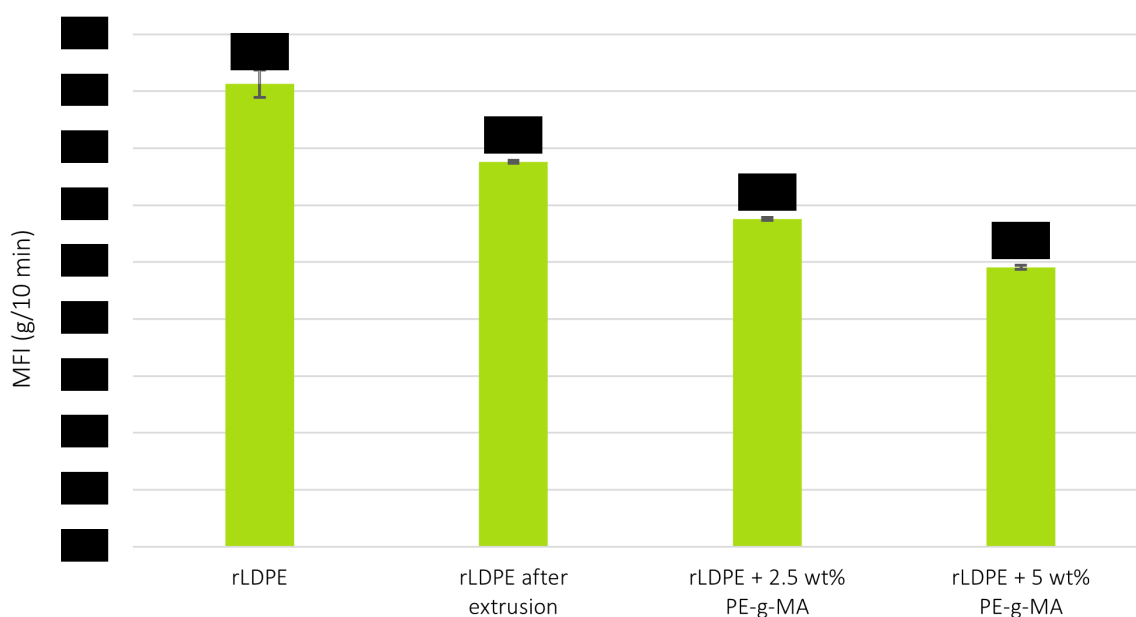


Figure 4.19: MFI values of references and formulations using recycled LDPE.

Interestingly, the same phenomenon is seen as before, where the extruded polymer has a lower MFI than the non-extruded one. In this case, however, the LDPE has already been extruded during the recycling process, so the two cases are not identical. The MFI decreases even further, upon adding and increasing the amount of compatibilizer. This behaviour might again be explained by complex forming, this time between PP and PE.

The rLDPE shows a significantly higher MFI value than the virgin LDPE. This makes it impossible to quantitatively compare the two. A virgin LDPE grade with a higher MFI would have been more suitable for the benchmarking. Starting with LDPE that already exhibits little flow, the contrast with the PA6-containing samples does not come forth as much as would be the case with highly flowing LDPE. Also, it would allow for a better comparison with the rLDPE.

4.5 DSC

The various DSC results are displayed in this section. For area (and therefore crystallinity) determinations, the starting point for peak integration was chosen based on the point where the first derivation of the curve shows a rapid increase.

In Figure 4.20, the DSC curves of the first and second heating cycle of virgin, untreated LDPE are given. The onset temperature is in accordance with the theoretical melting point of LDPE. A “step” increase can be observed between 70 and 80 °C on the first heating curve, which is not shown on the second one. The second cycle generally delivers a neater curve, since the polymer chains cooled slowly after the first heating cycle and their “thermal history” is effaced. The peaks for both cycles are relatively broad, more than might be expected from a virgin polymer.

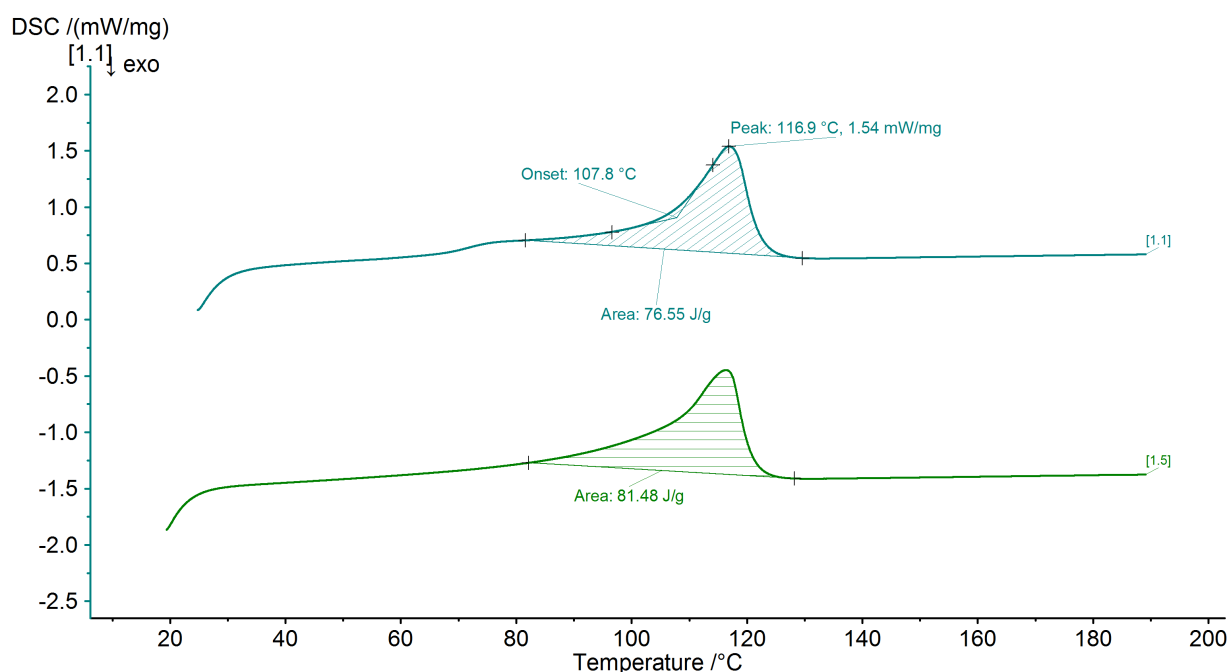


Figure 4.20: DSC curve of virgin LDPE.

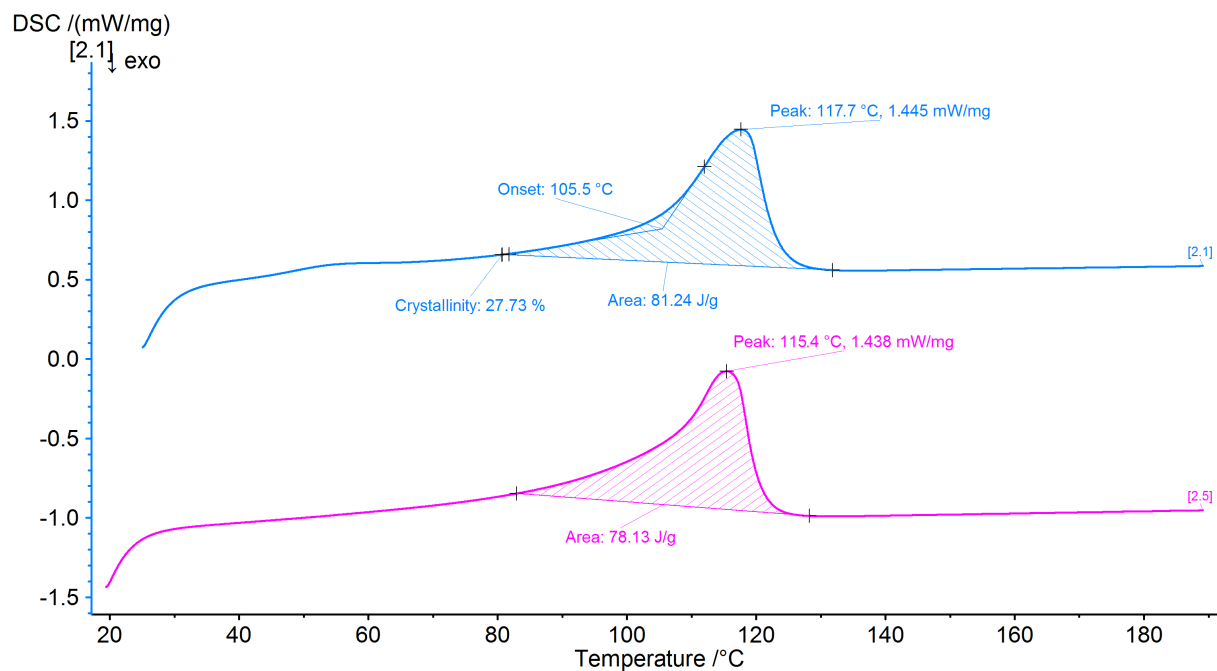


Figure 4.21: DSC curve of virgin LDPE after extrusion.

Figure 4.21 shows the first and second heating curve of LDPE after having passed through the extruder. The onset of 105.5 °C is accordance with the theoretical melting point (or range) of LDPE.

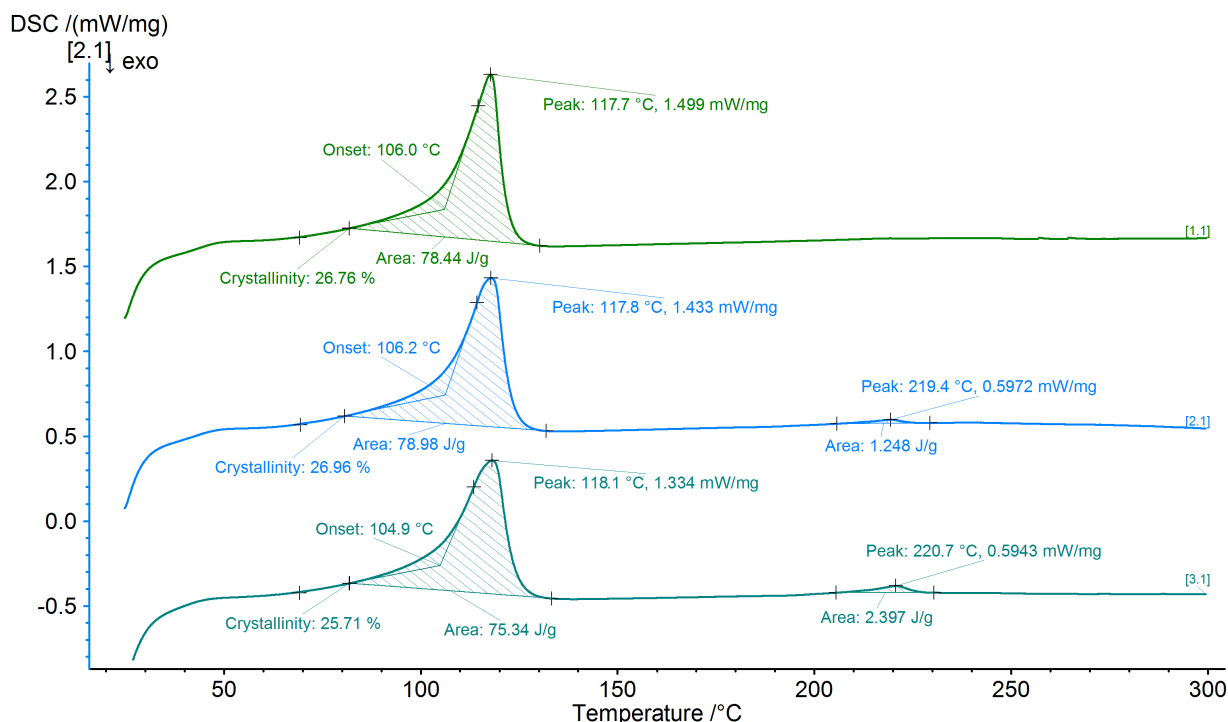


Figure 4.22: DSC curve of the first heating cycle of virgin LDPE with, from top to bottom, 1 wt%, 5 wt% and 10 wt% of PA6, respectively.

In Figure 4.22, the DSC curves of virgin LDPE with 1 wt%, 5 wt% and 10 wt% of PA6 are shown. A similar onset and peak of melting are seen as for pure LDPE. Besides this, for two of the three curves, a peak can be distinguished at around 220°C, belonging to the present PA6. At 1 wt%, no peak was visible, indicating that no sufficient amount of PA6 was present in this sample for it to be detected. This points to the fact that due to the inhomogeneity of the blend, a certain threshold quantity is needed for it to be represented in all pellets formed during extrusion. The peak has the largest area for the highest amount of PA6.

The crystallinity of the LDPE roughly remains constant for all curves, meaning that based on this measurement, it is not impeded by the PA6 phase. It should be noted, though, that through manual determination of the peak area like was done here, the human error is substantial and will overrule one percentage point of difference in crystallinity.

In Figure 4.23, DSC curves are displayed of the same blends of LDPE and PA6 as Figure 4.22, only this time with 5 wt% of PE-g-MA added to them.

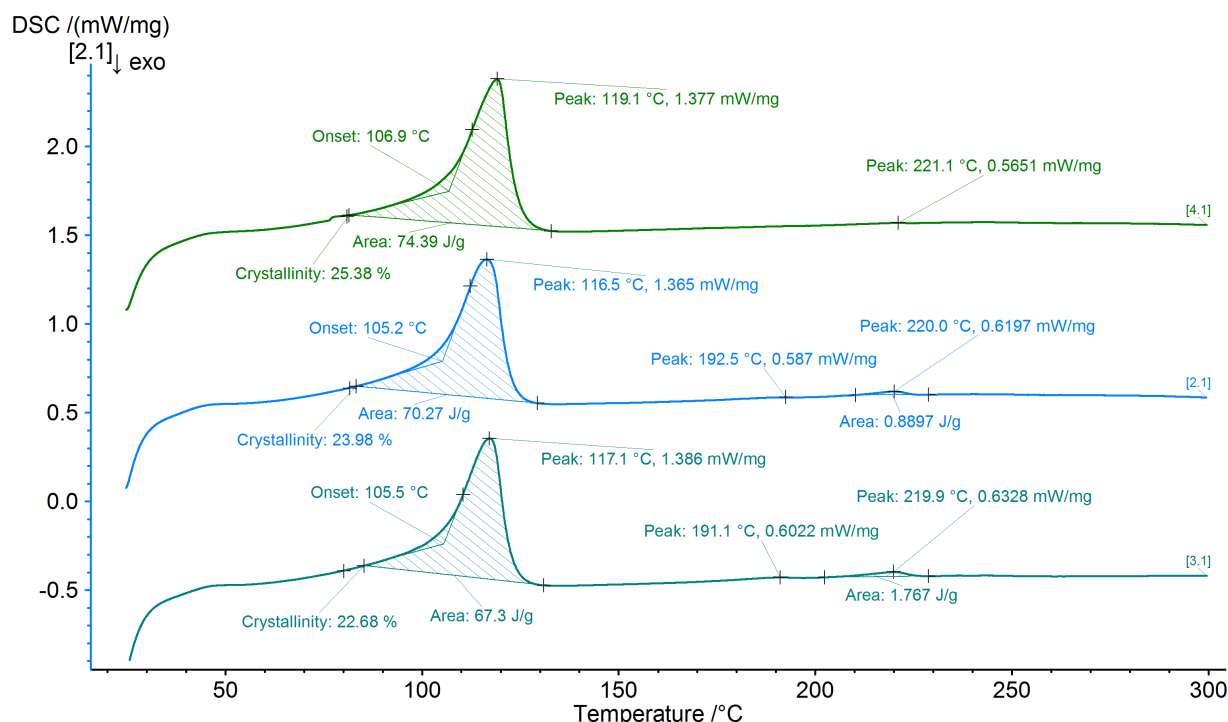


Figure 4.23: DSC curve of the first heating cycle of virgin LDPE with, from top to bottom, 1 wt%, 5 wt% and 10 wt% of PA6, respectively, with 5 wt% of PE-g-MA added to each blend.

Interestingly, a peak can be distinguished for PA6 in the 1 wt% curve, albeit extremely small, where this was not possible before. This can be explained by the higher dispersion of PA6 in the LDPE matrix, meaning a higher likelihood of detecting it in a random sample.

Moreover, a new peak has arisen around 192 °C for the two bottom curves. This can be explained when looking at Figure 4.24, where the two heating cycles are shown of both PA6 grades that were used in this study. The curves denoted by [1.1] and [1.5] belong to Ultramid 40L, having a typical melting point of 220 °C according to the data sheet provided by BASF. This is in accordance with what is seen in the heating cycles and is in accordance with temperature of the aforementioned peak in Figure 4.23. The curves [2.1] and [2.5] stem from Ultramid B36LN, which was said to have a melting point of 189 °C, which was seen in both Figure 4.22 and Figure 4.23.

It appears that after compatibilization, the phases of the two PA6 grades are more segregated, relative to before. This could be caused by the reaction with the PE-g-MA, interfering with the crystallinity of the phases. Furthermore, the additive might react more readily with either of the two grades. Finally, the two grades of PA6 will certainly not distribute themselves among the LDPE matrix in identical fashion. Since the C40L grade is a copolyamide of PA6 and polyamide 6,6 (PA66), the amount of amide groups will be slightly higher, perhaps causing a larger repulsion from the PE. As a result, in order to quantitatively assess the results of the DSC spectra, the number of inspected samples ought to be much higher.

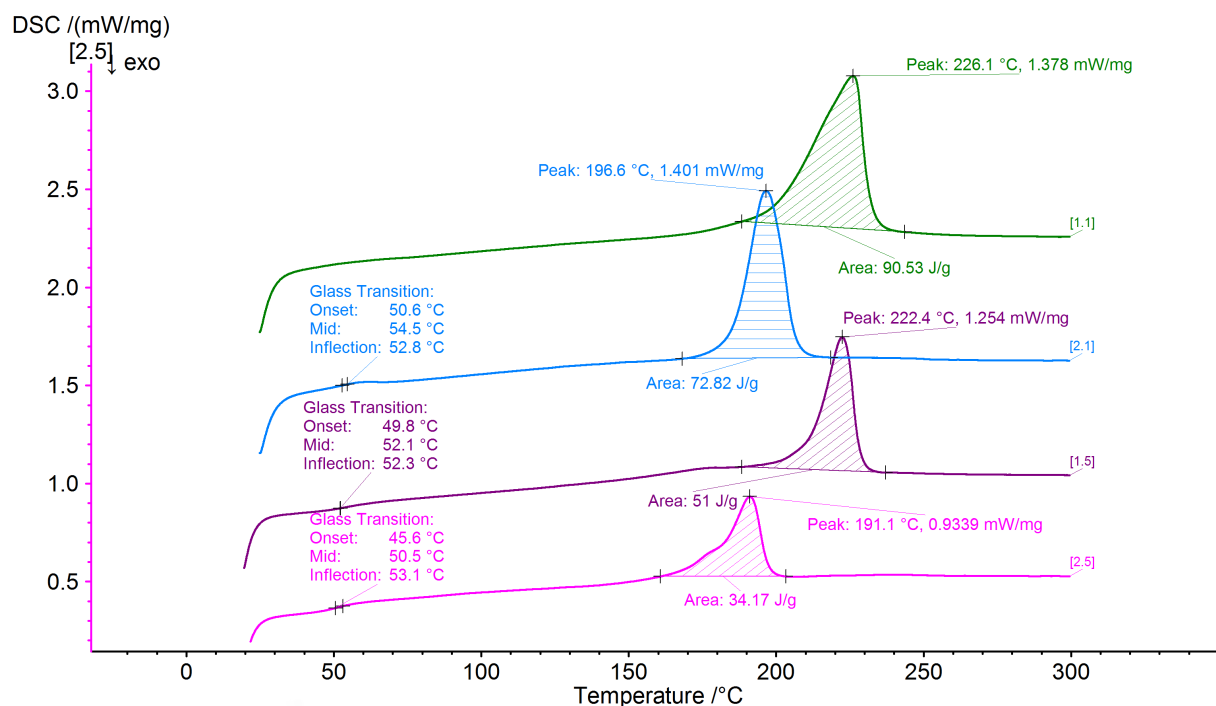


Figure 4.24: DSC curves of the first heating cycle of the two different PA6 grades, followed by their respective second heating cycle.

In Figure 4.25, the DSC curves of both the first and second heating cycle of a recycled PE material are shown.

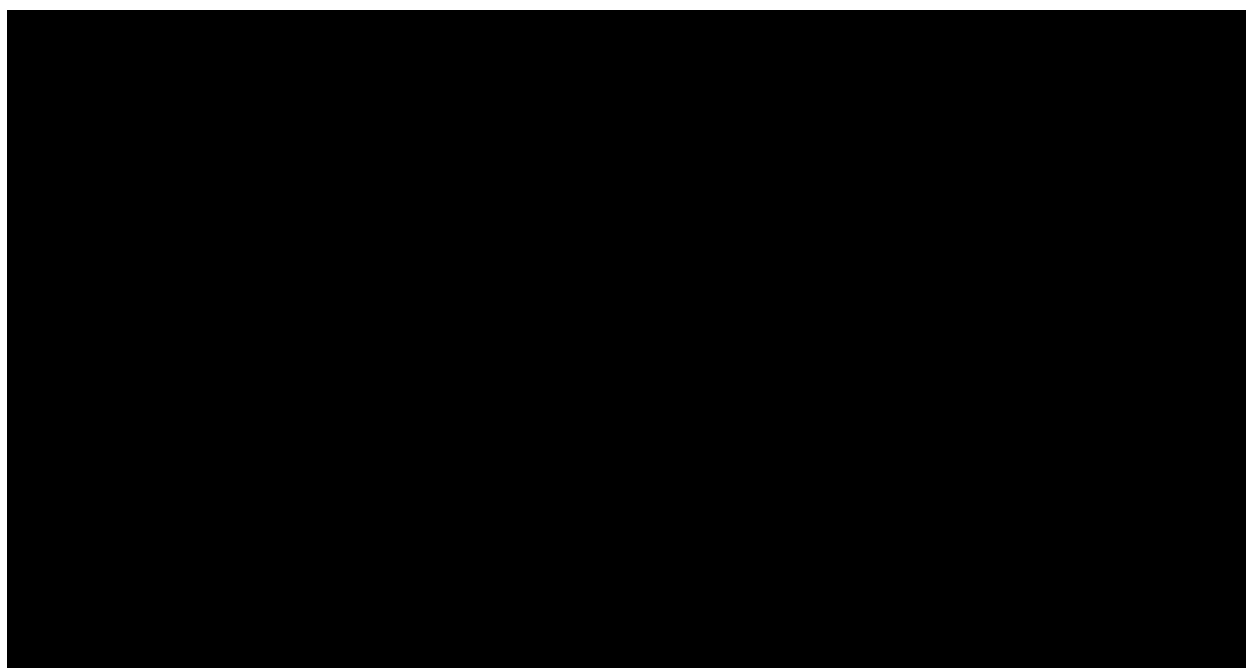
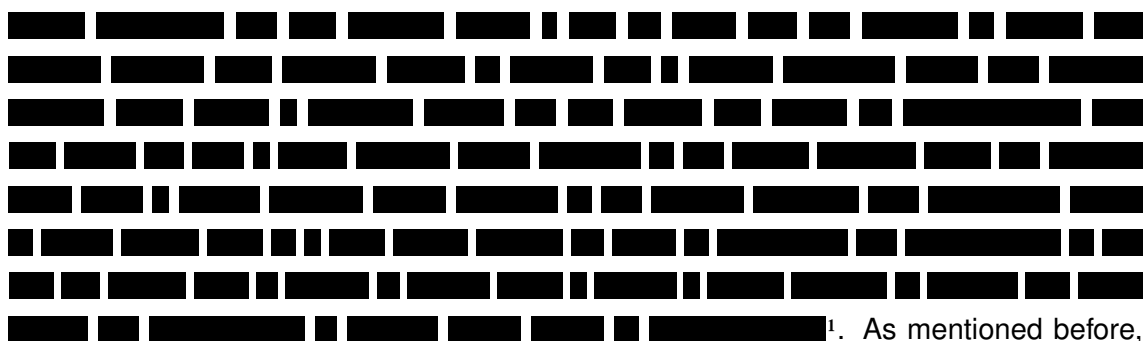


Figure 4.25: DSC curve of the first and second heating cycle of recycled industrial film as received from the recycling plant.



¹. As mentioned before, this merely provides a rough indication, since a proper result can only be obtained from using a deconvolution software, through which the respective areas of two overlapping peaks can be precisely identified. Using the melting enthalpies obtained through DSC, a correlation curve can be created for determination of compositions of LDPE/LLDPE mixtures^[155].



It became clear from Figure 4.22 that as much as 1 wt% can go unnoticed during a DSC test, due to inhomogeneity, small samples sizes and low number of samples studied. A possible explanation for the fact that PP is detected where PA6 is not, could be their difference in intermolecular forces. PP relies on van der Waals forces, which are of less strong nature than the hydrogen bonding that is present in the PA6. Furthermore, since PP does not have any polar end groups, the repulsion force towards the PE will be smaller. The PP would then be naturally more dispersed than PA6.

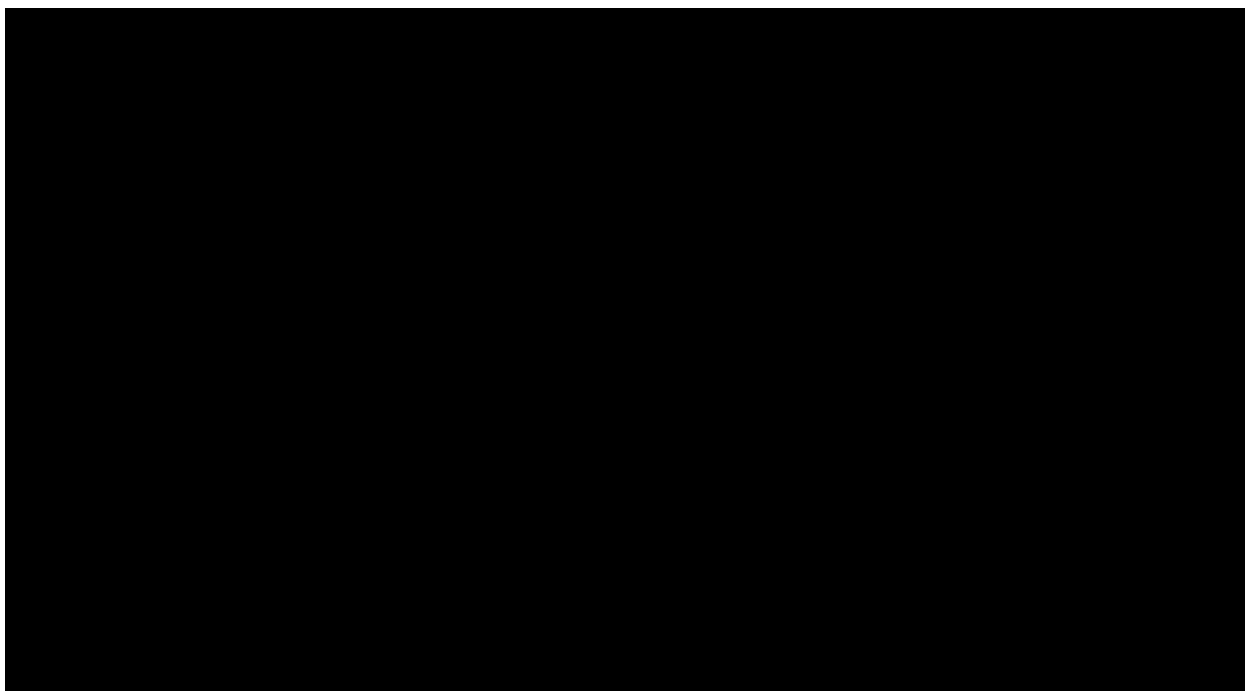


Figure 4.26: Second cycle from Figure 4.25, with partial areas indicating LDPE/LLDPE ratio.

¹This information follows from prior research within SUEZ.

In Figure 4.27, the first and second heating cycle of the rLDPE is shown, after having gone through one extrusion step.

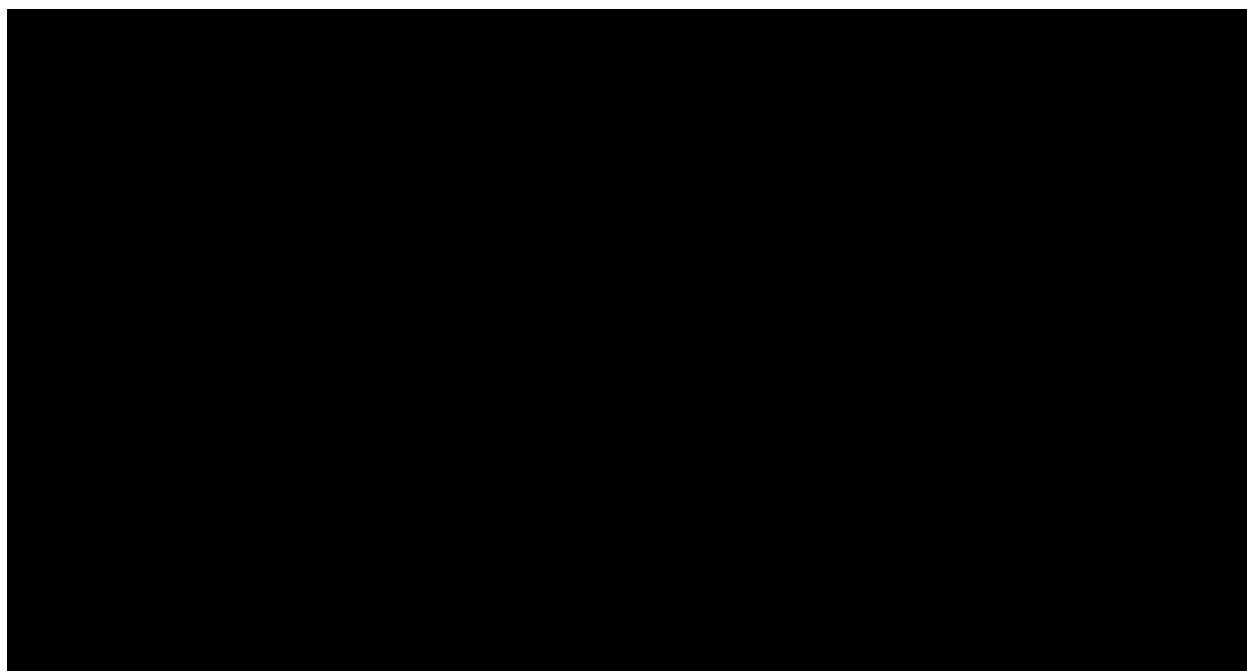


Figure 4.27: First and second heating cycle of rLDPE after going through an extrusion step.

When comparing the curves of Figure 4.25 and Figure 4.27, it appears that the in the first heating curve of the mix after extrusion, the “step” at around 60°C has vanished, which was there before extrusion. The peak has a more gradual and neater run-up. The contrary might have been expected, since the extrusion leads to a small amount of polymer degradation, which can cause the peak to become broader (due to a larger molecular weight distribution). The second heating curve of both specimens are nearly identical.

In Figure 4.28, the two DSC heating cycles are displayed, of rLDPE with 2.5 wt% of PE-g-MA added to it.

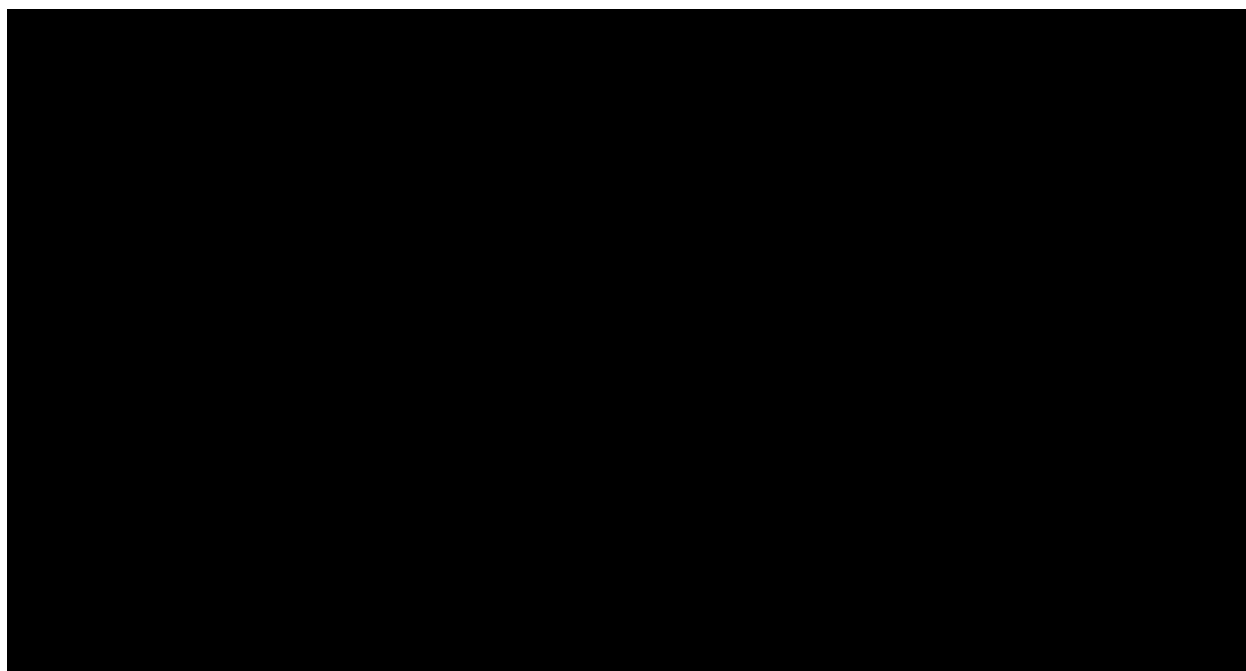


Figure 4.28: First and second heating cycle of rLDPE after reactive extrusion with 2.5 wt% of PE-g-MA.

The two cycles are, in all aspects, extremely similar to those shown in Figure 4.27, where no additive was introduced. The first peak of the first cycle has a slightly different shape, but this does not lead to any hard conclusions, since it is just a matter of the extent to which the two PE types are blended.

The same goes for the two cycles of the rLDPE with 5% of PE-g-MA added, as shown in Figure 4.29. The crystallinity seems to marginally decrease upon increasing the amount of additive, but since the peak area determination is performed manually, it is impossible to say with certainty. Besides, the grafted MA monomers' size most likely does not make a difference compared to the vast (side) chains of the PE.

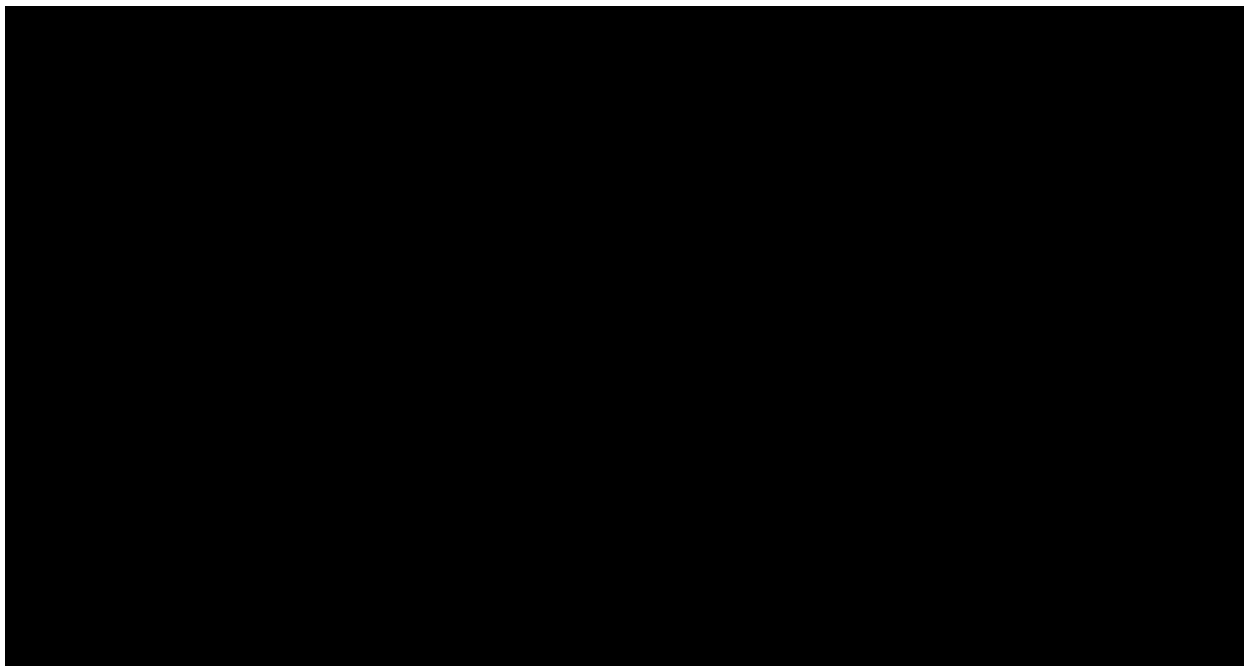


Figure 4.29: First and second heating cycle of rLDPE after reactive extrusion with 5 wt% of PE-g-MA.

4.6 SEM

This section covers the results of the SEM images that were attempted to be made. First of all, it should be said that getting clear and useful images turned out to be incredibly difficult. Naturally, the proper imaging of polymer materials is less straightforward than that of metals, due to the low electric conduction. However, with the use of the right coating, appreciable images should be possible nonetheless, as evidenced by literature. At the very beginning, images were made in low-vacuum mode without coating the samples. This gave highly blurry images, especially at higher magnitudes. For this reason, the coatings were applied. Merely coating the top surface of the pellet, though, will not benefit the measurement, since the incoming electrons will still create a charge build-up in this closed system. The final mount setup was therefore chosen to include a strip of copper tape connecting the coated surface with the metal mount (recall Figure 3.2).

Despite having created a seemingly well-conducting system for analysis, a huge accumulation of charge was seen when using the apparatus in full vacuum mode. Thus, it seemed as though the coating did not function properly. Combining this setup with low-vacuum mode, however, gave the sharpest images of all approaches that were taken. The next difficulty was finding a suitable part at which the focus could be optimal. Perhaps because the pellet's top surface was slightly tilted or because the surface morphology showed too much relief.

Finally, not all samples turned out to be equally fit for examination. Having only a few wt% contaminant makes it nearly impossible to give a good overview of the surface. When it concerns samples of composition 25/75 or 50/50, this is entirely different. This being said, the sample with 10 wt% of PA6 did yield an appreciable result, seeming to be representative for the bulk. In Figure 4.30, the SEM image for this sample can be observed.

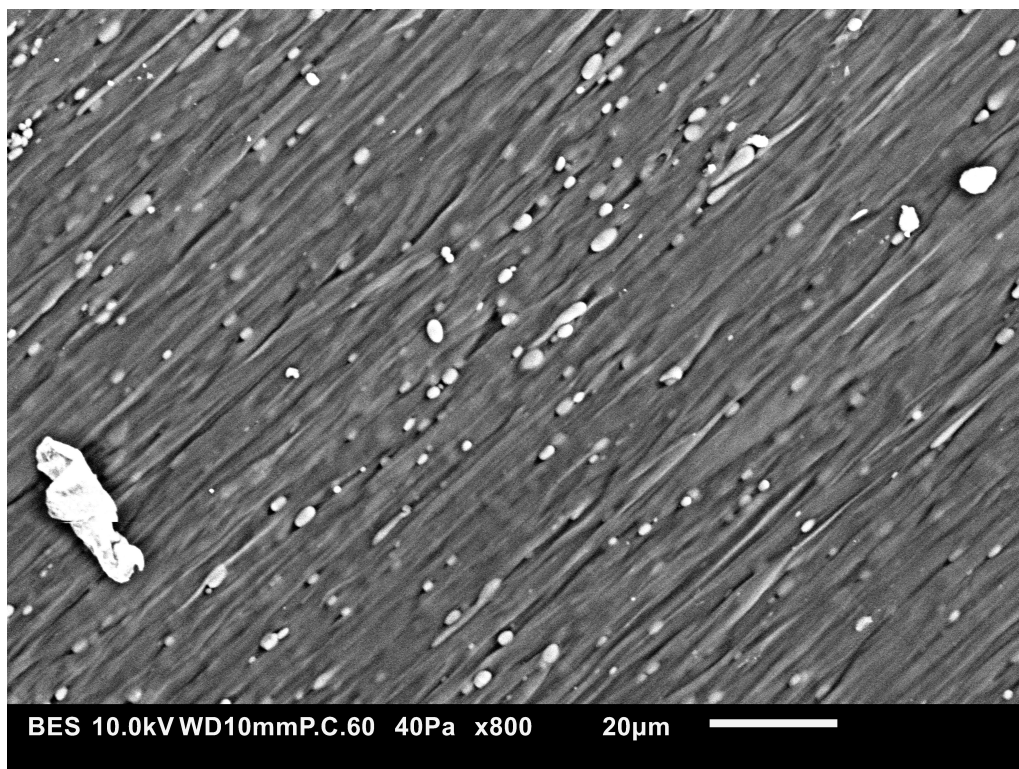


Figure 4.30: SEM image of the fracture surface of a pellet containing virgin LDPE with 10 wt% of PA6.

The two distinct polymer phases that are present can be clearly distinguished. PA6, containing atoms of larger atom number, will turn white compared to the PE. The diagonal pattern that is seen across the image is created by slicing of the pellet. On the left, a large white shape can be identified. Looking at the sharp edges of this shape, it is most likely not PA6, but some other contaminant. Whether it rests on the surface or is embedded in it, is hard to say.

Then, for comparison, the image of the sample after compatibilization is displayed in Figure 4.31.

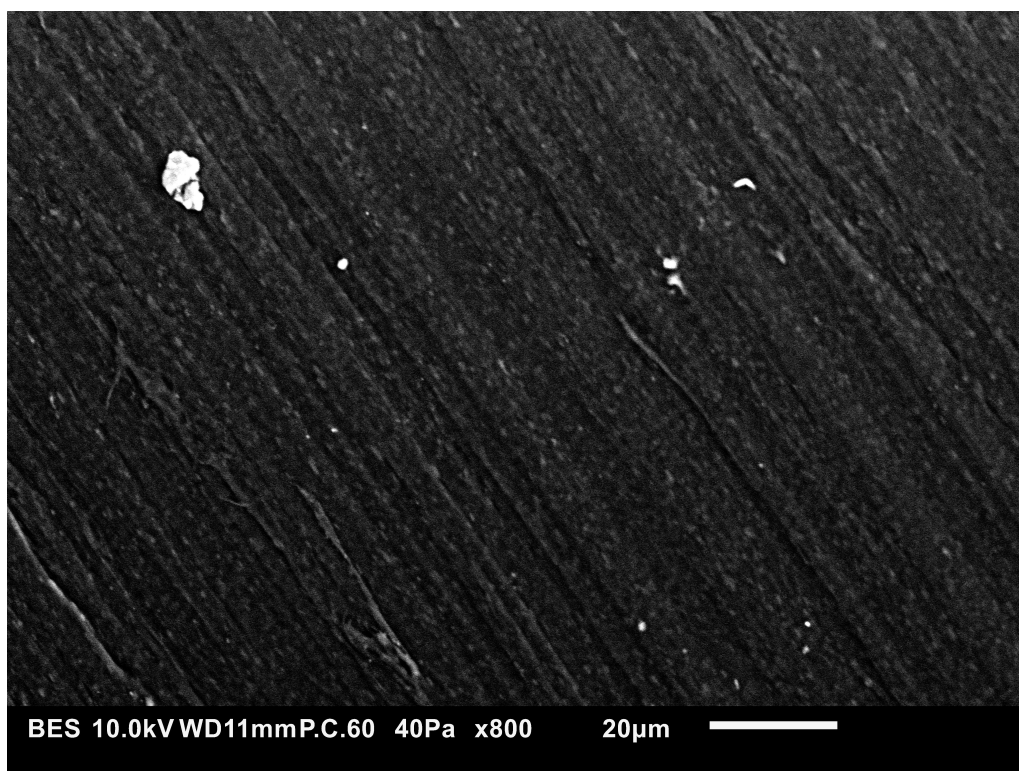


Figure 4.31: SEM image of the fracture surface of a pellet containing virgin LDPE with 10 wt% of PA6 and PE-g-MA.

The difference between the two surfaces is striking. The PA6 seems to have dispersed itself to a great extent in the LDPE matrix. Where the matrix was mostly plain grey before compatibilizing, it is now filled with small grey/white speckles. A few solid white shapes can still be identified, albeit much fewer. A white sharp-edged object is seen at the top left, similar to before.

In Figure 4.32, the SEM image is shown for the rLDPE, after extrusion.

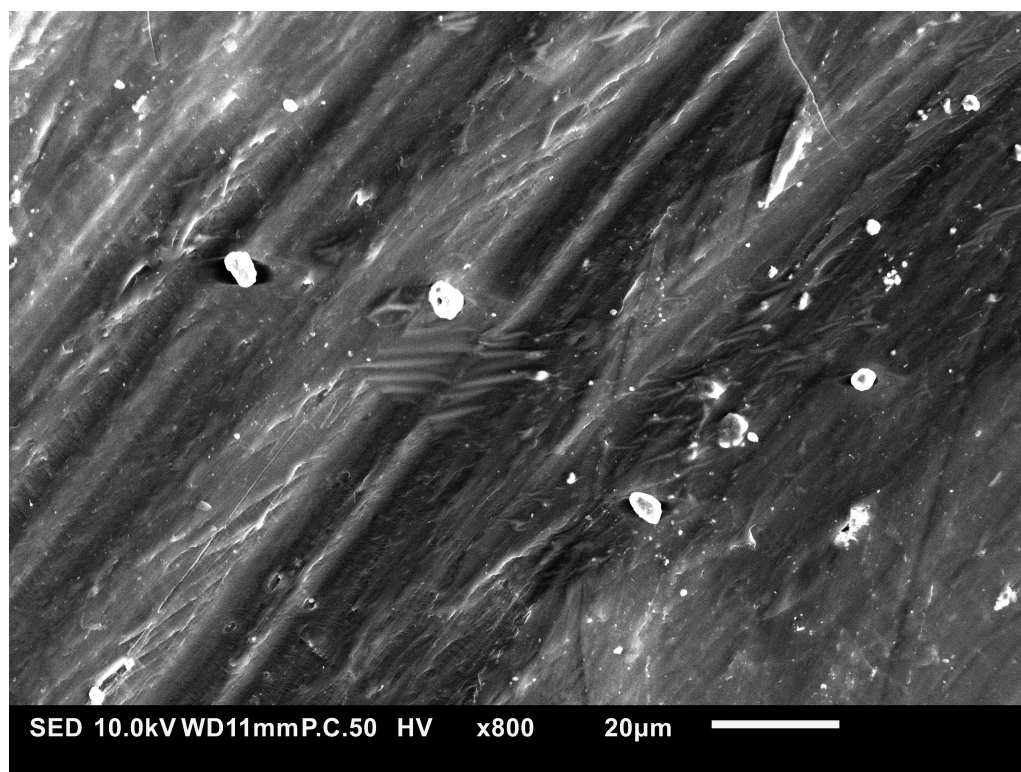


Figure 4.32: SEM image of the fracture surface of a pellet containing recycled LDPE after extrusion.

Again, a grey PE phase contrasts with solid white particles of varying sizes. For the biggest among them, it is not clear whether or not they are embedded in the matrix. In order to assess the structure of this sample well, the use of energy-dispersive X-ray spectroscopy (EDS) is imperative. EDS allows for an elemental analysis of the elements for which $Z > 5$. A certain threshold quantity (about 0.5 wt%) is needed for this^[156]. Unfortunately, EDS cannot be performed in low-vacuum mode. Since PP does not contain any other elements than PE, the white particles have to be of other origin.

Finally, in Figure 4.33, the image can be found of the same recycled polymer, extruded with 5 wt% PE-g-MA.

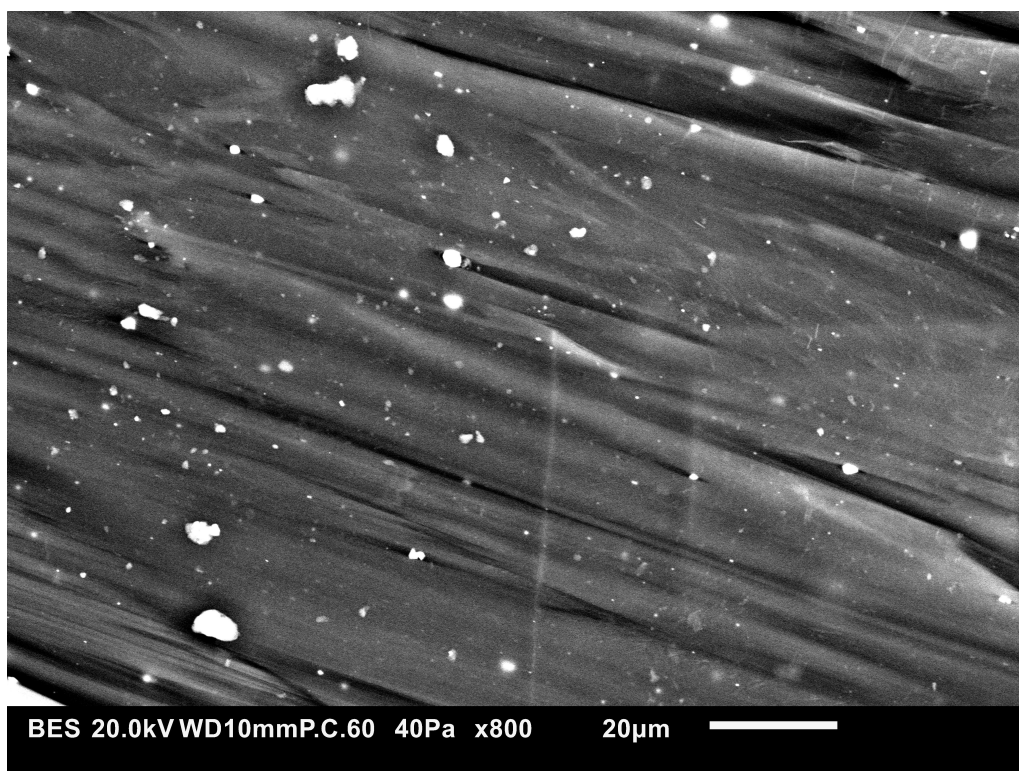


Figure 4.33: SEM image of the fracture surface of a pellet containing recycled LDPE and 5 wt% PE-g-MA.

It is impossible to state with certainty if a change has occurred with regard to the surface morphology. The sample exhibits very similar white particles to before. Since the DSC measurements pointed out that no large quantity of PA6 or PET is present in the recycled LDPE, it comes to no surprise that the compatibilization effect is not comparable to that of the virgin blend above.

4.7 Gel and black spots

During extrusion blowing, the gel spots and black spots present in the film were quantified. Holes in the film are detected in the same way, but none were found throughout all experiments. The spots were all categorised into different sizes: 100-150 μm^2 , 150-250 μm^2 and larger than 250 μm^2 . The values for the various sizes are presented in the form of stacked columns, but nearly 100% of all numbers is accounted for by the lowest size category.

The average number of black spots that were counted per m^2 of film for all references and formulations using virgin polymers, is given in Figure 4.34. As expected, the virgin, untreated LDPE shows the lowest number of black spots. This number increases when the polymer is extruded, although very slightly for the second try (denoted by [2]). Then,

when 1 wt% PA6 is added, the number rises significantly. 5 wt% of PA6 nearly gives a tenfold increase, before increases once more by a factor of ten for 10 wt% of PA6. Extruding at a higher temperature (230 °C instead of 200 °C) seems to marginally lower the number of spots.

Passing on to the compatibilized blends, for the lowest amount of PA6, the number of black spots sees an increase compared to the non-compatibilized blend. This increase is even more substantial for the second try, even though the number slightly decreased previously. Moreover, the number seems to rise even further when the extrusion blowing is performed at 230 °C, contrarily to what was seen before. A great reduction, by more than sixfold, is seen for 5 wt% of PA6 after compatibilization, which is followed by a tremendous decrease for the case of 10 wt% of PA6, by a stunning factor of 60. Oddly enough, the two latter numbers are the lowest of all compatibilized blends, meaning the PE-g-MA negatively influences the number of black spots for low amounts of PA6.

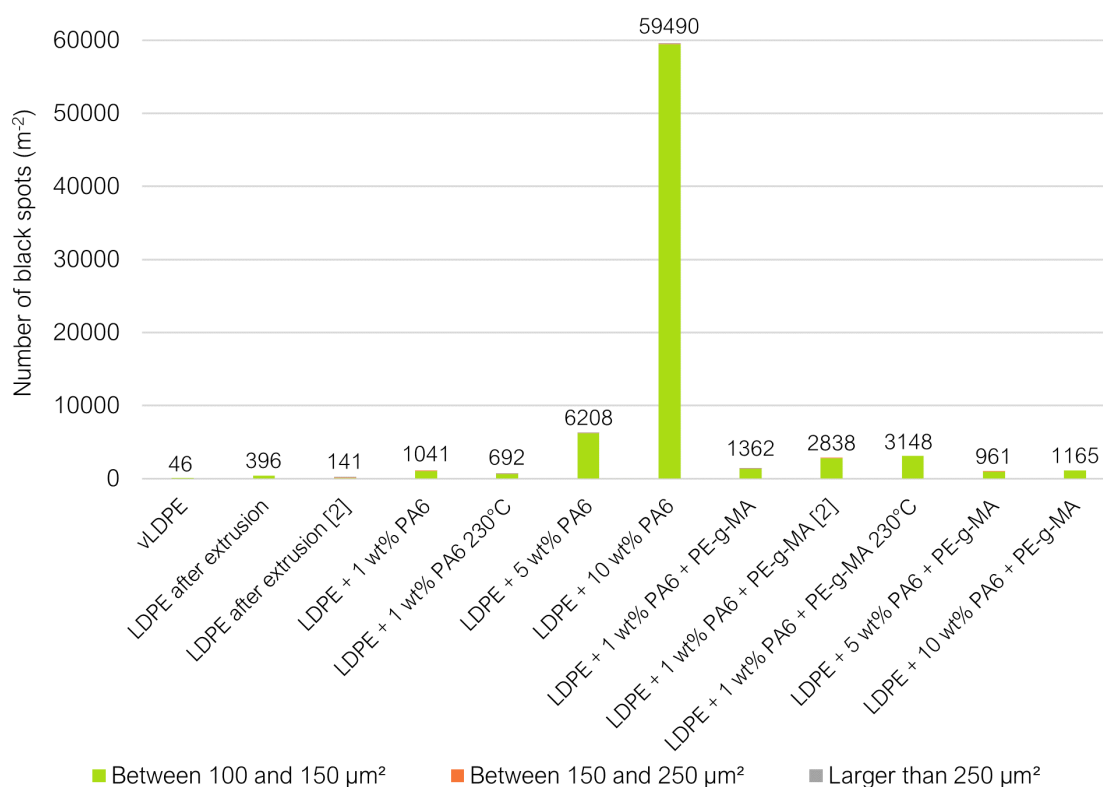


Figure 4.34: Average number of black spots per m² of film for the references and formulations using virgin polymers.

It should be noted that the term black spot, although suggested by the name, does not necessarily imply that the spot in question has a black colour. The software connected to the camera makes an evaluation based on opacity of the spot. If the spot shows (close to) full opacity, it is marked as a black spot. However, in this case, these spots are predominantly white due to the nature of the PA6 present. Using the term opaque spots

would perhaps be better suited in light of the current results.

What follows in Figure 4.35, is the average number of gel spots per m² of film for the references and formulations using virgin polymers. The trend that is shown across the samples, is identical to that of Figure 4.34. This proves that the manifestation of black spots and gel spots are inextricably linked, at least for the combination of polymers and additive that are presented here.

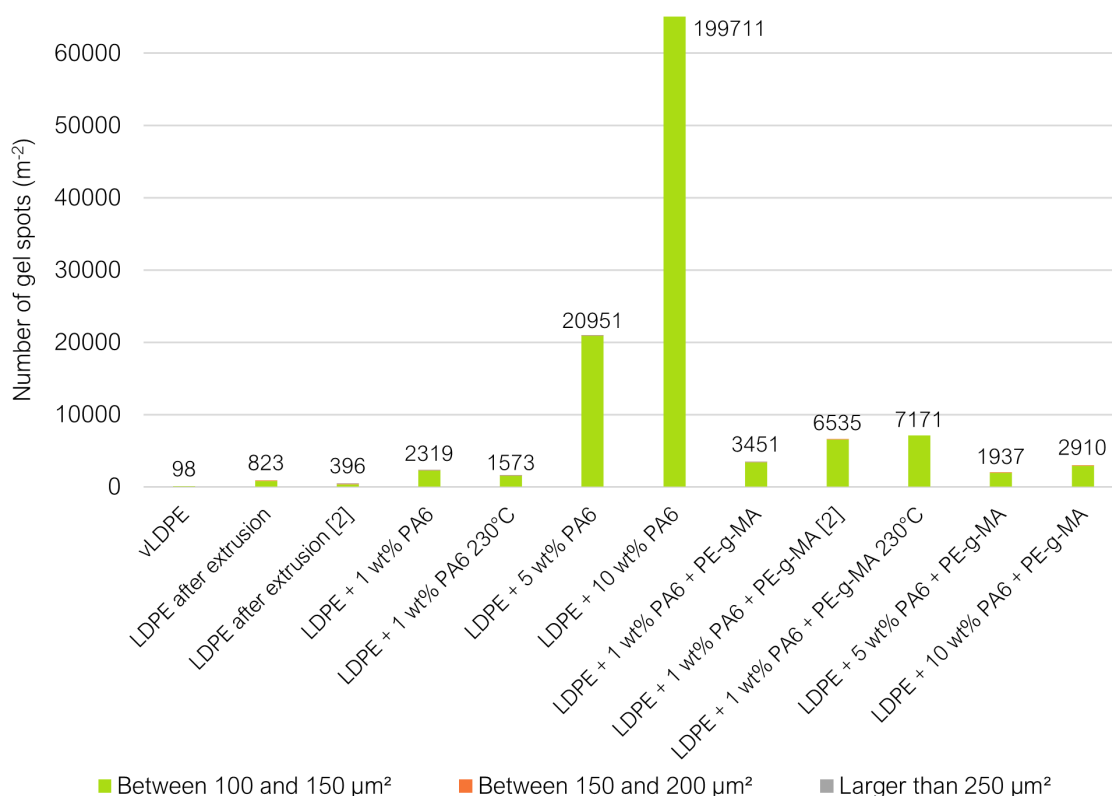
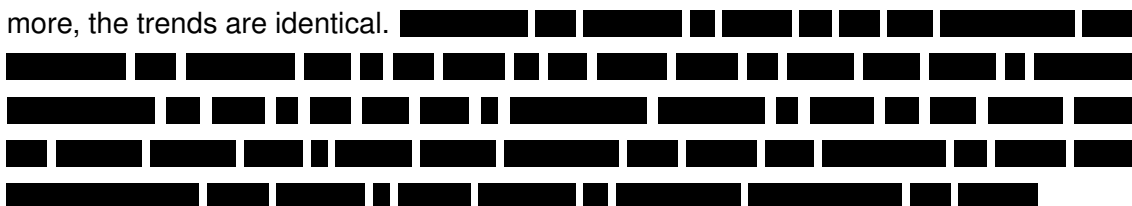


Figure 4.35: Average number of gel spots per m² of film for the references and formulations using virgin polymers.

Highly noteworthy is the astronomical number of gel spots for the non-compatibilized blend with 10 wt% PA6, which would take at least twice more the size of the graph to be depicted. Incredibly enough, the number is brought down by the additive to lower amounts than those for the case of 1 wt% of PA6, similar to before. Again, the additive seems to negatively affect the number of gel spots at the lowest amount of PA6.

Additionally, the number of black spots and gel spots per m² of film for the references and formulations using rLDPE are given in Figure 4.36 and Figure 4.37, respectively. Once more, the trends are identical.



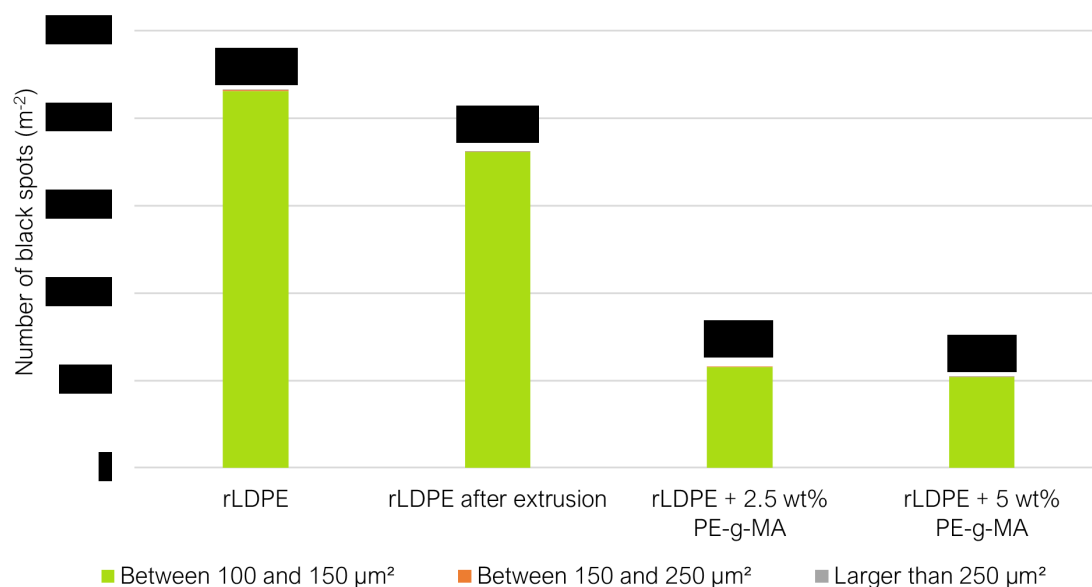


Figure 4.36: Average number of black spots per m^2 of film for the references and formulations using rLDPE.

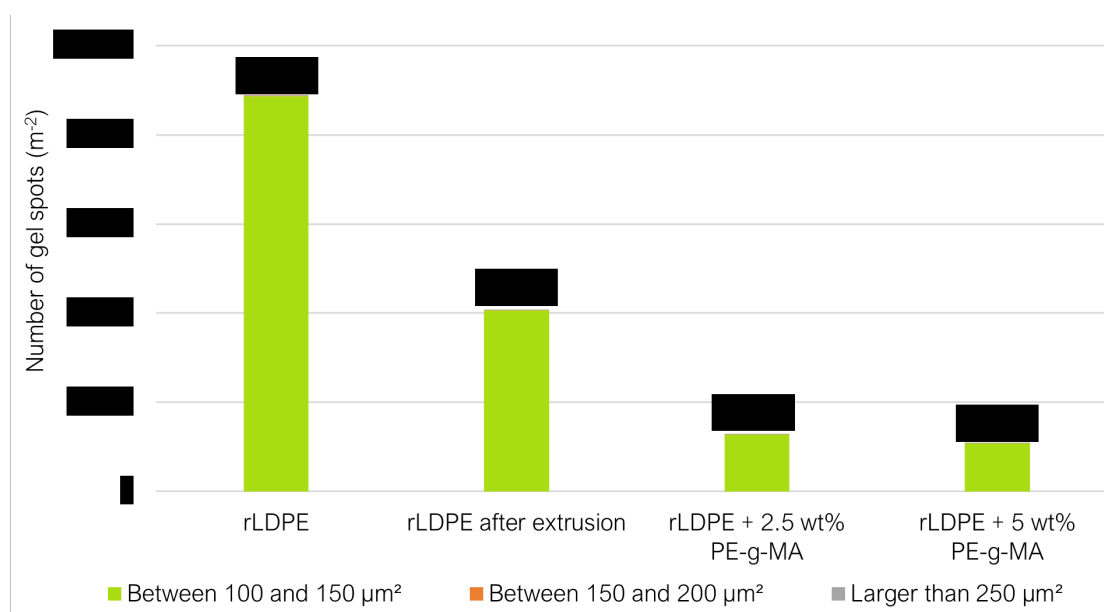


Figure 4.37: Average number of gel spots per m^2 of film for the references and formulations using rLDPE.

An important feat is the significant decline for both types of spots, with the addition of PE-g-MA. Since there cannot be more than 1 wt% of PA6 in the recycled stream, and there is a certain amount of PP present, it is interesting to see that the additive still managed to achieve that for which it was deployed.

For all of the results on black (or opaque) spots and gel spots, an important remark needs to be made. When a change in the number of spots is determined, this means the number of spots of that specific size range has evolved. This does not necessarily

mean that the whole spot has vanished; it might just as well mean that it has undergone a size transformation (in this case: gotten smaller, since the number of spots in larger categories does not increase). A decreasing number of spots should therefore also be interpreted as a better dispersion of impurities and gels throughout the polymer matrix.

4.8 Colorimetry

After turning the samples into film, the haze, L^* and YI were measured. The L^* value is a measure of whiteness or milkiness of the film. The higher the L^* , the whiter it is. The YI provides similar information, but for a yellow colouration. All values are stated together with the thickness of the film, to show whether or not a correlation exists. An important side note, though, is the fact that the thickness varies enormously throughout the film. For this reason, an average thickness was taken from multiple measurements, over the exact area that was to be analysed by the colorimeter. Although the average thickness turned out to be fairly constant, the standard deviation of the thickness remained substantial (about 20%). For the sake of clarity, the individual standard deviation values of the thickness are not depicted in the graphs.

First of all, in Figure 4.38, the average haze values are given for all references and formulations using virgin polymers.

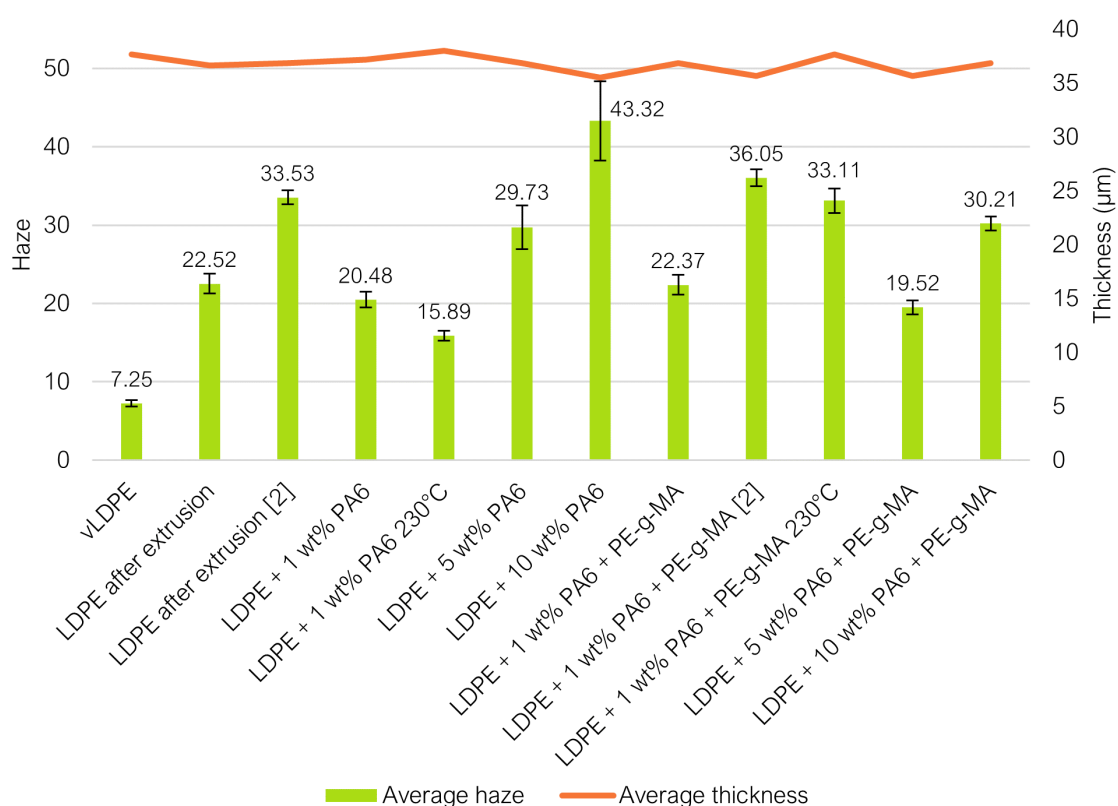


Figure 4.38: Haze and thickness values for the references and formulations using virgin polymers.

These results provide a number of takeaways about the development of haze during extrusion blowing. When looking at the haze of virgin LDPE, before and after an extrusion step, a huge difference is seen, of a factor 3-4. Furthermore, the virgin LDPE after extrusion shows a higher haze value than when 1 wt% of PA6 is added (especially in the second try), which seems utmost strange. The haze increases when the amount of PA6 is increased, which is in line with expectations. The same goes for the standard deviation, meaning the film gets less and less homogeneous, which is also in line with expectations.

Then, concerning the positive impact of compatibilization on haze, this seems to only be the case for higher PA6 contents (a rise in haze is seen after compatibilization for 1 wt% of PA6). It is unclear why the second measurement of the two samples yields such an increase in haze. Especially when looking at the thickness of the film, which was either the same or even lower for the second try. What becomes clear, though, is that the compatibilization has a positive influence on homogeneity, since the standard deviation remains constant throughout those blends.

Carrying out the extrusion blowing at higher temperatures seems to diminish the haze of the film. This is most likely because of better dispersion of PA6 throughout the matrix, since it is melted to a larger extent and will show much better flow.

For the same samples, the L^* values are shown in Figure 4.39.

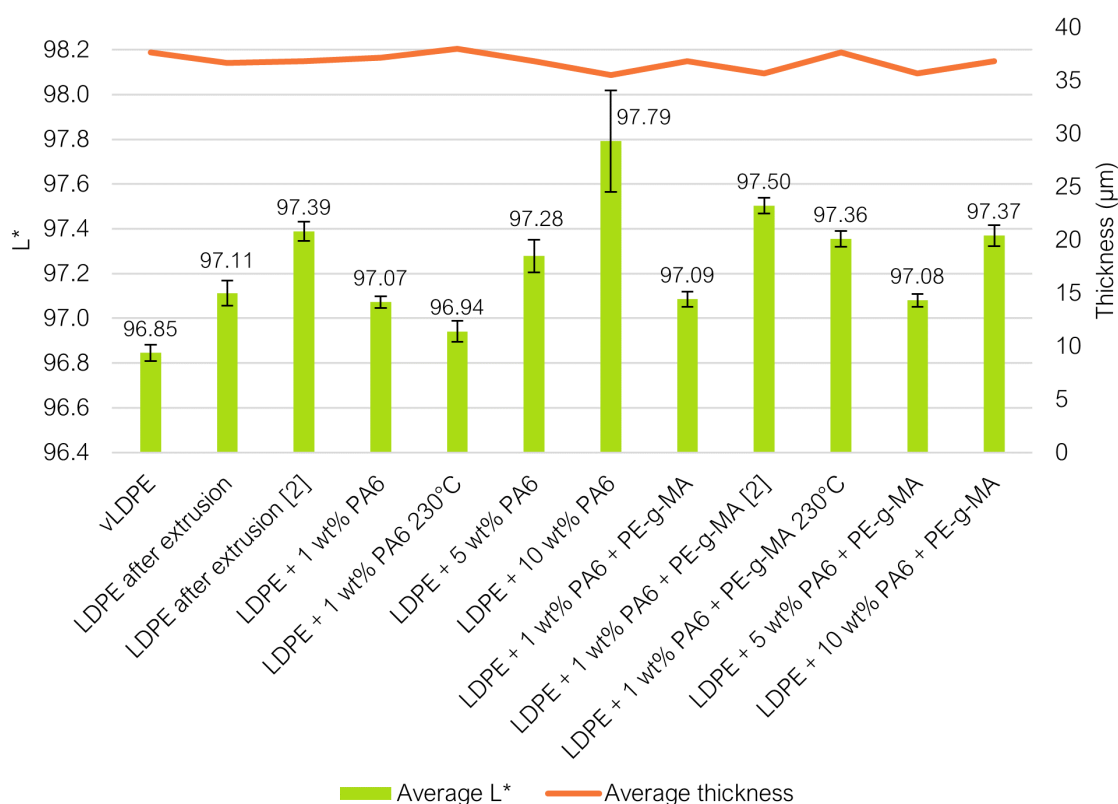


Figure 4.39: L^* and thickness values for the references and formulations using virgin polymers.

The first thing that strikes the eye, is the fact that the L^* shows the exact same trend throughout the different samples as the haze. This confirms what might have been obvious, the milkier a film turns, the less transparent it becomes. Furthermore, the same trend of standard deviation is noticeable throughout the three non-compatible LDPE/PA6 blends.

In Figure 4.40, the YI values are displayed. Most of previously seen trends are prevalent in this graph as well. For the first time, however, does the non-compatible blend with 1 wt% of PA6 not seem to show an inferior value to the LDPE after extrusion.

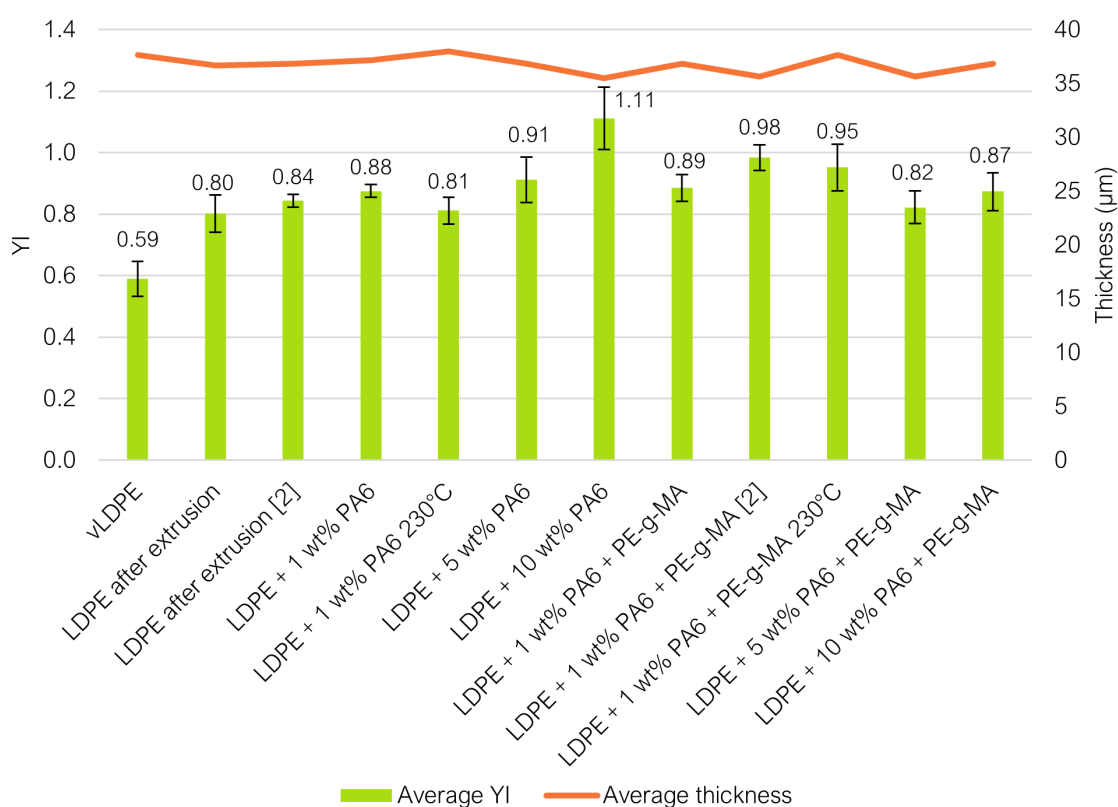


Figure 4.40: YI and thickness values for the references and formulations using virgin polymers.

Subsequently, the same graphs were made for the references and formulations using rLDPE. The first one, displaying haze, can be observed in Figure 4.41. Overall, there does not seem to be a great difference between all four samples. The haze does increase from the LDPE as received to the LDPE after extrusion, but so did the thickness, so it cannot be said with certainty. The haze seems to marginally increase upon extruding with additive, but the standard deviations overlap.

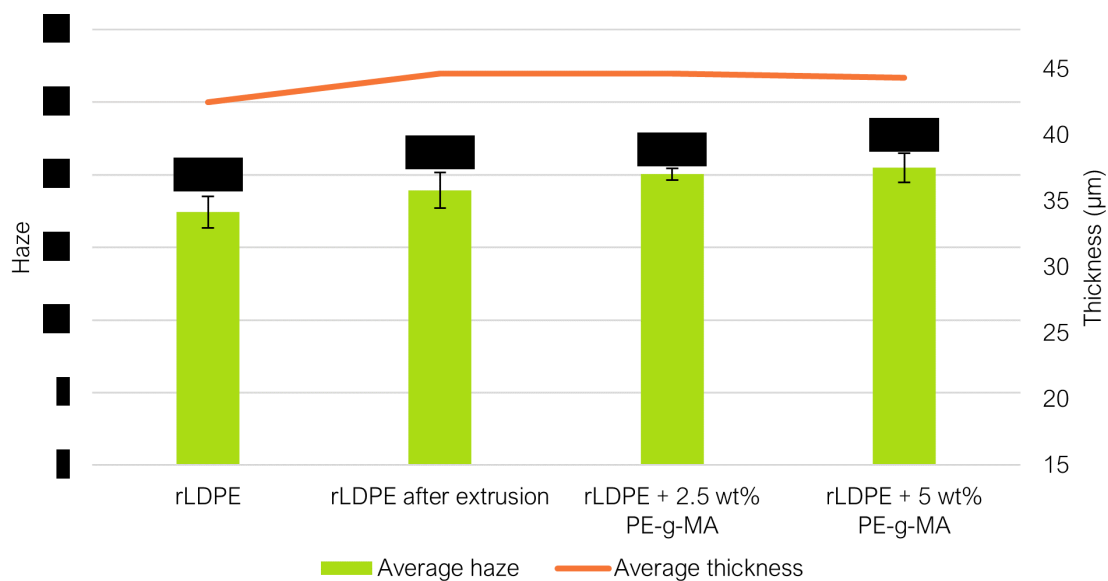


Figure 4.41: Haze and thickness values for the references and formulations using rLDPE.

The L^* values for the rLDPE are shown in Figure 4.42.

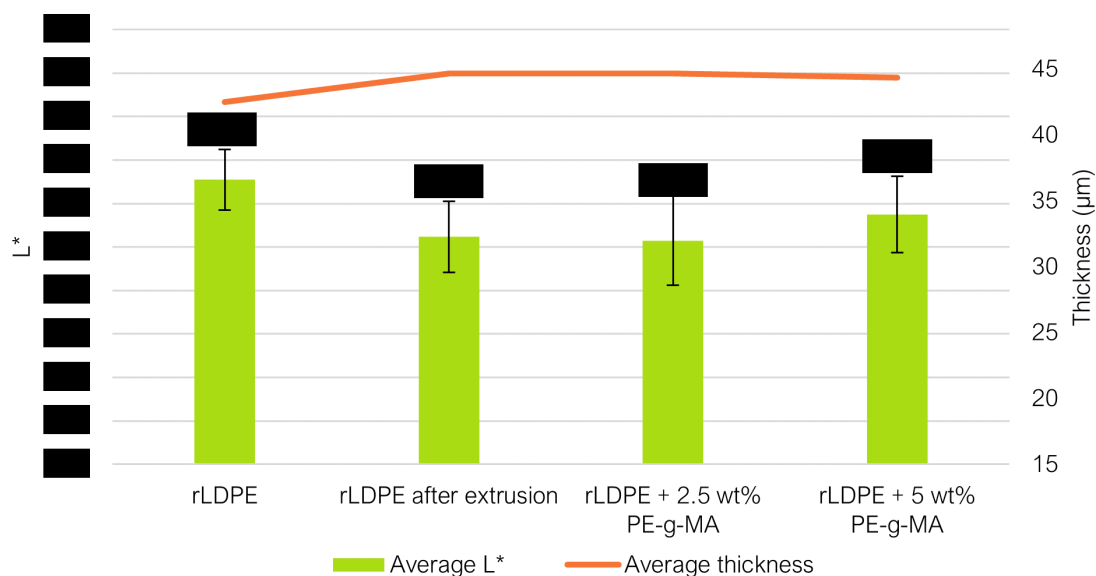


Figure 4.42: L^* and thickness values for the references and formulations using rLDPE.

The L^* value does not follow the same trend as the haze. After extrusion, the lightness decreases, even with (slightly) increasing film thickness. The additive does not seem to affect the L^* value much. What is noteworthy, though, is the larger variance than the one that was seen in Figure 4.40.

Finally, the YI values of the references and formulations using rLDPE follow in Figure 4.43.

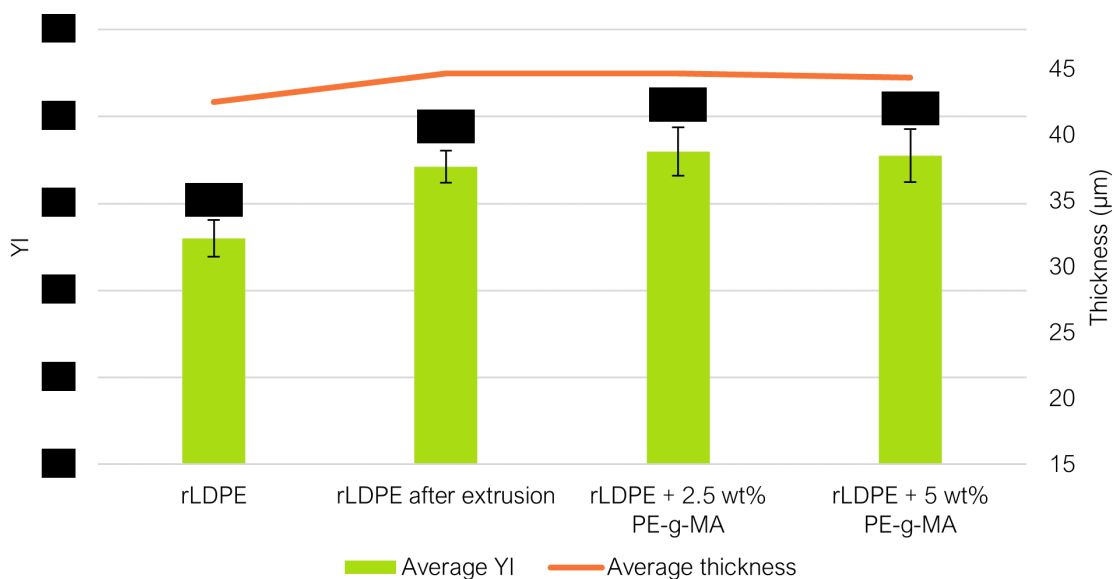


Figure 4.43: YI and thickness values for the references and formulations using virgin polymers.

Similarly to Figure 4.42, the value for YI seems to be affected by the extrusion itself, not by the additive with which it is extruded. An increase is seen for the LDPE after extrusion, after which it remains more or less constant for both additive quantities.

4.9 Tensile tests

The last characterisation method that was carried out to evaluate the effect of compatibilization, was tensile testing of the films. In this test, both the tensile strength and the deformation at break are given as output. As was mentioned in Chapter 3, this was done in both the machine direction and transverse direction.

In Figure 4.44 and Figure 4.45, the tensile strength and elongation at break values for both testing directions are displayed, for all references and formulations using virgin polymers.

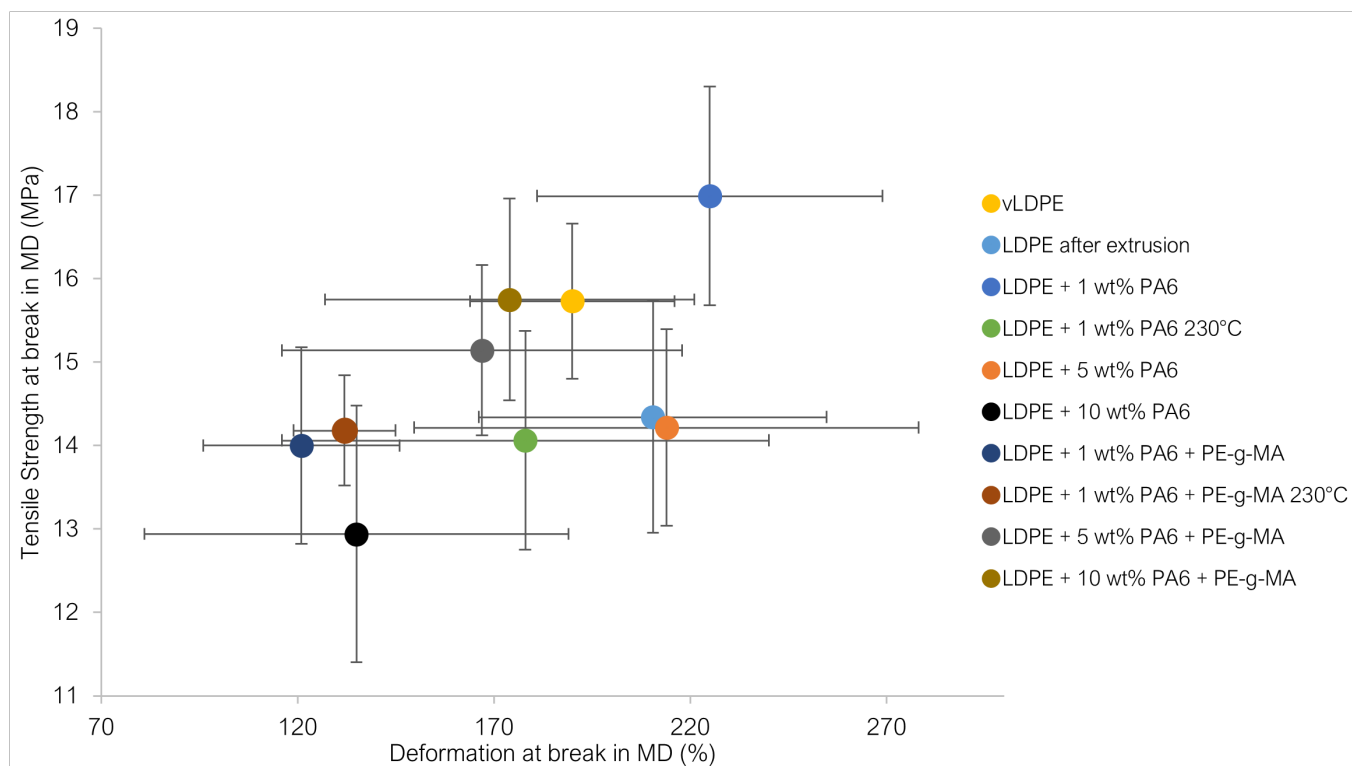


Figure 4.44: Values of tensile strength and elongation at break in machine direction of films of all references and formulations using virgin polymers.

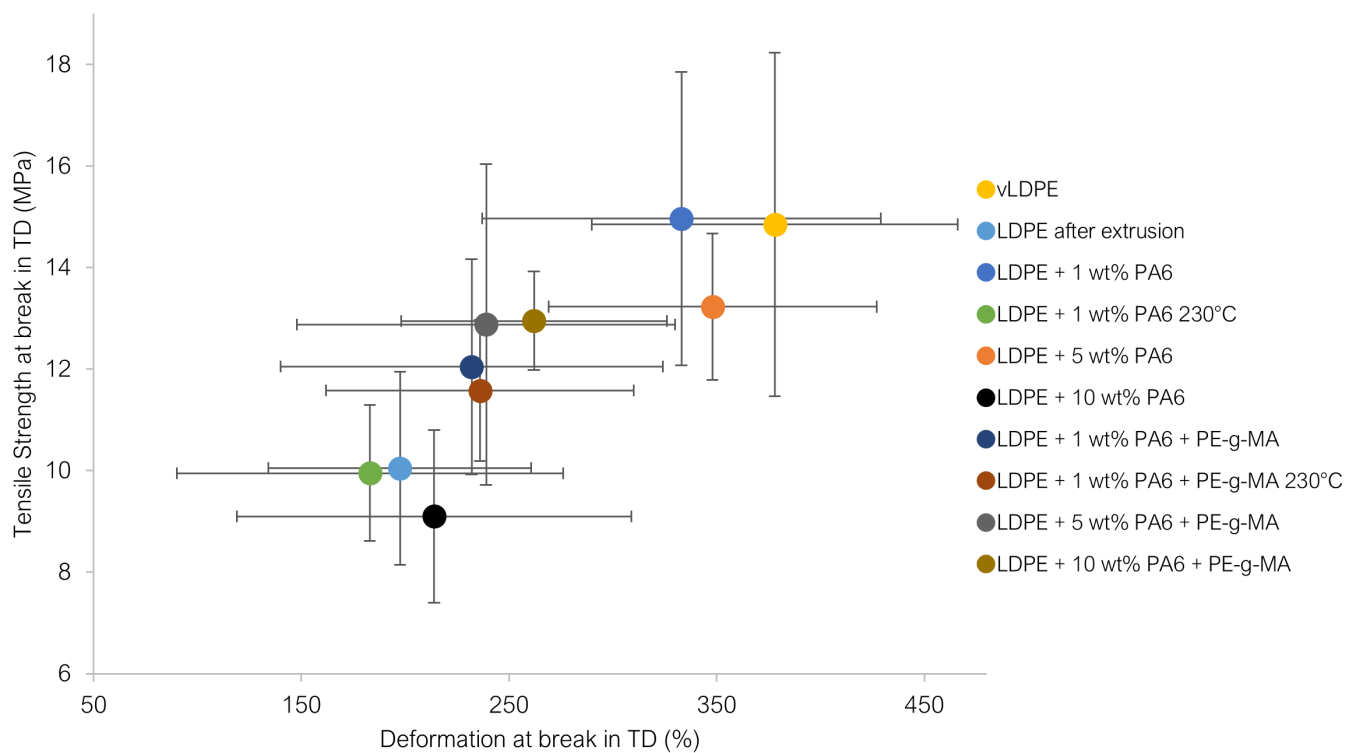


Figure 4.45: Values of tensile strength and elongation at break in transverse direction of films of all references and formulations using virgin polymers.

As expected, the virgin LDPE gives one of the best results, especially in TD. After merely one extrusion step, however, the mechanical properties show a vast decay. At first, this particular sample seemed to perform the lowest of all samples, for both directions. For this reason, it was tested again, giving entirely different results. In the figures, the average of the two tests is given. It does indicate, though, that the film might have inconsistent properties throughout its length.

The LDPE + 1 wt% PA6 sample shows a relatively high strength and EaB, in MD even larger than vLDPE. Perhaps there was no significant amount of PA6 present in the studied samples, yet this would be contradictory with the results of the gel and black spots measurement. A possible explanation could be that the PA6 at this quantity has a lubricating effect. For both directions, the sample with 5 wt% PA6 shows inferior properties and the one with 10 wt% even more so, following expectations. Bizarrely, the contrary is exhibited by the compatibilized blends; the one with 10 wt% PA6 shows the best results, followed by the 5 wt% sample. This phenomenon is more dominantly present in MD.

Comparing the reciprocal blends with one another, yields interesting results. For both directions, the 1 wt% sample shows superior properties before compatibilization, the ones containing 5 wt% are about the same and the one with 10 wt% is significantly better after compatibilization. It seems as though the compatibilization only starts to make a real difference at PA6 contents of at least 5 wt%. When recalling Figure 4.18, the exact same trend was observed between the three samples.

Performing the extrusion blowing at a higher temperature gives divergent results. Where it might have been expected to improve the mechanical properties due to better dispersion of PA6 in the LDPE, the contrary is the case for the non-compatibilized blend; their properties decrease deteriorate significantly for both directions. The compatibilized blends demonstrate something different, their values are nearly identical for both directions after extrusion blowing with both temperatures.

It should be noted that the standard deviations are very high overall. The measured values vary greatly among different specimen because the measurement is heavily dependent on external factors. Since the film is manually placed between the clamps, a variance will intrinsically be present between the exact vertical orientation of the samples. Furthermore, when the film is too thin, the clamps will not be able to hold it completely at its place and it can start to slide. When this happens excessively, it is obvious in the graph and the specimen is not considered. However, when it happens to a very small degree, it can go unnoticed while still affecting the result. All in all, the outcome of a tensile test on film looks to be highly volatile,

A clear difference can be seen between the results of both directions. The machine direction shows a higher tensile strength overall, while the transverse direction fails after a much larger elongation. This has everything to do with the orientation of the polymer chains as they exit the extruder, right before the melt is blown into film. The chains tend to

orient themselves along with the direction of flow, in order to minimise strain as they are pushed through the die. The chains will, therefore, generally be oriented more towards the machine direction rather than the transverse direction. Since the polymer poses the largest resistance in the direction parallel to its chains, a larger tensile strength will be seen for the MD tests. However, since most chains are already aligned in this direction, there will be less margin to pull them, resulting in a lower elongation when the film fails.

On the other hand, when the film is pulled in the transverse direction, most chains are not yet in their most stretched state, providing more leeway when pulling the film. The chains will be orienting them towards the direction of pulling for the whole duration of the test, which is why eventual elongation will be much higher by the time the chains are oriented parallel this direction. The strength of the film at this point, however, will be significantly lower since the polymer has to cover a higher length with the same amount of material.

In Figure 4.46 and Figure 4.47, the TS and EaB values are given of the films of all references and formulations using recycled PE. The LDPE before and after extrusion, show generally similar behaviour, although the EaB seems a little higher for LDPE in TD. Then, a significant improvement is seen upon addition of the PE-g-MA, for both directions. This improvement is continued when doubling the additive content, notably for MD.

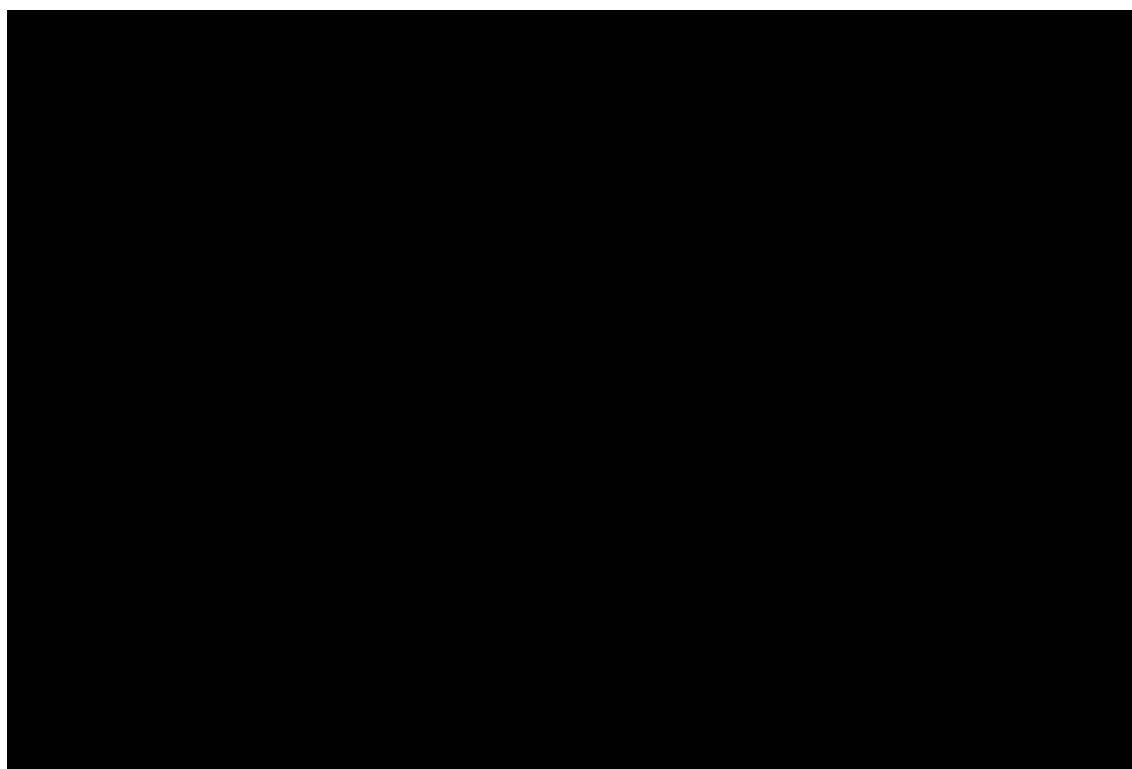


Figure 4.46: Values of tensile strength and elongation at break in machine direction of films of all references and formulations using rLDPE.

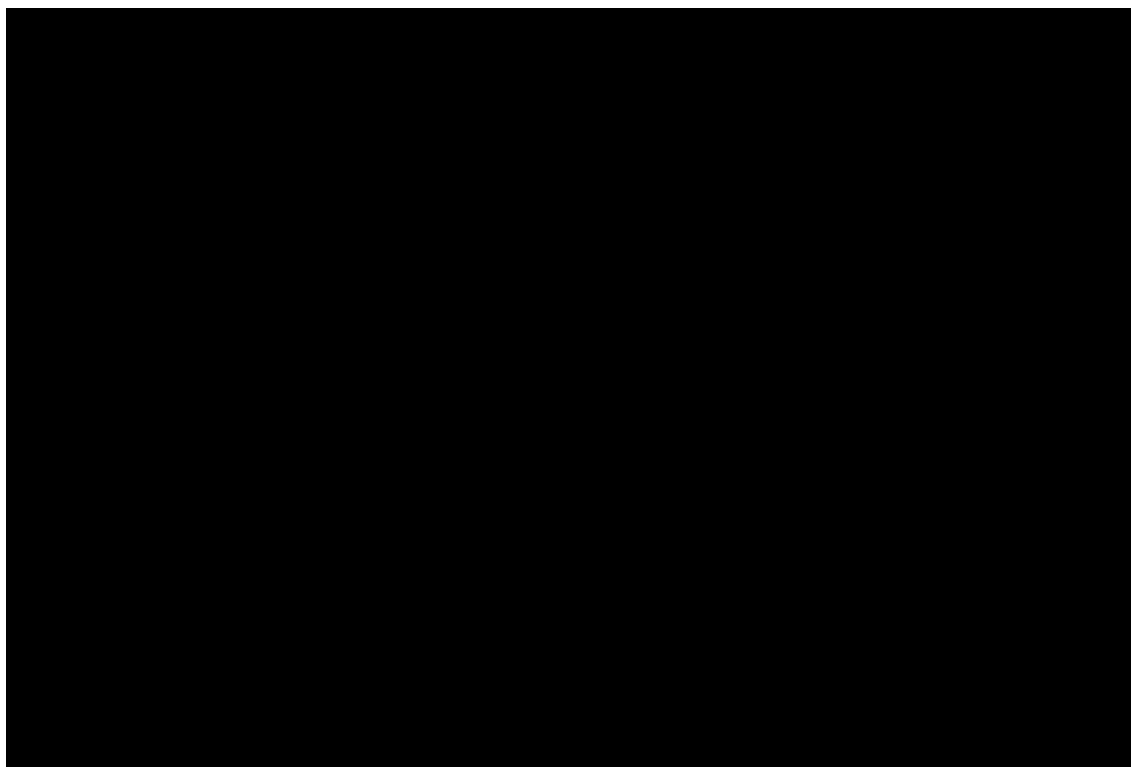


Figure 4.47: Values of tensile strength and elongation at break in transverse direction of films of all references and formulations using rLDPE.

4.10 Synthesis of results

In this section, an overall synthesis will be given of the results, with a focus on the mechanical and optical properties of the various samples as a result of compatibilization. This means that characterisation methods to quantify content or molecular structure/morphology (FTIR, DSC and SEM) will not be taken into account. In Table 4.1, the results of the four other characterisation experiments are summarised. The results that could be perceived as surprising, are underlined. The synthesis is set up to take on the structure of the two experimental research questions with regard to compatibilization.

Starting with the virgin polymer blends, the sample with 1 wt% of PA6 shows very little response to the compatibilizing additive. The MFI decreases, but only very slightly. The number of film defaults seems to rise marginally, showing the opposite of what was intended. It is possible that 1 wt% is simply not enough for the compatibilizing molecules to sufficiently find the PA6 molecules since the dispersion is very low and the blend is non-homogeneous. The PE-g-MA will in this case perhaps only contribute to the film spots, instead of counteracting them. Analogously, it might interfere with the molecular structure of the LDPE, causing the inferior tensile properties that were observed. All in all, the results of this sample were least in agreement with expectations, as pointed out by the full underlined row in Table 4.1.

The sample containing 5 wt% of PA6 gives varying results. The MFI values before and after compatibilization are identical, while both the number of film spots and the colorimetric values have decreased. The tensile tests do not show any significant response to compatibilization. It could be the case that for the MFI, a balance exists between the increased flow due to dispersion and the decreased flow due to high molecular weight complexes. Compatibilization is evidenced by the optical properties of the film. The drop in film defects might have been expected to improve the tensile properties of the film, but this is not clearly portrayed. The vast range in which the tensile test results are encountered, however, makes it difficult to base hard conclusions for this portion of the analysis.

For the 10 wt% sample the results are the most straightforward, also becoming clear from its designated row in Table 4.1. The MFI was greatly enhanced by compatibilization. However, as was mentioned in Section 4.4, the result might look entirely differently when the test is performed at a temperature at which the PA6 phase is allowed proper melting. In this context the augmentation is explicable, since the only partially molten PA6 will obstruct the flow to a much lesser degree, due to its increased dispersion. The monumental decrease of black and gel spots after compatibilization is noteworthy for this sample. As was mentioned in the Section 4.7, it does not inextricably mean that they have vanished; they can be more dispersed and smaller.

Moving on to the recycled PE samples, two different quantities of PE-g-MA were evaluated. The sample containing 2.5 wt% showed a consistent response to compatibilization throughout the conducted experiments. A drop in MFI was observed as compared to the non-compatibilized sample, possibly resulting from complex formation. Interestingly, the number of film defects showed a substantial reduction, while the colorimetric values either stayed the same or slightly increased. A plausible explanation could be that the gel and black spots are no (significant) contributors to the colorimetric values haze, YI and L*. The rLDPE already had a fairly brown colour to begin with (recall Figure 4.3), which might not be affected much by the degree of dispersion of PP and (possibly) other polymer contaminants. Finally, an amelioration in tensile properties was seen upon compatibilization, which is a promising result.

Doubling the PE-g-MA quantity to 5 wt% with the rLDPE leads to a further continuation of all observations stated in the previous paragraph. This also becomes clear from Table 4.1, where a comparison of this sample is outlined with the two precedent ones. It seems that having more additive in the system leads to a slightly better compatibilization. However, the effect is much less between the two samples with additive than between either of the two with the non-compatibilized rLDPE (the curves for MFI, film spots and tensile properties all flatten out). Therefore, 5 wt% is likely not far from the optimal quantity for this batch of rLDPE. Similarly to before, the colorimetric values did not exhibit any change.

Sample	Compared to:	MFI	Gel/black spots	Haze, L*, YI	Tensile strength/EaB
vLDPE					
LDPE after extrusion	vLDPE	<u>Decrease</u>	Increase	Increase	<u>No difference</u>
LDPE + 1 wt% PA6	LDPE after extrusion	Increase	Increase	<u>Decrease</u>	<u>Increase</u>
LDPE + 1 wt% PA6 230 °C	LDPE + 1 wt% PA6		Decrease	Decrease	<u>Decrease</u>
LDPE + 5 wt% PA6	LDPE + 1 wt% PA6	Decrease	Increase	Increase	Decrease
LDPE + 10 wt% PA6	LDPE + 5 wt% PA6	Decrease	Increase	Increase	Decrease
LDPE + 1 wt% PA6 + PE-g-MA	LDPE + 1 wt% PA6	<u>Decrease</u>	<u>Increase</u>	<u>No difference</u>	<u>Decrease</u>
LDPE + 1 wt% PA6 + PE-g-MA 230 °C	LDPE + 1 wt% PA6 + PE-g-MA		<u>Increase</u>	Decrease	<u>No difference</u>
LDPE + 5 wt% PA6 + PE-g-MA	LDPE + 5 wt% PA6	<u>No difference</u>	Decrease	Decrease	<u>No difference</u>
LDPE + 10 wt% PA6 + PE-g-MA	LDPE + 10 wt% PA6	Increase	Decrease	Decrease	Increase

Table 4.1: Summary of trends in mechanical and optical properties of the samples discussed in this chapter.

Conclusion and recommendations

5.1 Conclusion

The goal of this study was to research the effects of compatibilizing virgin LDPE with polymer impurities as well as recycled industrial PE film, through reactive extrusion. As the basis for this, a literature review of the current state-of-the-art on the reactive compatibilization of (recycled) PE-containing polymer blends through reactive extrusion was created. What follows first, are the answers to the research questions regarding the literature review.

Which main types of PE exist and what are their characteristics?

A number of different types of PE are distinguished based on their density, which largely follows from their production process. Their difference in microscopic structure causes them to have distinct mechanical properties, which are outlined in Table 2.1.

With which immiscible polymers is PE usually mixed in plastic industrial film waste and what causes the immiscibility?

PE materials constitute the largest group of plastic materials that are used globally. Their main application is film material. Since the majority of plastic use concerns packaging, the PE demand is tremendously high. However, due to the design of packaging becoming continuously more complex, PE often finds itself thoroughly mixed with PET, PP and PA6 at its EoL. Because of structural differences, the free energy of mixing is nearly never equal to zero for blends of these polymers. Intermolecular forces are therefore needed to ensure miscibility.

Which types of polymer compatibilization exist and what is their current state-of-the-art?

Compatibilization of a polymer blend is rendering the two phases miscible with one another. Reactive compatibilization does so by means of chemically altering at least one of the polymers. Reactive copolymers covalently bind to one polymer in the blend, while being miscible with the other. This way, interfacial tension are significantly lowered and the blend is homogenised. These copolymers can be block copolymers (Table 2.3), mostly using a GMA block, or grafted copolymers (Table 2.4), mostly using an MA group, to bind to the hydroxide or ester group of a polar polymer. A third method of reactive compatibilization is chain functionalisation. Here, a polymer is converted to a

macroradical, after which a chain crosslink, an indirect crosslink or an attached functional group can cause compatibilization.

What does the reactive extrusion process look like?

Reactive extrusion is a means to combine polymer chemistry with polymer processing. A conventional twin-screw extruder can be used for the reactive compatibilization of polymers, after which it can directly be processed into the desired material, as would happen with a pure polymer. The twin-screw extruder consists of several different zones: feeding, melting, side-feeding, dispersing, homogenising, degassing and discharging. The zones are each associated with particular screw characteristics.

How is the reactive extrusion process carried out for polymer compatibilization in the current state-of-the-art?

A huge range of different extruders, with different screw dimensions, are used for the reactive compatibilization of PE-containing blends. The extruder present at SUEZ falls nicely within this range. The barrel temperature varies for the melting temperature of the different polymers that are blended. As for the screw speed, there seems to be no general consensus as to which value seems to be best. The difference between certain studies is as much as an order of magnitude. It can therefore be said that the process is highly empirical and not based on theory and correlations.

The *in-situ* grafting reaction is highly reliant on reactions conditions such as temperature and screw speed (determining residence time). The course of the decomposition reaction of the initiator determines the success of the experiment. Using the rate law of the (first order) decomposition reaction, an equation can be established for the rate constant. This constant can be calculated based on the peroxide and reaction conditions. Through the rate constant, the peroxide level at the end of extruder can be estimated, providing valuable information for the experiment.

Hereafter, the answers follow to the research questions with regard to the experimental work.

What is the effect on the mechanical and optical properties of compatibilizing virgin LDPE and PA6 of different compositions through reactive extrusion?

The effect on the mechanical and optical properties of compatibilizing virgin LDPE and PA6 of different compositions through reactive extrusion was determined. For 1 wt% of PA6, the response to compatibilization is negligible. For 5 wt% of PA6, the effect is significant for the optical properties of produced film, and slightly less so for the mechanical properties. Then, for 10 wt% of PA6, the effects are monumental for the optical properties of the film, as well as being substantial for the mechanical properties. The compatibilizing effect was also made visible through SEM for this blend. All in all, it can be concluded that the compatibilizing effect of PE-g-MA in LDPE/PA6 blends grows importance with increasing PA6 content, with a threshold value for having effect between 1 and 5 wt%.

the amount of specimen per sample analysed through DSC, should be higher. Two 10 mg samples out of a 2 kg batch proved to be insufficient for the detection of 1 wt% of PA6. This number can be increased to five, or even ten, for a more accurate evaluation of the contents in the rLDPE.

Then, the reader might have noticed the discrepancy between the listed materials in Section 3.1 and the results in Chapter 4. Due to time constraints, the formulations destined for *in situ* compatibilization were not carried out. This does not mean that this part is less relevant; this approach might serve as much more economically interesting alternative due to the one-step extrusion method and no reliability on costly pre-grafted additives. This one-step extrusion method has not yet been examined to achieve chain functionalisation by means of functional group attachment. If the grafting of the monomer to the PE can happen simultaneously to the compatibilization with a polymer impurity, an entire step in the process can be omitted. This is of course economically and energetically advantageous, but another large benefit is not having to subject the polymers to a second extrusion step, unnecessarily inflecting degradation and thereby weakening the material. On top of this, the peroxide might lead to an additional compatibilizing effect between the PP and PE by means of chain crosslinking, which has been pursued by other studies found in literature.

As was mentioned in Section 2.3.3, though, this approach is much more delicate when it comes to process conditions. The calculations for peroxides decomposition kinetics ought to serve as guideline for this research. Several variables in this process should again be subject of scrutiny. The temperature and screw speed during extrusion, changes of which will likely be highly impactful. Of course, the amount of both peroxide and monomer will need to be varied. This can be done through a threefold experiment: two parts where one additive is changed and the other is kept constant, and a third one where both are changed. Combining the results of this experiment might yield great insight in the optimal additive quantities.

If the *in situ* compatibilization approach is to be pursued, the different formulations using DBPB and MA as stated in Section 3.1, are the recommended starting point. Recalling the Arrhenius constants for DBPB and Equation 2.13, it follows that at the current conditions of extruding (300 rpm, 230 °C), the peroxide would decompose too quickly. Assuming the residual peroxide quantity should be between 0 and 1 % at the die, the temperature should be changed to 200 °C (which was the example used in Section 2.3.3). Some adjustments will have to be made to other parts of the extrusion line, such as feed rate and pulling speed of the pelletizer.

It should be noted that the temperature has a much larger effect on the residual peroxide quantity than the screw speed, due to the exponential term in the Arrhenius equation. If a temperature of 230 °C is used, a residence time of around 5 seconds would be needed to satisfy the aforementioned residual peroxide requirement. This is practically impossible, since the extruder is not able to reach such screw speeds (see Appendix A), but more

importantly, the polymer would never have time to melt and no reaction could ever take place. It is therefore recommended that the extrusion temperature is tweaked first.

Then, a massive role in reactive extrusion is played by the design of the screw. The design that was used in this study was not intended for reactive extrusion specifically. Naturally, if no reaction is expected to take place in the extruder and the aim is merely to melt and homogenise, then a different screw set-up might be expected than when a precise reaction needs to occur. Certain screw elements might exert excessive pressure on some of the additives, causing them to behave distortedly. Or perhaps several modules that cause back-flow are needed, in order to increase residence time at a certain screw speed. A new study ought to take place, where the ideal screw design is developed for reactive extrusion in this particular extruder.

Finally, further research is most definitely needed on suitable monomers for chain functionalisation. MA and GMA seem to be only monomers that are commonly employed in literature. However, both of these compounds are categorised to be CMR^[157,158]. This almost immediately implies insurmountable difficulties in translating the process to an industrial scale. The safety procedures that are in place in plastic recycling plants would have to undergo massive changes. Safety and health measures would need to be created for all workers that handle the compounds, as well as all personnel working in the direct vicinity. Additionally, depending on the quantities of CMR compounds managed and stored at the plant, appropriate measures would have to be put in place regarding hazards, possibly involving public authorities.

References

- [1] Recyclon. (2020). *LDPE Granulates*. Retrieved January 19, 2023, from <http://recyklon.pl/en/offer.html>
- [2] Global Sources. (2023). *Recycle LDPE 80-20 Plastic Scrap LDPE Film*. Retrieved January 19, 2023, from https://www.globalsources.com/product/ldpe-recycled-plastic-scrap_1186724836f.htm
- [3] Richel, A. (2021, November 10). *Plastics and bioplastics: a 200-year history of research and development*. Retrieved June 5, 2022, from <http://www.chem4us.be/plastics-and-bioplastics-a-200-year-history-of-research-and-development/>
- [4] Geyer, R. (2020). A Brief History of Plastics. In M. Streit-Bianchi, M. Cimadevila & W. Tretnak (Eds.), *Mare plasticum - the plastic sea: Combatting plastic pollution through science and art* (pp. 31–47). Springer International Publishing. https://doi.org/10.1007/978-3-030-38945-1_2
- [5] Cabernard, L., Pfister, S., Oberschelp, C., & Hellweg, S. (2022). Growing environmental footprint of plastics driven by coal combustion. *Nature Sustainability*, 5, 139–148. <https://doi.org/10.1038/s41893-021-00807-2>
- [6] Jambeck, J. R., Geyer, R., Wilcox, C., Siegler, T. R., Perryman, M., Andrady, A., Narayan, R., & Law, K. L. (2015). Plastic waste inputs from land into the ocean. *Science*, 347(6223), 768–771. <https://doi.org/10.1126/science.1260352>
- [7] Kosior, E., & Mitchell, J. (2020). Chapter 6 - Current industry position on plastic production and recycling. In T. M. Letcher (Ed.), *Plastic Waste and Recycling* (pp. 133–162). Academic Press. <https://doi.org/10.1016/B978-0-12-817880-5.00006-2>
- [8] European Commission. (2018a). *Directive (EU) 2018/852 of the European Parliament and of the Council of 30 May 2018 amending Directive 94/62/EC on packaging and packaging waste*. Retrieved December 19, 2022, from <https://eur-lex.europa.eu/legal-content/EN/TXT/?uri=celex:32018L0852>
- [9] Plastics Europe. (2021). *Plastics - the Facts 2021*. <https://plasticseurope.org/wp-content/uploads/2021/12/Plastics-the-Facts-2021-web-final.pdf>
- [10] Plastics recyclers europe. (2020). Report on plastics recycling statistics 2020. https://www.plasticsrecyclers.eu/_files/ugd/dda42a_2544b63cfb5847e39034fadafbac71bf.pdf
- [11] Sudhakar, M., Doble, M., Murthy, P. S., & Venkatesan, R. (2008). Marine microbe-mediated biodegradation of low- and high-density polyethylenes. *International Biodeterioration & Biodegradation*, 61(3), 203–213. <https://doi.org/10.1016/j.ibiod.2007.07.011>
- [12] Cornwall, W. (2021). The plastic eaters. *Science*, 373(6550), 36–39. <https://doi.org/10.1126/science.373.6550.36>
- [13] Letcher, T. (2020). *Plastic Waste and Recycling: Environmental Impact, Societal Issues, Prevention, and Solutions*. Elsevier Science. https://books.google.nl/books?id=Ma%5C_SDwAAQBAJ

- [14] Caresana. (2020). *Market Study: Polyethylene LDPE (3rd edition)*. <https://www.ceresana.com/en/market-studies/plastics/polyethylene-ldpe>
- [15] Kaiser, K., Schmid, M., & Schlummer, M. (2018). Recycling of Polymer-Based Multilayer Packaging: A Review. *Recycling*, 3(1). <https://doi.org/10.3390/recycling3010001>
- [16] Ghosh, A. (2021). Performance modifying techniques for recycled thermoplastics. *Resources, Conservation and Recycling*, 175, 105887. <https://doi.org/10.1016/j.resconrec.2021.105887>
- [17] Lahtela, V., Silwal, S., & Kärki, T. (2020). Re-Processing of Multilayer Plastic Materials as a Part of the Recycling Process: The Features of Processed Multilayer Materials. *Polymers*, 12(11), 2517. <https://doi.org/10.3390/polym12112517>
- [18] Feldman, D. (2005). Polyblend Compatibilization. *Journal of Macromolecular Science, Part A*, 42(5), 587–605. <https://doi.org/10.1081/MA-200056331>
- [19] Tzoganakis, C. (1989). Reactive extrusion of polymers: A review. *Advances in Polymer Technology*, 9(4), 321–330. <https://doi.org/10.1002/adv.1989.060090406>
- [20] Cabrera, G., Li, J., Maazouz, A., & Lamnawar, K. (2022). A Journey from Processing to Recycling of Multilayer Waste Films: A Review of Main Challenges and Prospects. *Polymers*, 14(12). <https://doi.org/10.3390/polym14122319>
- [21] Ragaert, K., Delva, L., & Van Geem, K. (2017). Mechanical and chemical recycling of solid plastic waste. *Waste Management*, 69, 24–58. <https://doi.org/10.1016/j.wasman.2017.07.044>
- [22] Horodytska, O., Valdés, F., & Fullana, A. (2018). Plastic flexible films waste management – A state of art review. *Waste Management*, 77, 413–425. <https://doi.org/10.1016/j.wasman.2018.04.023>
- [23] Acomb, J. C., Wu, C., & Williams, P. T. (2014). Control of steam input to the pyrolysis-gasification of waste plastics for improved production of hydrogen or carbon nanotubes. *Applied Catalysis B: Environmental*, 147, 571–584. <https://doi.org/10.1016/j.apcatb.2013.09.018>
- [24] Fazil, A., Kumar, S., & Mahajani, S. M. (2022). Downdraft co-gasification of high ash biomass and plastics. *Energy*, 243, 123055. <https://doi.org/10.1016/j.energy.2021.123055>
- [25] Farooq, A., Moogi, S., Jang, S.-H., Kannapu, H. P. R., Valizadeh, S., Ahmed, A., Lam, S. S., & Park, Y.-K. (2021). Linear low-density polyethylene gasification over highly active Ni/CeO₂-ZrO₂ catalyst for enhanced hydrogen generation. *Journal of Industrial and Engineering Chemistry*, 94, 336–342. <https://doi.org/10.1016/j.jiec.2020.11.005>
- [26] Kannan, P., Al Shoaibi, A., & Srinivasakannan, C. (2014). Process simulation and sensitivity analysis of waste plastics gasification in a fluidized bed reactor. *WIT Transactions on State-of-the-art in Science and Engineering*, 84, 177–186. <https://doi.org/10.495/WM120171>

- [27] Farooq, A., Song, H., Park, Y.-K., & Rhee, G. H. (2021). Effects of different Al₂O₃ support on HDPE gasification for enhanced hydrogen generation using Ni-based catalysts [Special issue on the 2nd International Symposium on Hydrogen Energy and Energy Technologies (HEET 2019)]. *International Journal of Hydrogen Energy*, 46(34), 18085–18092. <https://doi.org/10.1016/j.ijhydene.2020.05.199>
- [28] Lopez, G., Erkiaga, A., Artetxe, M., Amutio, M., Bilbao, J., & Olazar, M. (2015). Hydrogen Production by High Density Polyethylene Steam Gasification and In-Line Volatile Reforming. *Industrial & Engineering Chemistry Research*, 54(39), 9536–9544. <https://doi.org/10.1021/acs.iecr.5b02413>
- [29] Cho, I. J., Park, H.-W., Park, D.-W., & Choi, S. (2015). Enhancement of synthesis gas production using gasification-plasma hybrid system. *International Journal of Hydrogen Energy*, 40(4), 1709–1716. <https://doi.org/10.1016/j.ijhydene.2014.12.007>
- [30] Vollmer, I., Jenks, M. J. F., Roelands, M. C. P., White, R. J., van Harmelen, T., de Wild, P., van der Laan, G. P., Meirer, F., Keurentjes, J. T. F., & Weckhuysen, B. M. (2020). Beyond Mechanical Recycling: Giving New Life to Plastic Waste. *Angewandte Chemie International Edition*, 59(36), 15402–15423. <https://doi.org/10.1002/anie.201915651>
- [31] Al-Salem, S., Lettieri, P., & Baeyens, J. (2009). Recycling and recovery routes of plastic solid waste (PSW): A review. *Waste Management*, 29(10), 2625–2643. <https://doi.org/10.1016/j.wasman.2009.06.004>
- [32] European Commission. (n.d.). *Waste Framework Directive*. Retrieved December 19, 2022, from https://environment.ec.europa.eu/topics/waste-and-recycling/waste-framework-directive_en
- [33] European Commission. (2018b). *Landfill waste*. Retrieved December 19, 2022, from https://environment.ec.europa.eu/topics/waste-and-recycling/landfill-waste_en
- [34] Rouch, D. (2021). Plastic future: How to reduce the increasing environmental footprint of plastic packaging. https://www.researchgate.net/publication/337506127_Plastic_future_How_to_reduce_the_increasing_environmental_footprint_of_plastic_packaging
- [35] Fellows, P. (2009). 25 - Packaging. In P. Fellows (Ed.), *Food Processing Technology (Third Edition)* (Third Edition, pp. 713–781). Woodhead Publishing. <https://doi.org/10.1533/9781845696344.5.713>
- [36] TART. (2011). *Polyethylene (PE) Foils*. Retrieved June 8, 2022, from <https://www.tart.eu/en/products/packaging-materials/pe-foils>
- [37] Parker Hannifin Corporation. (unknown). *Polyethylene Instrument Grade Tubing - E/EB Series*. Retrieved June 8, 2022, from <https://ph.parker.com/us/fr/polyethylene-instrument-grade-tubing-e-eb-series>
- [38] CROW polymer database. (n.d.). *Polyolefins (polyalkenes)*. Retrieved April 12, 2022, from <https://polymerdatabase.com/polymer%5C%20classes/Polyolefin%20type.html>
- [39] Jeremic, D. (2014). Polyethylene. In *Ullmann's Encyclopedia of Industrial Chemistry* (pp. 1–42). John Wiley & Sons, Ltd. https://doi.org/10.1002/14356007.a21_487.pub3

- [40] Biron, M. (2020). 10 - Transition of Plastics to Renewable Feedstock and Raw Materials: Bioplastics and Additives Derived From Natural Resources. In M. Biron (Ed.), *A Practical Guide to Plastics Sustainability* (pp. 469–555). William Andrew Publishing. <https://doi.org/10.1016/B978-0-12-821539-5.00010-0>
- [41] Pruitt, L. (2017). 1.23 - Load-Bearing Medical Polymers (Non-Degradable). In P. Ducheyne (Ed.), *Comprehensive Biomaterials II* (pp. 507–515). Elsevier. <https://doi.org/10.1016/B978-0-12-803581-8.10214-0>
- [42] Hato, M. J., & Luyt, A. S. (2007). Thermal fractionation and properties of different polyethylene/wax blends. *Journal of Applied Polymer Science*, 104(4), 2225–2236. <https://doi.org/10.1002/app.25494>
- [43] SUEZ France. (2019). *L'usine de Landemont & le recyclage des films plastiques - SUEZ France (video)*. Retrieved December 19, 2022, from https://www.youtube.com/watch?v=F2hN7Cp8EJY&ab_channel=SUEZFrance
- [44] Nofar, M. (2021). Chapter 2 - Introduction to polymer blends. In M. Nofar (Ed.), *Multiphase Polylactide Blends* (pp. 17–96). Elsevier. <https://doi.org/10.1016/B978-0-12-824150-9.00002-9>
- [45] Fink, J. K. (2018). 16 - Compatibilization. In J. K. Fink (Ed.), *Reactive Polymers: Fundamentals and Applications (Third Edition)* (Third Edition, pp. 497–546). William Andrew Publishing. <https://doi.org/10.1016/B978-0-12-814509-8.00016-6>
- [46] David, D., & Sincock, T. (1992). Estimation of miscibility of polymer blends using the solubility parameter concept. *Polymer*, 33(21), 4505–4514. [https://doi.org/10.1016/0032-3861\(92\)90406-M](https://doi.org/10.1016/0032-3861(92)90406-M)
- [47] Ajitha A.R. & Thomas, S. (2020). Chapter 1 - Introduction: Polymer blends, thermodynamics, miscibility, phase separation, and compatibilization. In A. A.R. & S. Thomas (Eds.), *Compatibilization of Polymer Blends* (pp. 1–29). Elsevier. <https://doi.org/10.1016/B978-0-12-816006-0.00001-3>
- [48] Li, J., Shanks, R. A., & Long, Y. (2000). Mechanical properties and morphology of polyethylene–polypropylene blends with controlled thermal history. *Journal of Applied Polymer Science*, 76(7), 1151–1164. [https://doi.org/10.1002/\(SICI\)1097-4628\(20000516\)76:7<1151::AID-APP19>3.0.CO;2-H](https://doi.org/10.1002/(SICI)1097-4628(20000516)76:7<1151::AID-APP19>3.0.CO;2-H)
- [49] Zhao, L., & Choi, P. (2006). A Review of the Miscibility of Polyethylene Blends. *Materials and Manufacturing Processes*, 21(2), 135–142. <https://doi.org/10.1081/AMP-200068644>
- [50] Muthuraj, R., Misra, M., & Mohanty, A. (2015). 5 - Studies on mechanical, thermal, and morphological characteristics of biocomposites from biodegradable polymer blends and natural fibers. In M. Misra, J. K. Pandey & A. K. Mohanty (Eds.), *Biocomposites* (pp. 93–140). Woodhead Publishing. <https://doi.org/10.1016/B978-1-78242-373-7.00014-7>
- [51] Subramanian, M. N. (2017). *Polymer blends and composites: chemistry and technology*. John Wiley & Sons. <https://doi.org/10.1002/9781119383581.ch5>
- [52] Shanks, R. A. (2020). Chapter 2 - Concepts and classification of compatibilization processes. In A. A.R. & S. Thomas (Eds.), *Compatibilization of Polymer Blends* (pp. 31–56). Elsevier. <https://doi.org/10.1016/B978-0-12-816006-0.00002-5>

- [53] Spalding, M., Garcia-Meitin, E., Kodjie, S., Campbell, G., & Womer, T. (2017). Troubleshooting and mitigating gels in polyethylene film products. *Journal of Plastic Film Sheeting*, 34, 875608791772258. <https://doi.org/10.1177/8756087917722586>
- [54] Imre, B., & Pukánszky, B. (2013). Compatibilization in bio-based and biodegradable polymer blends. *European Polymer Journal*, 49(6), 1215–1233. <https://doi.org/10.1016/j.eurpolymj.2013.01.019>
- [55] Coleman, E. A. (2011). 23 - Plastics Additives. In M. Kutz (Ed.), *Applied Plastics Engineering Handbook* (pp. 419–428). William Andrew Publishing. <https://doi.org/10.1016/B978-1-4377-3514-7.10023-6>
- [56] Heino, M., Kirjava, J., Hietaoja, P., & A Seppälä, J. (1997). Compatibilization of polyethylene terephthalate/polypropylene blends with styrene–ethylene/butylene–styrene (SEBS) block copolymers. *Journal of Applied Polymer Science*, 65(2), 241–249. [https://doi.org/10.1002/\(SICI\)1097-4628\(19970711\)65:2<241::AID-APP4>3.0.CO;2-O](https://doi.org/10.1002/(SICI)1097-4628(19970711)65:2<241::AID-APP4>3.0.CO;2-O)
- [57] Zhang, Y., Zhang, H., Yu, Y., Guo, W., & Wu, C. (2009). Recycled poly(ethylene terephthalate)/linear low-density polyethylene blends through physical processing. *Journal of Applied Polymer Science*, 114(2), 1187–1194. <https://doi.org/10.1002/app.30030>
- [58] Lei, Y., Wu, Q., Clemons, C. M., & Guo, W. (2009a). Phase structure and properties of poly(ethylene terephthalate)/high-density polyethylene based on recycled materials. *Journal of Applied Polymer Science*, 113(3), 1710–1719. <https://doi.org/10.1002/app.30178>
- [59] SUEZ France. Additives for improving recycled plastics properties. *Internal report*.
- [60] Chen, R. S., Ab Ghani, M. H., Salleh, M. N., Ahmad, S., Gan, S., et al. (2014). Influence of blend composition and compatibilizer on mechanical and morphological properties of recycled HDPE/PET blends. *Materials Sciences and Applications*, 5(13), 943. <https://doi.org/10.4236/msa.2014.513096>
- [61] Correnti, A., Bocchino, M., Filippi, S., Magagnini, P. L., Polacco, G., & La Mantia, F. P. (2005). Recycling of inside upholstery of end-of-life cars. *Journal of Applied Polymer Science*, 96(5), 1716–1728. <https://doi.org/10.1002/app.21638>
- [62] Lei, Y., Wu, Q., & Zhang, Q. (2009b). Morphology and properties of microfibrillar composites based on recycled poly (ethylene terephthalate) and high density polyethylene. *Composites Part A: Applied Science and Manufacturing*, 40(6), 904–912. <https://doi.org/10.1016/j.compositesa.2009.04.017>
- [63] Li, S.-C., & Lu, L.-N. (2008). Melt rheological properties of reactive compatibilized HDPE/PET blends. *Journal of Applied Polymer Science*, 108(6), 3559–3564. <https://doi.org/10.1002/app.28031>
- [64] Pluta, M., Bartczak, Z., Pawlak, A., Galeski, A., & Pracella, M. (2001). Phase structure and viscoelastic properties of compatibilized blends of PET and HDPE recyclates. *Journal of Applied Polymer Science*, 82(6), 1423–1436. <https://doi.org/10.1002/app.1980>

- [65] Pawlak, A., Morawiec, J., Pazzagli, F., Pracella, M., & Galeski, A. (2002). Recycling of postconsumer poly(ethylene terephthalate) and high-density polyethylene by compatibilized blending. *Journal of Applied Polymer Science*, 86(6), 1473–1485. <https://doi.org/10.1002/app.11307>
- [66] Pracella, M., Rolla, L., Chionna, D., & Galeski, A. (2002). Compatibilization and properties of poly(ethylene terephthalate)/polyethylene blends based on recycled materials. *Macromolecular Chemistry and Physics*, 203(10-11), 1473–1485. [https://doi.org/10.1002/1521-3935\(200207\)203:10/11<1473::AID-MACP1473>3.0.CO;2-4](https://doi.org/10.1002/1521-3935(200207)203:10/11<1473::AID-MACP1473>3.0.CO;2-4)
- [67] Dagli, S. S., & Kamdar, K. M. (1994). Effects of component addition protocol on the reactive compatibilization of HDPE/PET blends. *Polymer Engineering & Science*, 34(23), 1709–1719. <https://doi.org/10.1002/pen.760342302>
- [68] Pietrasanta, Y., Robin, J.-J., Torres, N., & Boutevin, B. (1999). Reactive compatibilization of HDPE/PET blends by glycidyl methacrylate functionalized polyolefins. *Macromolecular Chemistry and Physics*, 200(1), 142–149. [https://doi.org/10.1002/\(SICI\)1521-3935\(19990101\)200:1<142::AID-MACP142>3.0.CO;2-W](https://doi.org/10.1002/(SICI)1521-3935(19990101)200:1<142::AID-MACP142>3.0.CO;2-W)
- [69] Uehara, G. A., França, M. P., & Canevarolo Junior, S. V. (2015). Recycling assessment of multilayer flexible packaging films using design of experiments. *Polimeros*, 25, 371–381. <https://doi.org/10.1590/0104-1428.1965>
- [70] Pracella, M., Chionna, D., Ishak, R., & Galeski, A. (2004). Recycling of PET and polyolefin based packaging materials by reactive blending. *Polymer-Plastics Technology and Engineering*, 43(6), 1711–1722. <https://doi.org/10.1081/PPT-200040075>
- [71] Benhamida, A., Kaci, M., Cimmino, S., Silvestre, C., & Duraccio, D. (2009). Melt mixing of ethylene/butyl acrylate/glycidyl methacrylate terpolymers with LDPE and PET. *Macromolecular Materials and Engineering*, 294(2), 122–129. <https://doi.org/10.1002/mame.200800214>
- [72] Fasce, L., Seltzer, R., Frontini, P., Pita, V. R., Pacheco, E., & Dias, M. (2005). Mechanical and fracture characterization of 50:50 HDPE/PET blends presenting different phase morphologies. *Polymer Engineering & Science*, 45(3), 354–363. <https://doi.org/10.1002/pen.20282>
- [73] Morawiec, J., Krasnikova, N. P., Galeski, A., & Pracella, M. (2002). Oriented films from recycled poly(ethylene terephthalate)/recycled high-density polyethylene compatibilized blends. *Journal of Applied Polymer Science*, 86(6), 1486–1496. <https://doi.org/10.1002/app.11308>
- [74] Guerrero, C., Lozano, T., González, V., & Arroyo, E. (2001). Properties and morphology of poly(ethylene terephthalate) and high-density polyethylene blends. *Journal of Applied Polymer Science*, 82(6), 1382–1390. <https://doi.org/10.1002/app.1975>
- [75] Fang, C., Nie, L., Liu, S., Yu, R., An, N., & Li, S. (2013). Characterization of polypropylene–polyethylene blends made of waste materials with compatibilizer and nano-filler. *Composites Part B: Engineering*, 55, 498–505. <https://doi.org/10.1016/j.compositesb.2013.06.046>

- [76] Chiono, V., Filippi, S., Yordanov, H., Minkova, L., & Magagnini, P. (2003). Reactive compatibilizer precursors for LDPE/PA6 blends. iii: Ethylene–glycidylmethacrylate copolymer. *Polymer*, 44(8), 2423–2432. [https://doi.org/10.1016/S0032-3861\(03\)00134-4](https://doi.org/10.1016/S0032-3861(03)00134-4)
- [77] Tuampoemsab, S., Riyajan, S., Sritapunya, T., & Pakeyangkoon, P. (2014). Effect of Epoxide Group in Thermoplastic Elastomer on the Properties of Polyamide 6 and Low-Density Polyethylene Blends. In W. Mekhum, N. Sangwaranatee, P. Limsuwan, H. Kim, M. Djamal & J. Kaewkhao (Eds.), *Applied Physics and Material Science* (pp. 143–146). Trans Tech Publications Ltd. <https://doi.org/10.4028/www.scientific.net/AMR.979.143>
- [78] Zhang, X., Li, B., Wang, K., Zhang, Q., & Fu, Q. (2009). The effect of interfacial adhesion on the impact strength of immiscible PP/PETG blends compatibilized with triblock copolymers. *Polymer*, 50(19), 4737–4744. <https://doi.org/10.1016/j.polymer.2009.08.004>
- [79] Maris, J., Bourdon, S., Brossard, J.-M., Cauret, L., Fontaine, L., & Montembault, V. (2018). Mechanical recycling: Compatibilization of mixed thermoplastic wastes. *Polymer Degradation and Stability*, 147, 245–266. <https://doi.org/10.1016/j.polymdegradstab.2017.11.001>
- [80] Zhang, H., Guo, W., Yu, Y., Li, B., & Wu, C. (2007). Structure and properties of compatibilized recycled poly(ethylene terephthalate)/linear low density polyethylene blends. *European Polymer Journal*, 43(8), 3662–3670. <https://doi.org/10.1016/j.eurpolymj.2007.05.001>
- [81] Araujo, J., Vallim, M., Spinacé, M., & De Paoli, M. A. (2008). Use of postconsumer polyethylene in blends with polyamide 6: Effects of the extrusion method and the compatibilizer. *Journal of Applied Polymer Science*, 110, 1310–1317. <https://doi.org/10.1002/app.28441>
- [82] Atiqah, A. M., Salmah, H., Firuz, Z., & Lan, D. (2015). Effect of Different Blend Ratios and Compatibilizer on Tensile Properties of Recycled Poly(propylene)/Recycled High Density Polyethylene Blends. *Macromolecular Symposia*, 353(1), 70–76. <https://doi.org/10.1002/masy.201550309>
- [83] Kasama, J., & Chareunkvun, S. (2007). Compatibilization of recycled high density polyethylene (HDPE)/polyethylene terephthalate (PET) blends. *Suranaree Journal of Science Technology*, 14(1), 1–8. <http://ird.sut.ac.th/e-journal/document/contents/01.pdf>
- [84] Pazzagli, F., & Pracella, M. (2000). Reactive compatibilization of polyolefin/PET blends by melt grafting with glycidyl methacrylate. *Macromolecular Symposia*, 149(1), 225–230. [https://doi.org/10.1002/1521-3900\(200001\)149:1<225::AID-MASY225>3.0.CO;2-8](https://doi.org/10.1002/1521-3900(200001)149:1<225::AID-MASY225>3.0.CO;2-8)
- [85] Liu, Y., Xu, H., Liu, G., & Pu, S. (2017). Core/shell morphologies in recycled poly(ethylene terephthalate)/linear low-density polyethylene/poly(styrene-*b*-(ethylene-co-butylene)-*b*-styrene) ternary blends. *Polymer Bulletin*, 74(10), 4223–4233. <https://doi.org/10.1007/s00289-017-1950-1>
- [86] Sambaru, P., & Jabarin, S. A. (1993). Properties and morphology of oriented ternary blends of poly(ethylene terephthalate), high density polyethylene, and compatibilizing agent. *Polymer Engineering & Science*, 33(13), 827–837. <https://doi.org/10.1002/pen.760331307>

- [87] Choudhury, A., Mukherjee, M., & Adhikari, B. (2006). Recycling of Polyethylene/Poly(ethylene terephthalate) Post-Consumer Oil Pouches using Compatibiliser. *Polymers and Polymer Composites*, 14(6), 635–646. <https://doi.org/10.1177/096739110601400609>
- [88] Torres, N., Robin, J. J., & Boutevin, B. (2001). Study of compatibilization of HDPE–PET blends by adding grafted or statistical copolymers. *Journal of Applied Polymer Science*, 81(10), 2377–2386. <https://doi.org/10.1002/app.1678>
- [89] Modified styrene–butadiene–styrene block copolymer as compatibiliser precursor in polyethylene/poly(ethylene terephthalate) blends [Special Issue on Chemical Modification of Polymers]. (2005). *Polymer Degradation and Stability*, 90(2), 211–223. <https://doi.org/10.1016/j.polymdegradstab.2005.03.016>
- [90] Klimovica, K., Pan, S., Lin, T.-W., Peng, X., Ellison, C. J., LaPointe, A. M., Bates, F. S., & Coates, G. W. (2020). Compatibilization of iPP/HDPE blends with PE-g-iPP graft copolymers. *ACS Macro Letters*, 9(8), 1161–1166. <https://doi.org/10.1021/acsmacrolett.0c00339>
- [91] Chouiref, C. C., & Belhaneche-Bensemra, N. (2012). Regenerated LDPE/PS blends: Characterization and compatibilization. *International Journal of Environmental Studies*, 69(6), 881–887. <https://doi.org/10.1080/00207233.2012.727234>
- [92] Atiqah, A. M., Salmah, H., Firuz, Z., & Uy Lan, D. N. (2014). Properties of Recycled High Density Polyethylene/Recycled Polypropylene Blends: Effect of Maleic Anhydride Polypropylene. In M. M. A. B. Abdullah, L. Jamaludin, A. Abdullah, R. A. Razak & K. Hussin (Eds.), *Advanced Materials Engineering and Technology II* (pp. 837–841). Trans Tech Publications Ltd. <https://doi.org/10.4028/www.scientific.net/KEM.594-595.837>
- [93] Al-Mulla, A., & Shaban, H. (2014). Study on compatibility of recycled polypropylene/high-density polyethylene blends using rheology. *Polymer bulletin*, 71(9), 2335–2352. <https://doi.org/10.1007/s00289-014-1191-5>
- [94] Moreno, D. D. P., & Saron, C. (2018). Influence of compatibilizer on the properties of low-density polyethylene/polyamide 6 blends obtained by mechanical recycling of multilayer film waste. *Waste Management & Research*, 36(8), 729–736. <https://doi.org/10.1177/0734242X18777795>
- [95] Minkova, L., Yordanov, H., Filippi, S., & Grizzuti, N. (2003). Interfacial tension of compatibilized blends of LDPE and PA6: The breaking thread method. *Polymer*, 44(26), 7925–7932. <https://doi.org/10.1016/j.polymer.2003.09.054>
- [96] Aradoaei, S. T., Darie, R. N., Vasile, C., Mosneagu, M., & Olariu, M. A. (2012). Morphology and dielectric properties of some LDPE/PA blends in presence of compatibilizers. In M. Nicoară, A. Răduță & C. Opriș (Eds.), *Advanced Materials and Structures IV* (pp. 268–274). Trans Tech Publications Ltd. <https://doi.org/10.4028/www.scientific.net/SSP.188.268>
- [97] Graziano, A., Tifton Dias, O. A., Sena Maia, B., & Li, J. (2021). Enhancing the mechanical, morphological, and rheological behavior of polyethylene/polypropylene blends with maleic anhydride-grafted polyethylene. *Polymer Engineering & Science*, 61(10), 2487–2495. <https://doi.org/10.1002/pen.25775>

- [98] Kumar, R., Kar, K. K., & Kumar, V. (2018). Studies on the effect of compatibilizers on mechanical, thermal and flow properties of polycarbonate/poly (butylene terephthalate) blends. *Materials Research Express*, 5(1), 015306. <https://doi.org/10.1088/2053-1591/aaa25c>
- [99] Bruice, P. (2016). 12 - Radicals. In P. Bruice (Ed.), *Organic Chemistry, eBook, Global Edition* (Eighth edition, pp. 532–566). Pearson Education. <https://books.google.nl/books?id=KCtPDAAAQBAJ>
- [100] Russell, K. (2002). Free radical graft polymerization and copolymerization at higher temperatures. *Progress in Polymer Science*, 27(6), 1007–1038. [https://doi.org/10.1016/S0079-6700\(02\)00007-2](https://doi.org/10.1016/S0079-6700(02)00007-2)
- [101] Passaglia, E., Coiai, S., & Augier, S. (2009). Control of macromolecular architecture during the reactive functionalization in the melt of olefin polymers. *Progress in Polymer Science*, 34(9), 911–947. <https://doi.org/10.1016/j.progpolymsci.2009.04.008>
- [102] Passaglia, E., Coiai, S., Cicogna, F., & Ciardelli, F. (2014). Some recent advances in polyolefin functionalization. *Polymer International*, 63(1), 12–21. <https://doi.org/10.1002/pi.4598>
- [103] Li, J.-L., & Xie, X.-M. (2012). Reconsideration on the mechanism of free-radical melt grafting of glycidyl methacrylate on polyolefin. *Polymer*, 53(11), 2197–2204. <https://doi.org/10.1016/j.polymer.2012.03.035>
- [104] Hettema, R., Van Tol, J., & Janssen, L. (1999). In-situ reactive blending of polyethylene and polypropylene in co-rotating and counter-rotating extruders. *Polymer Engineering & Science*, 39(9), 1628–1641. <https://doi.org/10.1002/pen.11557>
- [105] Jeong, H.-G., & Lee, K.-J. (1999). Effect of discontinuous phase size on physical properties of LLDPE/PP blends obtained in the presence of peroxide. *Advances in Polymer Technology: Journal of the Polymer Processing Institute*, 18(1), 43–51. [https://doi.org/10.1002/\(SICI\)1098-2329\(199921\)18:1<43::AID-ADV5>3.0.CO;2-2](https://doi.org/10.1002/(SICI)1098-2329(199921)18:1<43::AID-ADV5>3.0.CO;2-2)
- [106] Moad, G. (1999). The synthesis of polyolefin graft copolymers by reactive extrusion. *Progress in Polymer Science*, 24(1), 81–142. [https://doi.org/10.1016/S0079-6700\(98\)00017-3](https://doi.org/10.1016/S0079-6700(98)00017-3)
- [107] Clark, D. C., Baker, W. E., & Whitney, R. A. (2001). Peroxide-initiated comonomer grafting of styrene and maleic anhydride onto polyethylene: Effect of polyethylene microstructure. *Journal of Applied Polymer Science*, 79(1), 96–107. [https://doi.org/10.1002/1097-4628\(20010103\)79:1<96::AID-APP120>3.0.CO;2-X](https://doi.org/10.1002/1097-4628(20010103)79:1<96::AID-APP120>3.0.CO;2-X)
- [108] Bray, T., Damiris, S., Grace, A., Moad, G., O'Shea, M., Rizzardo, E., & van Diepen, G. (1998). Developments in the synthesis of maleated polyolefins by reactive extrusion. *Macromolecular Symposia*, 129(1), 109–118. <https://doi.org/10.1002/masy.19981290110>
- [109] Teh, J. W., & Rudin, A. (1992). Compatibilization of a polystyrene-polyethylene blend through reactive processing in a twin screw extruder. *Polymer Engineering & Science*, 32(22), 1678–1686. <https://doi.org/10.1002/pen.760322205>
- [110] Saki, T. A. (2015). Reactive melt blending of low-density polyethylene with poly(acrylic acid). *Arabian Journal of Chemistry*, 8(2), 191–199. <https://doi.org/10.1016/j.arabjc.2011.05.021>

- [111] Chodak, I., Repin, H., Bruls, W., & Janigova, I. (1996). Chemical modification of polyolefin blends. *Macromolecular Symposia*, 112(1), 159–166. <https://doi.org/10.1002/masy.19961120123>
- [112] Gu, J., Xu, H., & Wu, C. (2014). The Effect of Benzoyl Peroxide and Divinyl Benzene on the Properties of Cross-Linked Recycled Polyolefin Blends. *Journal of Macromolecular Science, Part B*, 53(12), 1777–1785. <https://doi.org/10.1080/00222348.2013.861297>
- [113] Wei, Q., Chionna, D., Galoppini, E., & Pracella, M. (2003). Functionalization of LDPE by melt grafting with glycidyl methacrylate and reactive blending with polyamide-6. *Macromolecular Chemistry and Physics*, 204(8), 1123–1133. <https://doi.org/10.1002/macp.200390081>
- [114] Gu, J., Xu, H., & Wu, C. (2013). The effect of PP and peroxide on the properties and morphology of HDPE and HDPE/PP blends. *Advances in Polymer Technology*, 32(1). <https://doi.org/10.1002/adv.21326>
- [115] Wei, Q., Chionna, D., & Pracella, M. (2005). Reactive compatibilization of PA6/LDPE blends with glycidyl methacrylate functionalized polyolefins. *Macromolecular Chemistry and physics*, 206(7), 777–786. <https://doi.org/10.1002/macp.200400362>
- [116] Iqbal, M., Chuai, C., Huang, Y., & Che, C. (2010). Modification of low-density polyethylene by graft copolymerization with maleic anhydride and blends with polyamide 6. *Journal of Applied Polymer Science*, 116(3), 1558–1565. <https://doi.org/10.1002/app.31439>
- [117] Kelar, K., & Jurkowski, B. (2000). Preparation of functionalised low-density polyethylene by reactive extrusion and its blend with polyamide 6. *Polymer*, 41(3), 1055–1062. [https://doi.org/10.1016/S0032-3861\(99\)00260-8](https://doi.org/10.1016/S0032-3861(99)00260-8)
- [118] Ganzeveld, K. J., & Janssen, L. P. B. M. (1992). The grafting of maleic anhydride on high density polyethylene in an extruder. *Polymer Engineering & Science*, 32(7), 467–474. <https://doi.org/10.1002/pen.760320703>
- [119] Machado, A. V., van Duin, M., & Covas, J. A. (2000). Monitoring polyolefin modification along the axis of a twin-screw extruder. II. Maleic anhydride grafting. *Journal of Polymer Science Part A: Polymer Chemistry*, 38(21), 3919–3932. [https://doi.org/10.1002/1099-0518\(20001101\)38:21<3919::AID-POLA90>3.0.CO;2-L](https://doi.org/10.1002/1099-0518(20001101)38:21<3919::AID-POLA90>3.0.CO;2-L)
- [120] Fang, H., Ma, X., Feng, L., Wang, K., & Cao, B. (2008). Effects of screw configurations on the grafting of maleic anhydride grafted low-density polyethylene in reactive extrusion. *Journal of Applied Polymer Science*, 108(6), 3652–3661. <https://doi.org/10.1002/app.27158>
- [121] Samay, G., Nagy, T., & White, J. L. (1995). Grafting maleic anhydride and comonomers onto polyethylene. *Journal of Applied Polymer Science*, 56(11), 1423–1433. <https://doi.org/10.1002/app.1995.070561105>
- [122] Mehrabzadeh, M., Kamal, M. R., & Quintanar, G. (2009). Maleic Anhydride Grafting onto HDPE by In situ Reactive Extrusion and its Effect on Intercalation and Mechanical Properties of HDPE-Clay Nanocomposites. *Iranian Polymer Journal*, 18(10), 833–842. https://www.researchgate.net/publication/267778849_Maleic_Anhydride_Grafting_onto_HDPE_by_In_situ_Reactive_Extrusion_and_its_Effect_on_Intercalation_and_Mechanical_Properties_of_HDPEClay_Nanocomposites

- [123] Li, C., Zhang, Y., & Zhang, Y. (2003). Melt grafting of maleic anhydride onto low-density polyethylene/polypropylene blends. *Polymer Testing*, 22(2), 191–195. [https://doi.org/10.1016/S0142-9418\(02\)00079-X](https://doi.org/10.1016/S0142-9418(02)00079-X)
- [124] Roy, P. K., Swami, V., Kumar, D., & Rajagopal, C. (2012). Investigating the Degradation Behavior of LDPE-grafted Maleic Anhydride for Use as Compatibilizer in Environmentally Degradable Compositions. *International Journal of Polymeric Materials and Polymeric Biomaterials*, 61(4), 241–262. <https://doi.org/10.1080/00914037.2011.574662>
- [125] Hopmann, C., Adamy, M., & Cohnen, A. (2018). 1 - Introduction to Reactive Extrusion. In G. Beyer & C. Hopmann (Eds.), *Reactive Extrusion: Principles and Applications* (pp. 3–10). Wiley. <https://books.google.nl/books?id=hsY2DwAAQBAJ>
- [126] Cassagnau, P., Bounor-Legaré, V., & Fenouillot, F. (2007). Reactive Processing of Thermoplastic Polymers: A Review of the Fundamental Aspects. *International Polymer Processing*, 22, 218–258. <https://doi.org/10.3139/217.2032>
- [127] Lechner, F. (2018). 2 - The Co-rotating Twin-Screw Extruder for Reactive Extrusion. In G. Beyer & C. Hopmann (Eds.), *Reactive Extrusion: Principles and Applications* (pp. 13–35). Wiley. <https://books.google.nl/books?id=hsY2DwAAQBAJ>
- [128] Formela, K., Zedler, Ł., Hejna, A., & Tercjak, A. (2018). Reactive extrusion of bio-based polymer blends and composites – Current trends and future developments. *eXPRESS Polymer Letters*, 12, 24–57. <https://doi.org/10.3144/expresspolymlett.2018.4>
- [129] IndiaMART. (n.d.). *Twin Screw Barrel Machine*. Retrieved April 15, 2022, from <https://www.indiamart.com/golden-mechanical-works/twin-screw-barrel-machine.html>
- [130] C.W. Brabender® Instruments. (n.d.). *Segmented Twin Screw Extruder 20mm Clamshell*. Retrieved April 15, 2022, from <https://www.cwbrabender.com/en/chemical/products/extrusion/twin-screw-extruders/twin-screw-extruder-2040-stand-alone>
- [131] Kohlgrüber, K. (2008). 1 Introduction. In K. Kohlgrüber & M. Bierdel (Eds.), *Co-rotating Twin-screw Extruders: Fundamentals, Technology, and Applications* (pp. 1–7). Carl Hanser Publishers. <https://books.google.nl/books?id=Z2nlwAEACAAJ>
- [132] Crawford, D. (2017). Extrusion - Back to the future: Using an established technique to reform automated chemical synthesis. *Beilstein Journal of Organic Chemistry*, 13, 65–75. <https://doi.org/10.3762/bjoc.13.9>
- [133] Wagner, J. R., Mount, E. M., & Giles, H. F. (2014a). 13 - Screw Design. In J. R. Wagner, E. M. Mount & H. F. Giles (Eds.), *Extrusion (Second Edition)* (Second Edition, pp. 171–179). William Andrew Publishing. <https://doi.org/10.1016/B978-1-4377-3481-2.00013-2>
- [134] Wagner, J. R., Mount, E. M., & Giles, H. F. (2014b). 1 - Extrusion Process. In J. R. Wagner, E. M. Mount & H. F. Giles (Eds.), *Extrusion (Second Edition)* (Second Edition, pp. 3–11). William Andrew Publishing. <https://doi.org/10.1016/B978-1-4377-3481-2.00001-6>
- [135] Jenck, J. F., Agterberg, F., & Droescher, M. J. (2004). Products and processes for a sustainable chemical industry: a review of achievements and prospects. *Green Chemistry*, 6(11), 544–556. <https://doi.org/10.1039/B406854H>

- [136] Wagner, J. R., Mount, E. M., & Giles, H. F. (2014c). 15 - Applications. In J. R. Wagner, E. M. Mount & H. F. Giles (Eds.), *Extrusion (Second Edition)* (Second Edition, pp. 193–198). William Andrew Publishing. <https://doi.org/10.1016/B978-1-4377-3481-2.00015-6>
- [137] Tselios, C., Bikiaris, D., Maslis, V., & Panayiotou, C. (1998). In situ compatibilization of polypropylene–polyethylene blends: a thermomechanical and spectroscopic study. *Polymer*, 39(26), 6807–6817. [https://doi.org/10.1016/S0032-3861\(98\)00132-3](https://doi.org/10.1016/S0032-3861(98)00132-3)
- [138] Shrivastava, A. (2018). 5 - Plastics Processing. In A. Shrivastava (Ed.), *Introduction to Plastics Engineering* (pp. 143–177). William Andrew Publishing. <https://doi.org/10.1016/B978-0-323-39500-7.00005-8>
- [139] Wagner, J. R., Mount, E. M., & Giles, H. F. (2014d). 4 - Plastic Behaviour in the Extruder. In J. R. Wagner, E. M. Mount & H. F. Giles (Eds.), *Extrusion (Second Edition)* (Second Edition, pp. 171–179). William Andrew Publishing. <https://doi.org/10.1016/B978-1-4377-3481-2.00013-2>
- [140] Fang, H., & Yang, G. (2010). Influence of in situ compatibilization on in situ formation of low-density polyethylene/polyamide 6 blends by reactive extrusion. *Journal of Applied Polymer Science*, 116(5), 3027–3034. <https://doi.org/10.1002/app.31843>
- [141] Christoph Burgstaller and Bernhard Riedl and Wolfgang Stadlbauer. (2015). *The Influence of Blend Composition and Additive Type on the Properties of LDPE-PA6-Blends*. <https://app.knovel.com/hotlink/khtml/id:kt010QWAJ2/antec-2015-proceedings/influence-blend-composition%7D>
- [142] Reyes, A. (2015). Differential and Integrated Rate Laws (university handout). <https://laney.edu/abraham-reyes/wp-content/uploads/sites/229/2015/08/Differential-and-Integrated-Rate-Laws1.pdf>
- [143] Molyneux, P. (1966). The arrhenius parameters for the thermal decomposition of organic peroxides, and the dissociation energy of the peroxide bond. *Tetrahedron*, 22(9), 2929–2943. [https://doi.org/10.1016/S0040-4020\(01\)82271-7](https://doi.org/10.1016/S0040-4020(01)82271-7)
- [144] Nouryon. (2022). Initiators for Thermoplastics (brochure). https://www.nouryon.com/globalassets/inriver/resources/brochure-initiators-for-thermoplastics-en_us.pdf
- [145] LUCOBIT AG. (2014). *Lucofin® 1492M HG*. http://www.lucobit-china.com/icoaster/files/lucofin_1492mhg_pds_en_2014_01.pdf
- [146] *ISO 1133-1:2022 – Plastics — Determination of the melt mass-flow rate (MFR) and melt volume-flow rate (MVR) of thermoplastics — Part 1: Standard method* (Standard). (2018). <https://www.iso.org/standard/83905.html>
- [147] *ISO 527-3:2018 – Plastics — Determination of tensile properties — Part 3: Test conditions for films and sheets* (Standard). (2018). <https://www.iso.org/standard/23637.html>
- [148] Gottschalk, T., Özbay, C., Feuerbach, T., & Thommes, M. (2022). Predicting Throughput and Melt Temperature in Pharmaceutical Hot Melt Extrusion. *Pharmaceutics*, 14(9), 1757. <https://doi.org/10.3390/pharmaceutics14091757>

- [149] Mélo, T., Pinheiro, L., & Canevarolo, S. (2009). Factorial Design to Quantify the Influence of Extrusion Parameters in the Mean Residence Time. *Polímeros*, 20, 322–326. <https://doi.org/10.1590/S0104-14282010005000050>
- [150] LyondellBasel. (2022a). *Lupolen 2420D*. Retrieved December 23, 2022, from <https://www.lyondellbasell.com/en/polymers/p/Lupolen-2420D/bd51db21-61a1-4d8f-b90a-27d75238169f>
- [151] LyondellBasel. (2022b). *Lupolen 2420F*. Retrieved December 23, 2022, from <https://www.lyondellbasell.com/en/polymers/p/Lupolen-2420F/61e46490-ed79-4c71-bd7a-35125886bb3a>
- [152] Aggour, Y. A., Al-Shihri, A. S., & Bazzt, M. R. (2012). Surface Modification of Waste Tire by Grafting with Styrene and Maleic Anhydride. *Open Journal of Polymer Chemistry*, 2(2), 70. <https://doi.org/10.4236/ojpcchem.2012.22009>
- [153] Barra, G., Crespo, J., R, B., Soldi, V., & Nunes, P. (1999). Maleic Anhydride Grafting on EPDM: Qualitative and Quantitative Determination. *Journal of the Brazilian Chemical Society*, 10. <https://doi.org/10.1590/S0103-50531999000100006>
- [154] Czarnecka-Komorowska, D., Nowak-Grzebyta, J., Gawdzińska, K., Mysiukiewicz, O., & Tomasik, M. (2021). Polyethylene/Polyamide Blends Made of Waste with Compatibilizer: Processing, Morphology, Rheological and Thermo-Mechanical Behavior. *Polymers*, 13(14), 2385. <https://doi.org/10.3390/polym13142385>
- [155] Wu, X., Chen, J., & Zeng, X. (1991). The application of DSC in identification of LDPE/LLDPE blends mulching film. *Die Angewandte Makromolekulare Chemie*, 189(1), 183–193. <https://doi.org/10.1002/apmc.1991.051890117>
- [156] Piccardo, P., Bongiorno, V., & Campodonico, S. (2013). 10 - Artistic patinas on ancient bronze statues. In P. Dillmann, D. Watkinson, E. Angelini & A. Adriaens (Eds.), *Corrosion and Conservation of Cultural Heritage Metallic Artefacts* (pp. 193–212). Woodhead Publishing. <https://doi.org/10.1533/9781782421573.3.193>
- [157] Thermo Fisher Scientific. (2021a). SAFETY DATA SHEET – Maleic anhydride. [https://www.fishersci.com/store/msds?partNumber=AC125240251&productDescription=MALEIC + ANHYDRIDE % 2C + 99 % 25 % 2C + P + 25KG & vendorId = VN00032119 & countryCode=US&language=en](https://www.fishersci.com/store/msds?partNumber=AC125240251&productDescription=MALEIC+ANHYDRIDE%2C+99%25%2C+P+25KG&vendorId=VN00032119&countryCode=US&language=en)
- [158] Thermo Fisher Scientific. (2021b). SAFETY DATA SHEET – Glycidyl methacrylate, stabilized. [https://www.fishersci.com/store/msds?partNumber=AC165890050 & productDescription = GLYCIDYL + METHACRYLATE + 97 % 25 + 5G & vendorId = VN00032119&countryCode=US&language=en](https://www.fishersci.com/store/msds?partNumber=AC165890050&productDescription=GLYCIDYL+METHACRYLATE+97%25+5G&vendorId=VN00032119&countryCode=US&language=en)
- [159] LABTECH ENGINEERING COMPANY LTD. (n.d.). *TWIN SCREW EXTRUDER 26 MM*. Retrieved June 18, 2022, from <https://www.labtechengineering.com/product/lte-26-and-item-26/>

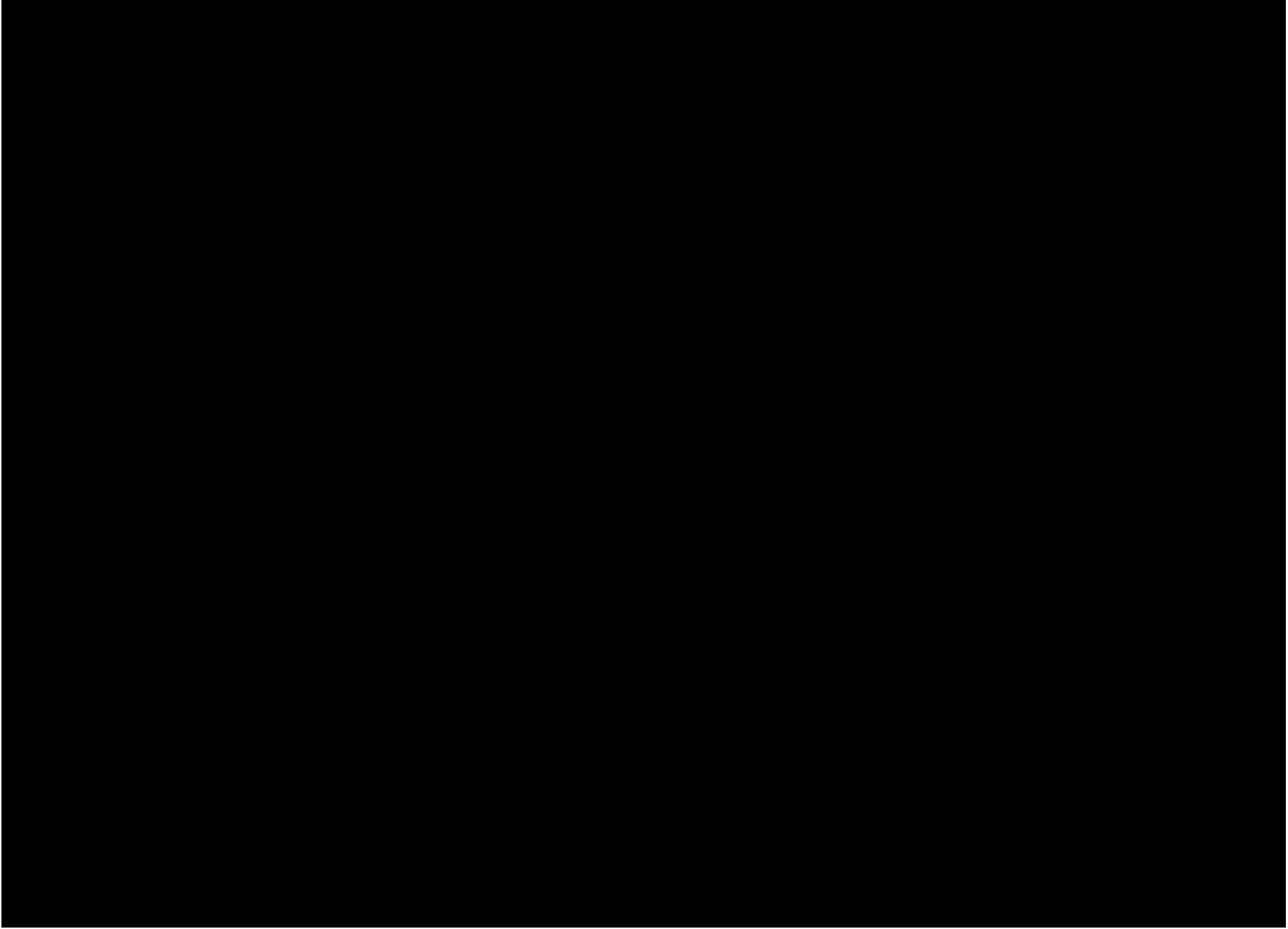
Appendices

A Specifications extruder set-up CIRSEE - PLAST'lab

Machine	Extruder
Brand	LABTECH
Type	LTE26-44 Standard
Screw type	Twin-screw, modular
Rotation orientation	Co-rotating
Screw diameter	26 mm
Maximum screw speed	800 rpm
Motor power	15 kW
Specific torque	9.8 Nm/cm ³
Maximum barrel temperature	400 °C
L/D	44
Approximate max. output (LDPE)	64 kg/hr

Table A.1: Extruder specifications^[159].

B Screw design of twin-screw extruder



C Extrusion blowing experiment



Figure C.1: The extrusion blowing setup during an experiment. The cylindrical plastic bubble can be identified, going from bottom to top.